

**Formation of Zinc Oxide Nanostructures and Their
Photo-Electrochemical Application**

JANUARY 2014

DOCTOR OF ENGINEERING

WAI KIAN TAN

TOYOHASHI UNIVERSITY OF TECHNOLOGY

Formation of Zinc Oxide Nanostructures and Their Photo-Electrochemical Application

Abstract

Nowadays, low-temperature and environmentally conservative methods of functional oxides formation have been the main motivation for many researchers. By using low temperature synthesis techniques, flexible device fabrication utilizing substrates with low thermal stability such as organic polymer substrates are envisaged. Initial investigations on the formation of ZnO nanostructures were performed using rapid thermal oxidation of Zn foils as a function time, temperature and atmosphere. One-dimensional (1-D) ZnO nanorods and two-dimensional (2-D) ZnO nanosheets on Zn foils were reported; the formation mechanism of the ZnO nanostructures and the photocatalytic properties were also documented. Subsequently, surface oxidation of Zn foils via hot-water treatment (HWT) was investigated at 90°C from 4 to 24 h. Chemical etching of Zn foils' surface was found to affect the morphologies of ZnO nanostructures generated due different diffusion route of Zn ions from the substrate to the surface of the foils; ZnO nanowires and nanorods were obtained on the surface of chemically etched Zn foils while ZnO nanosheets were formed on unetched Zn foils. However, the ZnO nanostructures formed exhibited good crystallinity and optical properties as demonstrated by photoluminescence, Raman measurements, and high-resolution transmission electron microscope (HR-TEM) observations. Moreover, HWT was performed on sol-gel derived coatings in order to study the formation mechanism of ZnO nanostructures. The effect of an external direct current (D.C.) electric field induction during HWT of sol-gel derived ZnO coatings for controlled formation of good crystalline ZnO films was investigated. The electric field induced hot-water treatment (EF-HWT) was found to influence the formation of crystalline ZnO nanostructures on the ZnO gel films at low-temperature of 50°C for 3 h. The effects of time, voltage and substrates used during the EF-HWT were investigated. Flower-like precipitates of hexagonal zinc oxide were generated from the zinc acetate derived ZnO gel film on a silicon single crystal substrate at the negative electrode by applying an electric field. In a separate study, Ce-doped ZnO nanostructured films were also prepared via HWT of Ce-doped ZnO sol-gel coatings. Rod-like undoped and Ce-doped ZnO nanostructures have been formed using hot-water treatment of the undoped and Ce-doped sol-gel derived coatings at low-temperature of 60°C for 30 min on glass substrates. The concentration of Ce doping was varied from 2 to 20 at %. Morphological structures and

optical properties of the hot-water treated ZnO films were investigated and compared with conventional, annealed ZnO films. The resultant undoped and Ce-doped ZnO nanostructures showed ultraviolet (UV) and strong blue emissions which can be used for the fabrication of optoelectronics devices. In a different study, well-aligned ZnO nanorod arrays were formed on seeded substrates via low-temperature hydrothermal process at 80°C. The oriented ZnO nanorod arrays were used as the photo-electrode for dye sensitized solar cells (DSSCs). The formation mechanism of the oriented ZnO nanorods arrays was investigated as a function of time (4 to 24 h) systematically. The maximum conversion efficiency of DSSCs obtained after a prolonged hydrothermal growth time of 24 h was 0.22 %. For photo-catalyst application, ZnO composite films consisting of ZnO nanorods and nanosheets were prepared by low-temperature hydrothermal at 80°C on seeded glass substrates. The seed layer was coated on glass substrates by sol-gel dip-coating and pre-heated at 300°C for 10 min prior to hydrothermal growth. The formation of composite one-dimensional ZnO nanorod arrays and two-dimensional ZnO nanosheet films using seeded substrates in a single low-temperature hydrothermal step would be beneficial for realization of device applications with properties exhibited in this unique morphology. The ZnO nanorods and nanosheets composite structure demonstrated higher photocatalytic activity during degradation of aqueous methylene blue under visible-light irradiation compared to only one-dimensional ZnO nanorod arrays. Based on all the studies, it can be concluded that the multi-dimensional and multi-functional ZnO nanostructures can be prepared using various low-temperature methods. HWT is also a promising method to generate ZnO nanostructures without any catalyst and therefore eliminating specimen contamination.

Contents

	Page
Abstract	i
Contents	iii
Chapter 1 General Introduction	1
1.1 ZnO structures	1
1.2 Optical structures of ZnO	2
1.3 Scope of studies	2
1.3.1 Thermal oxidation of Zn	3
1.3.2 Surface oxidation of Zn foils by HWT	3
1.3.3 Hot-water treatment of sol-gel derived coatings	4
1.3.4 Hydrothermal growth of ZnO nanostructures	5
Chapter 2 Formation of two-dimensional ZnO nanosheets by rapid thermal oxidation in oxygenated environment	12
2.1 Introduction	12
2.2 Experimental	14
2.3 Results & Discussions	16
2.3.1 Structural and morphological properties	16
2.3.2 Luminescence properties	25
2.3.3 Photocatalytic properties	29
2.3.4 Formation mechanism of ZnO nanosheets	31
2.4 Conclusion	34

Chapter 3 Formation of ZnO nanostructures via hot-water treatment	37
3.1 Hot-water treatment of Zn foils	37
3.1.1 Introduction	37
3.1.2 Experimental	38
3.1.3 Results and discussions of hot-water treated etched Zn foils	39
3.1.3.1 Morphological observation	39
3.1.3.2 XRD	42
3.1.3.3 Optical properties	43
3.1.4 Results and discussions of hot-water treated unetched Zn foils	47
3.1.4.1 Morphological observation of the ZnO nanosheets	47
3.1.4.2 XRD	51
3.1.4.3 Optical properties	52
3.1.5 Formation mechanism of the ZnO nanostructures	55
3.1.6 Conclusion	57
3.2 Hot-water treatment of sol-gel derived coatings	60
3.2.1 Morphology-control of crystallites precipitated from ZnO gel films by applying electric field during hot-water treatment.	60
3.2.1.1 Introduction	60
3.2.1.2 Experimental	62
3.2.1.2.1 Preparation of sol-gel coating	62
3.2.1.2.2 D.C. electric field induced hot-water treatment	62
3.2.1.2.3 Characterizations	64
3.2.1.3 Results & Discussions	64
3.2.1.3.1 Effect of electric field hot-water treatment on the morphological structures	64

3.2.1.3.2 Effect of substrate on ZnO crystals formation	75
3.2.1.4 Conclusion	81
3.2.2 Photoluminescence properties of rod-like Ce-doped ZnO nanostructured films formed by hot-water treatment of sol-gel derived coatings	84
3.2.2.1 Introduction	84
3.2.2.2 Experimental	86
3.2.2.3 Results & Discussions	87
3.2.2.4 Conclusion	101
Chapter 4 Hydrothermal growth of ZnO nanostructures	105
4.1 Enhance dye-sensitized solar cells performance of ZnO nanorod arrays grown by low-temperature hydrothermal reaction.	105
4.1.1 Introduction	105
4.1.2 Experimental	107
4.1.2.1 Preparation of ZnO seed-coated substrate	107
4.1.2.2 Hydrothermal growth of ZnO nanorod arrays by low-temperature hydrothermal reaction	107
4.1.2.3 Characterizations	108
4.1.2.4 DSSCs assembly	108
4.1.3 Results & Discussions	109
4.1.3.1 Morphology and the structure of the hydrothermally-derived ZnO nanorod arrays	109
4.1.3.2 XRD and HR-TEM observation	111
4.1.3.3 Optical properties of the ZnO nanorod arrays	114
4.1.3.4 DSSC efficiency measurement	118

4.1.3.5 ZnO nanorods growth mechanism	121
4.1.4 Conclusion	122
4.2 Synthesis of ZnO nanorod-nanosheet composite via facile hydrothermal method and their photocatalytic activities under visible light irradiation.	129
4.2.1 Introduction	129
4.2.2 Experimental	130
4.2.3 Results & Discussions	132
4.2.3.1 Sol-gel seed layer	133
4.2.3.2 Morphology and structure of hydrothermally-derived ZnO composite films	134
4.2.3.3 Luminescence properties	144
4.2.3.4 Photocatalytic activity	149
4.2.4 Conclusion	151
Chapter 5 General conclusion	158
Acknowledgements	162
List of publications	164

Chapter 1

GENERAL INTRODUCTION

Zinc oxide (ZnO) has attracted wide interest from many researchers on its processing methods, characterisations and applications due to its unique inter-correlation between morphologies and properties [1-3]. ZnO which is a wide band gap semiconductor with large exciton binding energy of 60 meV at room temperature which can be utilized for many applications such as bio/chemical sensors, photocatalyst, light emitting devices and dye sensitized solar cells (DSSCs) [4-6]. ZnO is also a better light emitting material compared to the widely used GaN due to its easy fabrication of high quality single crystals as oppose to GaN.

Ordered and aligned ZnO crystals can be formed into 1-dimensional (1-D) ZnO nanorod arrays using simple oxidation and chemical processes. Besides that, 2-dimensional (2-D) and 3-dimensional (3-D) ZnO nanostructures can be formed in order to achieve the desire properties required for specific applications. For example, 2-D and 3-D nanostructures have been explored for bio/chemical sensors as well as light sensing material due to its higher surface area which could enhance detection and sensing ability [7].

1.1 ZnO Structures

ZnO has well-defined crystal structures which are commonly in wurtzite, rocksalt, or cubic (zinc blende) structure. The ZnO wurtzite structure has the highest thermodynamic stability among the three structures and therefore the most common structure of ZnO. A rocksalt structure of ZnO can be yielded under high pressure thus ZnO in this structure is quite rare. The hexagonal wurtzite crystal structure has two lattice parameters, a and c with values of 0.3296 nm and 0.52065 nm respectively at ambient pressure and temperature. This

ZnO hexagonal wurtzite structure belongs to the $P6_3mc$ space group and exhibits a non-centrosymmetric structure which causes ZnO to be piezoelectric and pyroelectric.

The wurtzite ZnO consists of atoms forming hexagonal-close-pack sub-lattices which stack alternatively along the c-axis. Each Zn^{2+} sub-lattice contains four Zn^{2+} ions and are surrounded by four O^{2-} ions and vice versa, coordinated at the edges of a tetrahedron [8]. This tetrahedral coordination will form polar symmetry along the hexagonal axis which induces the effect of piezoelectricity and spontaneous polarization in the ZnO wurtzite crystal. The polarization effect is one of the major factors influencing the crystal growth during the synthesis of ZnO nanostructures.

1.2 Optical properties of ZnO

The luminescence properties of ZnO can be characterized using photoluminescence (PL). Typical PL spectra exhibited by ZnO nanostructures consist of two regions which are the ultraviolet (UV) and visible region. UV emission observed is also termed as deep-level emission which is attributed to the recombination of excitons (electron-hole pair recombination or band-to-band recombination). Highly crystalline ZnO would exhibit strong UV emission. The origin of the green band in the visible region in ZnO is attributed to various impurities and defects [8]. The visible emission could be related to the recombination of electrons with oxygen vacancies or with photo-excited holes in the valence band; hence higher defect concentrations may lead to higher emission intensity in this region [9].

1.3 Scope of studies

The evolution of ZnO nanostructures formation was initially investigated by a simple thermal oxidation process. The oxidation temperature, time and atmosphere were studied. After that, attention was given to formation of ZnO nanostructures by low-temperature

processes such as sol-gel, hydrothermal and hot-water treatment. The feasibility of controlled ZnO nanostructures formation in low-temperature would enable the utilization of flexible substrates which have low thermal stability such as organic polymers.

1.3.1 Thermal oxidation of Zn

In the initial study, investigations were performed on the formation of ZnO nanostructures by thermal oxidation of Zn foils as a function of time and temperature. By using this simple and facile method, formation of ZnO covering a large area in a short process time was demonstrated. Studies were performed at temperatures ranging from 100 to 500°C as the melting point of Zn is 419.5°C. At relatively low-temperature regime, porous nanosheets were formed and as the temperature increases, nanorods emerged and oxidation beyond the melting point of Zn resulted in the formation of blunt dendritic nanorods [10]. Thermal oxidation in oxygenated environment which resulted in the formation of 2-D ZnO nanosheets was also performed and included in this study.

In order to fabricate flexible devices utilizing ZnO nanostructures on substrates with low-thermal stability such as organic polymers, low-temperature syntheses are indispensable. Therefore, the main motivation of this project is to form ZnO nanostructures with good crystallinity using facile low-temperature processing methods for photo-electrochemical applications. Methods such as sol-gel, hot-water treatment and hydrothermal were used to generate ZnO nanostructures for its unique optical properties, as well as for DSSCs and photo-catalyst applications.

1.3.2 Surface oxidation of Zn foils by HWT

Xu *et al.* reported the effect of water vapour and oxygen during the growth of ZnO nanostructures by dry and wet oxidation of thermally evaporated Zn films on glass at elevated

temperature of 390°C [19]. Therefore, it is interesting to investigate on the surface oxidation of metallic Zn foils by HWT and study its optical properties and formation mechanism. Subsequent heat-treatment is not required and specimen contamination can be avoided using this facile method.

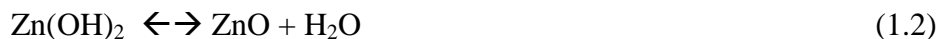
1.3.3 Hot-water treatment of sol-gel derived coatings

Sol-gel method portrays many advantages such as low-temperature fabrication, high purity precursor and good process control on molecular level. Part of this study involves the investigation of hot-water treatment on sol-gel derived coatings. Sol-gel is a simple method whereby the sol is coated onto a substrate, dried and annealed for phase transformation, densification, and crystallization of the film's desired phase [11, 12]. This method is derived from a liquid phase that consists of metal compounds as a source of oxides and alcohol as solvent. Water, acid or base is commonly added into the alcohol solution for the subsequent hydrolysis and poly-condensation reactions. The gel obtained would solidify forming a wet gel and upon evaporation of the remaining water and solvents, a dry gel is obtained. Heat-treatments of the gels at high temperature are commonly performed in order to acquire dense oxide materials as final products [11]. However, high temperature annealing will hinder the use of substrates with low thermal stability. HWT is deemed as a promising method to crystallize and form nanocrystals at low-temperature [13-15]. Works on HWT have been reported based on titanium gel coated on various substrates prior to annealing. This method could lead to the reduction of annealing temperature for the densification and crystallization of the sol-gel coated TiO₂ film. Besides that, the desired phase could be obtained without subsequent annealing. HWT was reportedly performed on ZrO₂ [16], and SiO₂-TiO₂ [17] in order to alter the morphologies of the sol-gel derived coatings. It is also demonstrated that resultant coatings obtained using HWT exhibit unique characteristics such as good photocatalytic activity and excellent water wettability [18].

1.3.4 Hydrothermal growth of ZnO nanostructures

Hydrothermal process is commonly used to generate ZnO nanostructures at low-temperatures. From previous reported work, controllable growth of ZnO nanorod arrays was achieved on seeded layers prepared by rapid thermal oxidation of Zn foil and thermal evaporated metallic Zn layer on polytetrafluoroethylene (PTFE) [20, 21]. Hydrothermal synthesis for thin film of ZnO nanostructures can be defined as a ZnO growth in a reactive bath (aqueous/non-aqueous) of a seeded or non-seeded substrate in a vessel under low-temperature heating. Under these conditions, autogenous pressure is generated within the hydrothermal vessel. The pressure is found to increase dramatically with temperature and is also dependent on volume fill percentage of the vessel as well as the concentration of the precursors. During hydrothermal growth, the formation of the ZnO nanostructures is highly dependent on the temperature, concentration, pH and the pressure of the solution. Correlation on the effect of the exposure time, growth temperature, precursor concentration of the precursor solutions during the formation of uniform ZnO nanorod arrays on seeded metallic Zn foil using Zn nitrate and methamine (HMT) was reported [21].

The growth of ZnO nanorods starts when supersaturation of Zn(OH)_2 from the reactive solution is achieved. Heterogenous nucleation would take place on the seeded substrate. The decomposition of HMT will provide OH^- ions to react with Zn^{2+} ions to form Zn(OH)_2 that will decompose to form ZnO. These are shown in Equation 1.1 and 1.2.



Apart from being a source of OH^- ions, HMT plays a crucial role in the oriented growth leading to the formation of high aspect ratio nanorods. The chelation of HMT onto the

non-polar side planes of the ZnO nanorods inhibits the horizontal growth (radial growth) of ZnO and hence oriented growth of the polarized plane occurs at a higher rate forming the high aspect ratio rod-like structure. In ZnO wurtzite structure, the polarized (002) plane grows faster than the six prismatic side planes. Zn^{2+} or OH^- ions are attracted towards the polar crystal plane which is negatively or positively charged depending on the terminating atoms and grow along c-axis direction.

Seed layer is indispensable for the hydrothermal growth of ZnO nanostructures. Homogenous nucleation of the solid phase in solution does not occur even though the system is beyond the supersaturation due to the surface energy resistance [22, 23]. On the other hand, heterogeneous nucleation onto a foreign surface occurs easier compared to homogenous nucleation. However, heterogeneous nucleation process is difficult to be controlled due to the random and complex nature of the nucleus forming on a foreign substrate. Therefore, substrates pre-coated with a thin layer of seed that consist of the similar material are vital to promote the growth, texture and orientation of the deposited crystals.

Based on these studies, further investigations were performed in order to explore new, novel and facile methods to form ZnO nanostructures at low-temperatures for its wide photo-electrochemical applications.

The studies in this thesis are presented in 5 chapters as indicated as follows:

Chapter 1

General introduction of ZnO, backgrounds, research motivations, and contents of this thesis are described in details.

Chapter 2

This chapter reports on the formation of 2-D ZnO nanosheets by rapid thermal oxidation of Zn foils in oxygenated environment. ZnO nanosheets were formed by rapid thermal oxidation at short period of 10 to 30 min at 300 and 400°C, respectively. The structural and optical properties of the as-formed ZnO nanosheets were characterized. The photocatalytic properties were also investigated and growth mechanism of the ZnO nanosheets was also described.

Chapter 3

In this chapter, the morphological evolution of the ZnO nanostructures generated on the surface of etched and unetched Zn foils by hot-water treatment (HWT) at 90°C is described. One-dimensional (1-D) and two-dimensional (2-D) crystallized ZnO nanostructures were generated using novel and facile HWT of Zn foils. Surface oxidation of metallic Zn foils by HWT without any catalyst was investigated as a function of time. ZnO nanostructures generated using this low-temperature method show good crystallinity and optical properties. 2-D ZnO nanosheets were obtained on unetched Zn foils compared to 1-D ZnO nanorods observed on hot-water treated etched Zn foils. It is believed that the formation mechanism of the ZnO nanosheets differ from the generation of ZnO nanorods on the surface of etched Zn foils. A different route of surface oxidation mechanism is proposed for the formation of ZnO nanosheets on Zn foils.

Hot-water treatment is also performed on sol-gel derived coatings. ZnO nanostructures were formed by dissolution and re-precipitation of the sol-gel derived coatings on FTO and Si. This part of study also describes on the effect of an applied electric field during HWT on the controlled deposition of ZnO crystal at low-temperature. The parameters investigated in this electric-field hot-water treatment (EF-HWT) include time, voltage, type

of substrate and electrode. Granular crystallites were precipitated on the surface of the sol-gel derived ZnO film on FTO during HWT, and the shape of the precipitates was changed to hexagonal columns when an electric field was applied during HWT. The EF-HWT of ZnO gel films on Si wafers influenced the morphology and orientation of the ZnO crystals formed; flower-like hexagonal ZnO crystals were obtained with the degree of branching increased with higher applied voltage during HWT.

The effect of cerium doping into ZnO nanostructured films and its photoluminescence properties by HWT of sol-gel derived coating was also investigated. The formation of crystallized Ce-doped thin film and nanostructures by annealing at 500 and 600°C are commonly reported by many researchers. In this work, thin film of Ce-doped ZnO films were formed by dip-coating of a sol-gel and subsequently hot-water treated without stirring at 60°C for 30 min to induce the crystallization of Ce-doped ZnO film. The undoped and Ce-doped ZnO sol-gel coatings were also annealed at 500°C for 3 h for comparison purposes. The optical properties of these Ce-doped ZnO films can be influenced by the defects induced from the doping as the electronic structure of the host might be changed. The effects of Ce doping on the optical and structural properties of the ZnO nanostructured films formed after hot-water treatment are described in this chapter.

Chapter 4

The study of well-aligned ZnO nanorod arrays formation on sol-gel seeded layer for prolonged hydrothermal exposure time of 4 to 24 h was systematically investigated and described in this chapter. The oriented ZnO nanorod arrays generated on indium-tin oxide (ITO) glass were used as photoanode for dye-sensitized solar cells application. The effect of prolonged hydrothermal growth time on the structural, crystallinity, optical properties, DSSC conversion efficiency and formation mechanism are described in details.

Simultaneous formation of ZnO nanorod arrays and nanosheets composite structures on glass substrates by hydrothermal process is also described in this chapter. The formation of these nanostructures was explored, focusing on the effect of development time for both nanosheets and nanorods. The ZnO nanorod arrays and nanosheets structure obtained were single crystalline and polycrystalline, respectively, and were obtained without any post-annealing treatment. The crystal structures, optical properties, growth mechanism and the photocatalytic activities of the composite films obtained are also reported in details.

Chapter 5

In this chapter, general conclusions are drawn for the studies and investigations performed in this thesis.

References

- [1] S. J. Chen, Y. C. Liu, Y. M. Lu, J. Y. Zhang, D.Z. Shen, X.W. Fan, *J. Cryst. Growth* 289(2006) 55-58.
- [2] R. Wahab, S. G. Ansari, Y. S. Kim, H. K. Seo, G. S. Kim, G. Khang, H. S. Shin, *Mater. Res. Bull.* 42 (2007) 1640-1648.
- [3] Z. Y. Fan, J. G. Lu, *J. Nanosci. Nanotechnol.* 5 (2005) 1561-1568.
- [4] A. B. Djurisic, A. M. C. Ng, X. Y. Chen, *Prog. Quant. Electron.* 34 (2010) 191-259.
- [5] Y.W. Heo, D. P. Norton, L. C. Tien, Y. Kwon, B.S. Kang, F.-Ren, S. J. Pearton, J. R. LaRoche, *Mat. Sci. Eng.* 47 (2004) 1-47.
- [6] O. Lupan, V. M. Guerin, I. M. Tiginyanu, V.V. Ursaki, L. Chow, H. Heinrich, T. Paupote, *J. Photochem. Photobiol., A* 211(2010) 65-73.

- [7] Z. Lockman, K.A. Razak, T.K. Huat, T.W. Kian, L.C. Li, G. Kawamura, A. Matsuda, *Materialwissenschaft und Werkstofftechnik* 43 (*Materials Science and Engineering Technology*) No.5 (2012) 457-460.
- [8] C. Jagadish, S. Pearton, *Zinc Oxide Bulk, Thin Films and Nanostructures: Processing, Properties and Applications*, Elsevier, Amsterdam, 2006.
- [9] S. S. Kurbanov, H. D. Cho, T. W. Kang, *Opt. Commun.* 284 (2011) 240-244.
- [10] W. K. Tan, K. Abdul Razak, K. Ibrahim, Z. Lockman, *J. Alloys Compd.* 509 (2011) No.24, 6806-6811.
- [11] S. Sakka, *Handbook of Sol-Gel Science and Technology, Processing Characterization and Applications Vol. 3, Applications of Sol-Gel Technology*. Edited by S. Sakka. Kluwer Academic Publisher, Boston, 2005.
- [12] W. K. Tan, K. Abdul Razak, K. Ibrahim, G. Kawamura, J. Hamagami, A. Matsuda, Z. Lockman, *Malaysian Journal of Microscopy* 6 (2010) 58-63.
- [13] A. Matsuda, Y. Kotani, T. Kogure, M. Tatsumisago, T. Minami, *J. Am. Ceram. Soc.*, 83 (2000) 229-231.
- [14] Y. Kotani, A. Matsuda, M. Tatsumisago, T. Minami, T. Kogure, *J. Sol-Gel Sci. Techn.*, 19 (2001) 585-588.
- [15] A. Matsuda, T. Matoda, K. Kogure, K. Tadanaga, T. Minami, M. Tatsumisago, *J. Mater. Res.*, 20 (2005) 256-263.
- [16] N. Prastomo, Y. Daiko, T. Kogure, H. Muto, M. Sakai, A. Matsuda, *Mater. Sci. Eng., B* 161 (2009) 170-174.

- [17] A. Matsuda, K. Kobayashi, T. Kogure, M. Sakai, K. Tadanaga, T. Minami, and M. Tatsumisago, *J. Non-Cryst. Solids* 354 (2008) 1263-1266.
- [18] A. Matsuda, Y. Kotani, T.Kogure, K. Tadanaga, T. Minami, *J. Sol-Gel. Sci. Techn.*, 22 (2001) 41-46.
- [19] C. H. Xu, H. F. Lui, C. Surya (2011) *Mater. Lett.* 65(2011) 27-30.
- [20] W. K. Tan, K. Abdul Razak, K. Ibrahim, Z. Lockman, *J. Alloys Compd.* 509 (2011)No.3, 820-826.
- [21] Z. Lockman, P. F. Yeo, W. K. Tan, K. Ibrahim, K. Abdul Razak, *J. Alloys Compd.* 493 (2010) No.1-2, 699-706.
- [22] M. Guo, P. Diao, S. Cai, *J. Solid State Chem.*, 178 (2005)1864-1873.
- [23] S. W. Chen, J. M. Wu, *Acta Mater.* 59 (2011) 841-847.

Chapter 2

FORMATION OF TWO-DIMENSIONAL ZnO NANOSHEETS BY RAPID THERMAL OXIDATION IN OXYGENATED ENVIRONMENT

2.1 INTRODUCTION

Nano-size functional materials have been the main focus of many researchers in the design and fabrication of nano-systems for nanotechnology which have been widely investigated for various applications [1]. Nanoscopic sciences at atomic level have established a new concept or paradigm for construction of functional materials from nanoscale building units with distinguished and enhanced properties [2]. Controlled synthesis of various nanostructures of materials such as nanotubes, nanoparticles, nanosheets and nanoporous into hierarchical and organized structures termed as ‘materials nanoarchitectonics’ is deemed as a new method to achieve the desired properties of a nano-system [1, 2]. Nanomaterials reviews towards nano-architectonics based on nanospace and nanosystems fabricated by layer-by-layer and mechanical stimuli have also been reported. Zinc oxide (ZnO) which has diverse morphological structures has been view as a potential material for nano-architectonics due to its unique interdependent morphologies and properties. Besides that, ZnO is also a chemically and thermally stable semiconductor with a wide direct band gap (3.37eV) and large excitation binding energy (60 meV) at room temperature [3-6]. ZnO is used in various applications such as luminescence devices, photocatalysts, piezoelectric devices, dye-sensitized solar cells and sensors as it exhibits good stability at elevated temperature and therefore could be applied for processing and applications at high temperature [1, 7-9]. The feasibility of ZnO to be formed into porous structures enable the

generation of large surface area which could improve the efficiency for photocatalytic applications.

Various methods can be used to generate ZnO nanostructures such as sputtering [4], hydrothermal [9], electrochemical methods [10-12] and thermal oxidation [13, 14]. Thermal oxidation is deemed as one of the facile methods being used as it is a simple, inexpensive, and no catalyst is required. During thermal oxidation, the oxide formation involves transportation, diffusion and absorption of oxygen to the surface of metallic zinc. In controlled condition such as controlled partial pressure of oxygen, nanocrystal ZnO thin films can be formed on metallic zinc substrate [8]. Variation in oxygen partial pressure during evaporation of Zn resulted in the formation of Zn microcrystal and nanowires while variation in nitrogen and argon gas flow does not affect the morphology of the crystals formation [3, 15]. Hong *et al.* reported that rapid oxidation of sputtered Zn layer under ambient condition occurred via a different route compared to conventional oxidation of metallic Zn films which enable the fabrication of amorphous transparent oxide thin films from low-melting-point metals [16].

Masuda *et al.* reported the formation of self-assembled ZnO nanosheets from an aqueous solution at 60°C for 6 h and the solution was then allowed to cool for a long period of 42 h [17]. In this work, rapid thermal oxidation of etched Zn foils in excessive oxygen was performed to generate dense and porous ZnO nanosheets for a short period of 10 to 30 min. To the best knowledge of the author, no work has been reported on the formation of ZnO nanosheet by rapid oxidation of Zn in excessive oxygen presence. There are many advantages of forming ZnO nanosheets on Zn foils by thermal oxidation in oxygen environment; such as elimination of contamination compared to chemical approach methods, shorter fabrication time, simple low-cost technique with easy set-up and therefore economical for commercial

mass production. The structural and optical properties of the as-formed ZnO nanosheets were characterized. The photocatalytic properties were also investigated and reported in this work.

2.2 EXPERIMENTAL

Zn foils (Alfa Aesar) that consists of 99.95% purity was used. The Zn foils were cut into the desired dimension of 4 cm x 1 cm. The Zn foils were then ground using SiC paper with ascending grit. After that, the Zn foils are polished using alumina powder 1 μm and 0.05 μm , respectively prior to etching with 3 % HCl in ethanol for 5 min. Etching was done to remove the native oxide on the surface of the Zn foils as well as to expose the grain boundaries. After that, the Zn foils were thermally oxidized at elevated temperatures of 300°C and 400°C for 10, 20 and 30 min in the oxygenated condition. The flow of oxygen gas was allowed to stabilize and homogenize for 1 h at the desired temperatures before inserting the etched Zn foils into the heated tube furnace. After thermal oxidation, the Zn foil was removed from the furnace and cooled to room temperature in air. The experimental set up for the oxidation in oxygen is schematically illustrated as in Fig.1

The morphologies of the samples were characterized using a Field Emission Scanning Electron Microscope (FE-SEM, Zeiss Supra 55 VP PGT/HKL FESEM) and high-resolution transmission electron microscope observation was done using JEOL, JEM-2100F at an acceleration voltage of 200 kV. The crystal structure of the ZnO nanosheets was investigated using X-ray diffractometer (XRD, Bruker AXS D8 Advance with $\text{CuK}\alpha$ radiation and $\lambda = 1.5406 \text{ \AA}$). Photoluminescence (PL) was performed using a He-Cd laser with a wavelength of 325 nm, and Raman spectroscopy measurements were performed using a Raman laser spectrometer (Jasco NSR-3100) with a laser wavelength of 532 nm. Photocatalytic activity of the samples was also investigated by measuring the degradation of methyl orange (MO). The

oxidized sample was inserted into a quartz glass photo-reactor containing 15 ml 30 ppm MO and being photo-irradiated at room temperature using TUV 18WUVC germicidal light ($\lambda = 250$ nm). The concentration of degraded MO was measured using a Varian Cary 50 UV-Visible spectrophotometer.

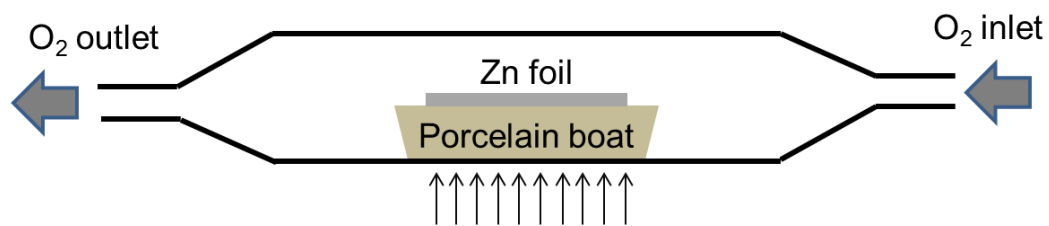


Fig. 1: Experimental schematic of etched Zn foils thermal oxidation in oxygen.

2.3 RESULTS AND DISCUSSION

2.3.1 Structural and morphological properties

Prior to thermal oxidation in oxygen, the surface morphologies of the Zn foils before and after etching are shown in Fig. 2 (a) and (b), respectively. The grain boundaries on the surface of the Zn foils are revealed and can be observed clearly after etching process. This would provide an easy diffusion path for Zn ions to diffuse from the substrate to the surface during oxidation [18]. From the higher magnification images shown in the inset of Fig. 2, the surface morphologies of the etched Zn foils appear to be rougher with ridge-like appearance compared to unetch Zn foils. The morphologies of the ZnO nanosheets formed after thermal oxidized in oxygen for 10 min, 20 min and 30 min for 300°C and 400°C were shown in Fig. 3 and Fig. 4, respectively. Images shown on the left hand column marked with an 'i' are the low magnification images and on the right hand column marked with an 'ii' are the higher magnification images of the sample. The surface morphology of the sample thermally oxidized at 300°C for 10 min consisted of porous-like and flaky nanosheets. The thickness of the porous nanosheets formed is approximately 32 nm with the size of the ridge-like particle at approximately 18 nm. The nanosheets appear to be consisted of loosely bound nanoparticles. When the oxidation time was increased to 20 min and 30 min, thicker and denser ZnO nanosheets with rougher surface were formed as shown in Fig. 3 (b) and Fig. 3(c), respectively. The size of the ridge-like structure on the surface of the nanosheets increased to approximately 36 nm and 40 nm while the average thickness of the nanosheets are approximately 128 nm and 80 nm after oxidized for 20 and 30 min, respectively. The surfaces of the nanosheets appear to be coarse and size of the ridge-like appearance on the surface increased with longer oxidation time.

At 400°C, thick and dense ZnO nanosheets with rough surface are observed after oxidized for only 10 min as shown in Fig. 4 (a). The average thickness of the nanosheets formed is approximately 88 nm with size of ridge-like structure at 90 nm as observed from the surface of the nanosheets. As for the samples oxidized for longer period of 20 and 30 min, the size of the ridge on the surface of the nanosheets increased. The average thickness of the nanosheets formed also increased with oxidation time to approximately 104 nm to 144 nm after oxidized for 20 and 30 min while the size of the ridge on the nanosheets surface increased to 94 nm and 118 nm, respectively. The thickness of the ZnO nanosheets layers obtained is determined from the cross-sectional SEM shown in Fig. 5. When oxidized at 300°C for 10 to 30 min, the thickness of the ZnO nanosheets generated increased from approximately 1.3 μm to 1.5 μm . Upon oxidation at 400°C for 10 and 30 min, the thickness of the ZnO nanosheets obtained was 4 μm and 6 μm , respectively. ZnO nanorods were not observed compared to the previous reported work where ZnO nanorods were formed after thermal oxidation at 400°C for 30 min in ambient air [13].

To have a further insight of the ZnO nanosheets crystallinity, the sample thermal oxidized at 400°C for 10 min was viewed using HR-TEM as shown in Fig. 6. Low-magnification image of a ZnO nanosheet shown in Fig. 6 (a) resemble the ZnO nanosheets observed in the SEM image of Fig. 4 (a)(ii) which possess a hexagonal structure with diameter of approximately 1 μm . High resolution TEM shown in Fig. 6 (b) and (c) show the inter-planar spacing of about 0.28 nm is observed, which indicates good ZnO wurtzite crystal structure formation. From HR-TEM observation, it can be observed that the ZnO nanosheets were consisted of smaller grains forming the hexagonal sheet-like structure [18].

Compared to our previous work, the presence of excess oxygen inhibited the growth dendritic ZnO nanorods while ZnO nanosheets with rough ridge-like surfaces were formed. With large areas of exposed polar basal planes of the nanosheets and the high roughness

factor, these ZnO nanosheets could enhance the photocatalytic properties for the decomposition of volatile organic compounds [19]. Table 1 shows the summary of the nanosheet thickness, size of the ridge on the surface of the nanosheets and the photoluminescence of the near-band edge emission obtained from all the samples.

XRD pattern of oxidized samples are shown in Fig. 7. From the XRD patterns, diffraction at (002) ZnO plane is observed at 34.70° (JCPDS 36-1451). This shows the ZnO nanosheets formed at a preferred orientation during the oxide formation. The diffraction pattern from the underlying Zn substrate is also observed. Note that the (002) peak of Zn overlaps with (101) ZnO peak, and therefore the peak at 36.2° could be attributed to both the underlying Zn layer and the ZnO nanosheets.

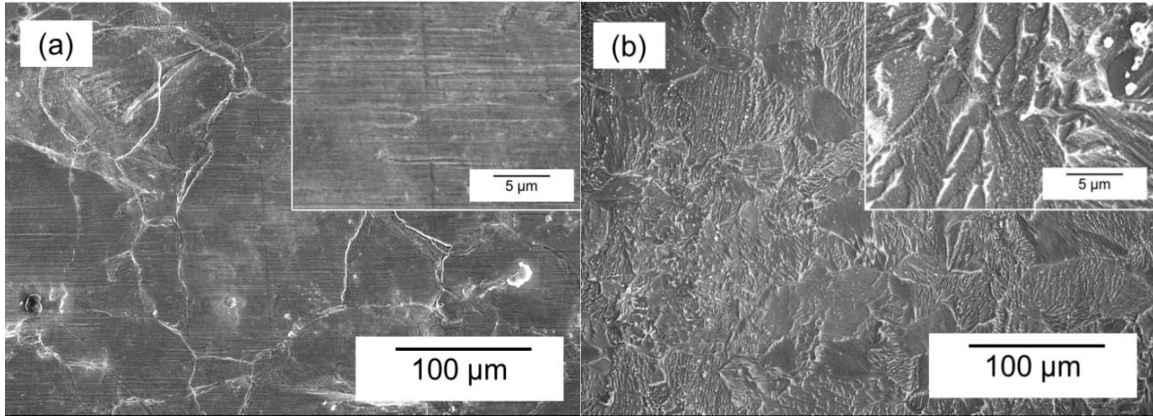


Fig. 2: Low and high (inset) magnification SEM images of the (a) unetch and (b) etched Zn foils.

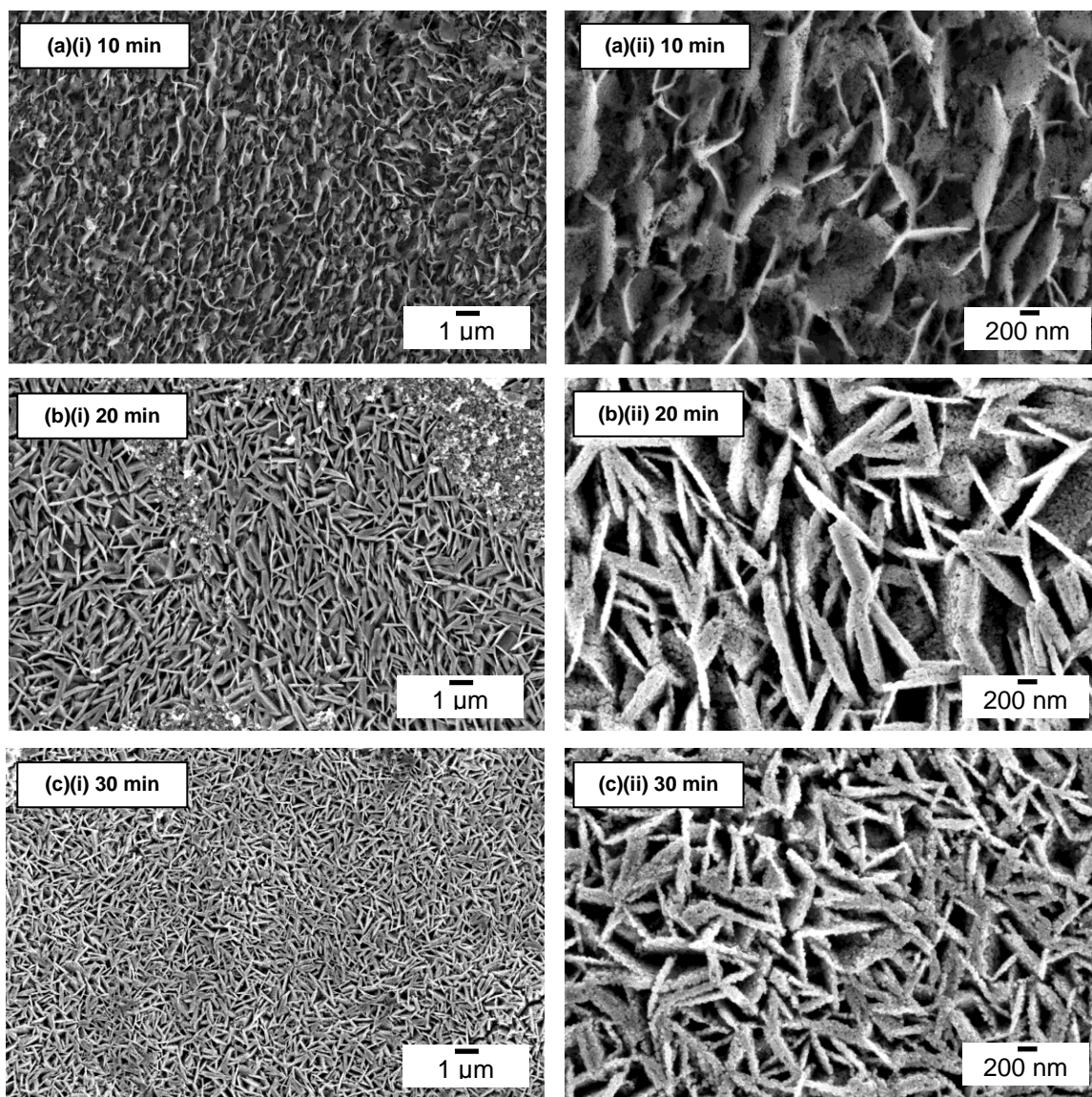


Fig. 3 : Morphologies of the ZnO nanostructures after thermal oxidation in oxygen at 300°C for (a) 10 min, (b) 20 min and (c) 30 min.

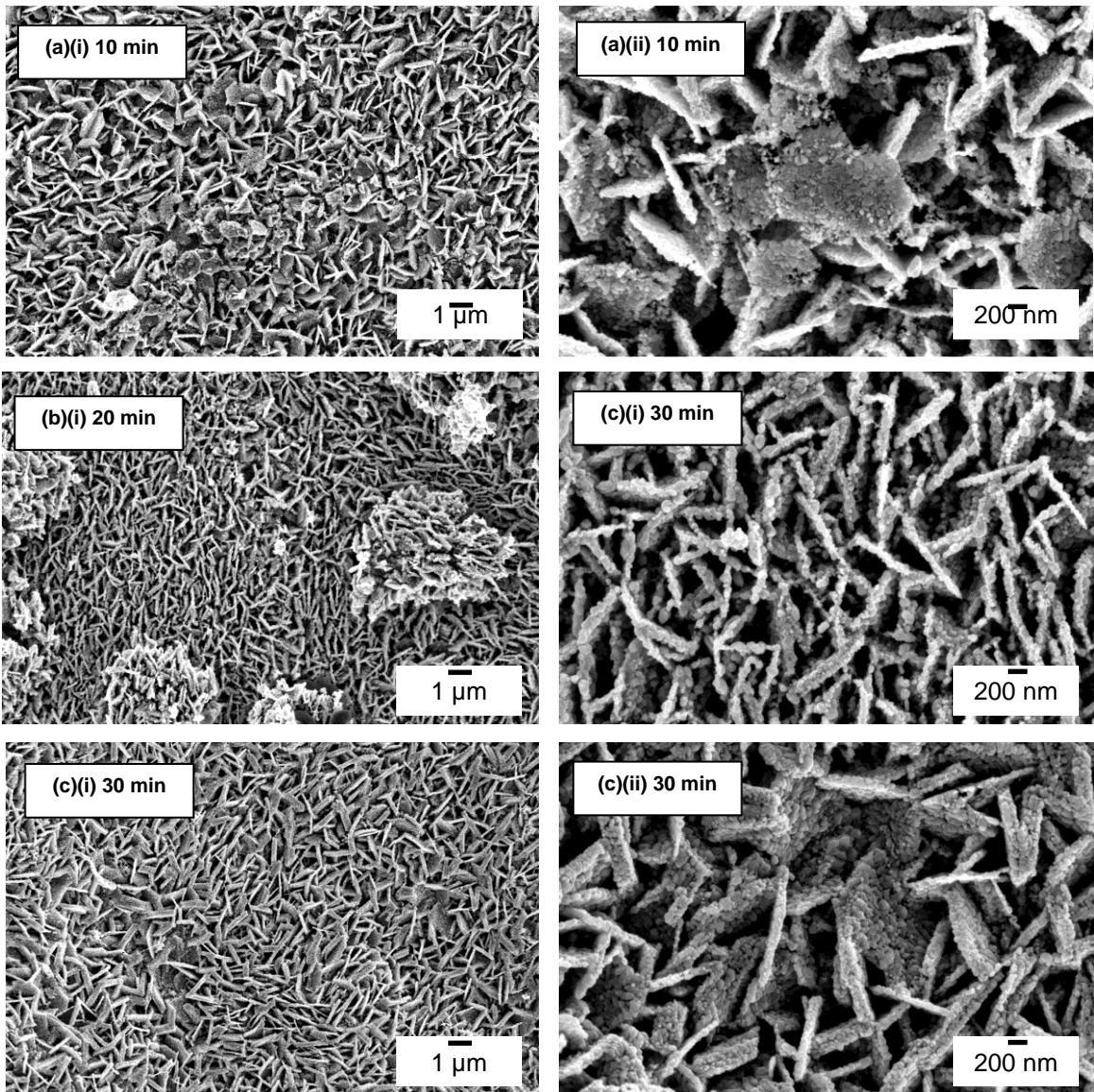


Fig. 4: Morphologies of the ZnO nanostructures after thermal oxidation in oxygen at 400°C for (a) 10 min, (b) 20 min and (c) 30 min.

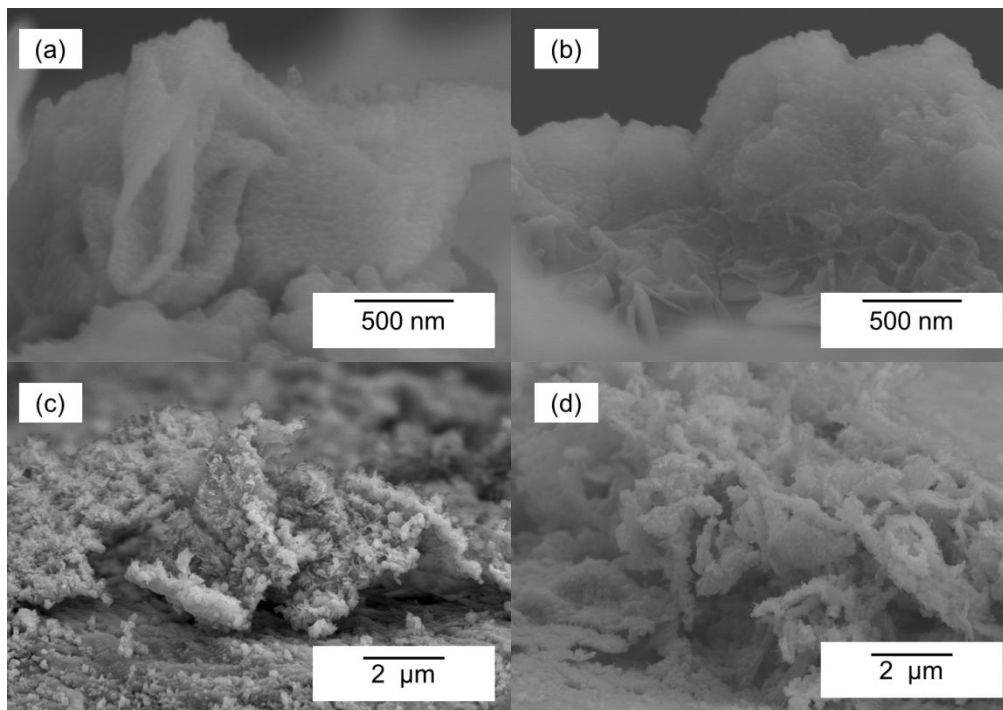


Fig. 5: Cross-sectional SEM images of the ZnO nanosheets after thermal oxidized in oxygen at 300°C for (a) 10 min, (b) 30 min and at 400°C for (c) 10 min and (d) 30 min.

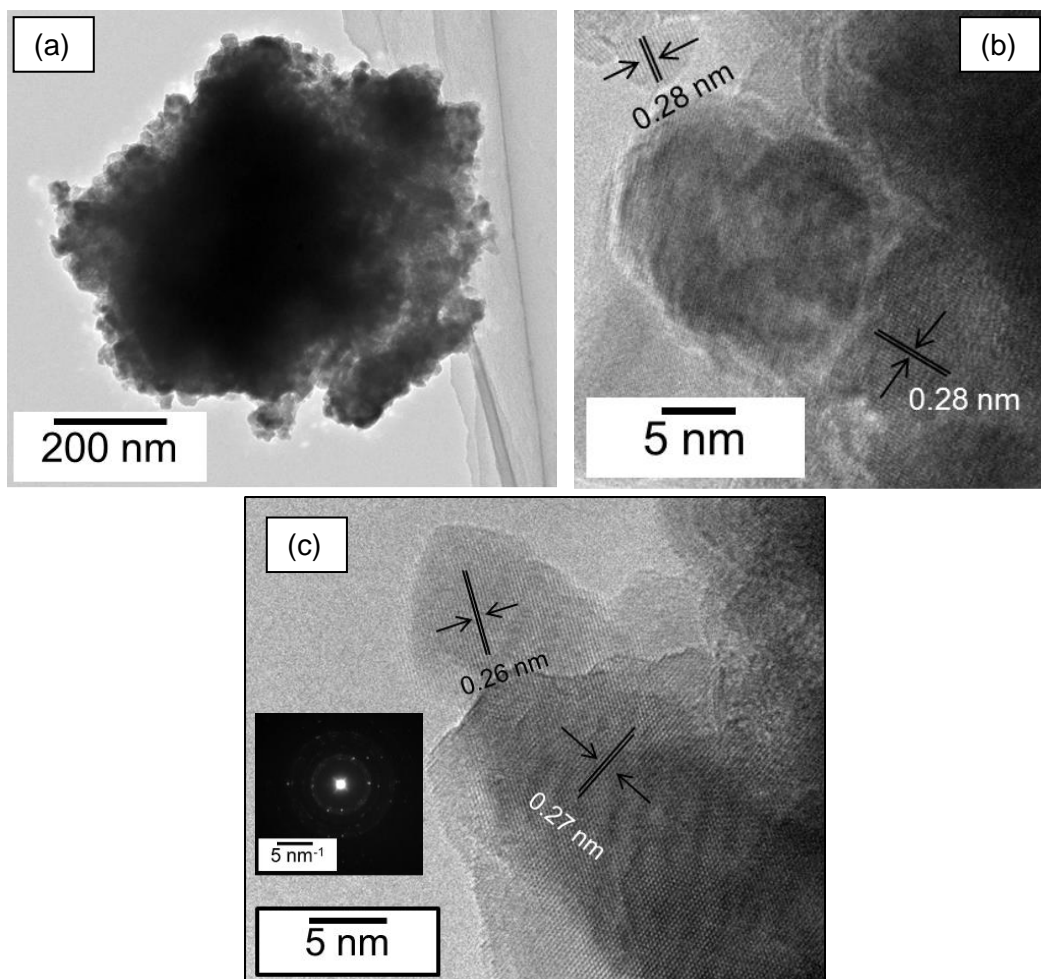


Fig. 6: High-resolution transmission electron microscope images of the ZnO nanosheets obtained after thermally oxidized at 400°C for 10 min in oxygen. (a) Low magnification image while (b) and (c) are the high-resolution images with SAED (inset).

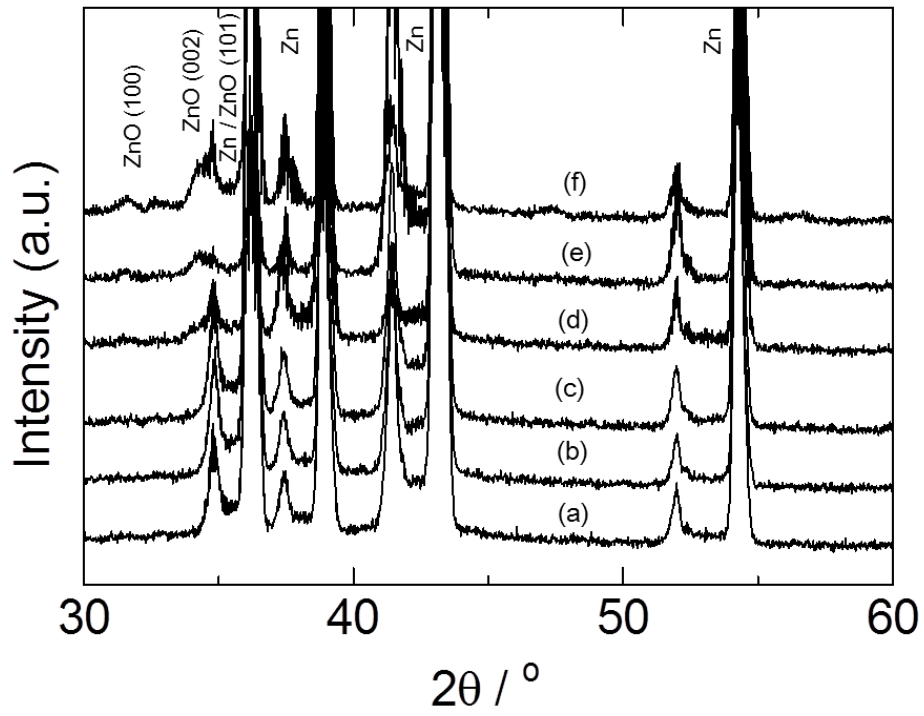


Fig. 7: XRD patterns for the Zn foils oxidized at 300°C for (a) 10 min, (b) 20 min, (c) 30 min and 400°C for (d) 10 min, (e) 20 min and (f) 30 min.

2.3.2 Luminescence properties

The photoluminescence spectra for the oxidized samples in oxygenated condition at 300°C and 400°C for 10 and 30 min is shown in Fig. 8. Inset is the enlarge spectra showing the photoluminescence spectra of the samples oxidized in 300°C which are suppressed by the relatively higher emission intensities of the samples oxidized at 400°C. Three emission peaks are observed at approximately 370 nm, 530 nm and 740 nm. These prominent peaks are attributed to the near-band edge UV emission and visible emissions which show that the ZnO nanosheets obtained possess good crystalline crystals. The peak at approximately 370 nm corresponds to near UV emission from the free exciton emission while visible emission peaks are due to the deep level emission. The deep level emission at the green and red region (visible) can be attributed to defects in the crystal structure such as O-vacancy, Zn-vacancy, O-interstitial, Zn-interstitial and substitution [3, 19]. The aspect ratio of UV emission to visible emission increased significantly for the samples oxidized at 400°C compared those oxidized at 300°C. The higher aspect ratio obtained demonstrates the formation of higher crystalline ZnO structures [15]. Blue-shift (~ 9 nm) of the near band edge emissions observed from approximately 374 nm to 365 nm with higher annealing temperature from 300°C to 400°C is also reported by other researchers [16]. The sharp and strong UV emissions with suppressed green emission indicate better crystalline quality with less structural defects [20]. This results show that rapid thermal oxidation in oxygenated condition can improve the quality of the ZnO crystals.

Raman spectra of the samples oxidized at 400°C for 10 and 30 min are shown in Fig. 9. No apparent band was observed for the samples oxidized at 300°C (not shown). The band at 439 cm^{-1} corresponds to the E_2 non-polar phonon of the hexagonal wurtzite phase is observed for the samples oxidized at 400°C. This confirms the good crystallinity of the ZnO nanosheets formed at 400°C. The Raman results are in agreement with the

photoluminescence results obtained as the relative PL intensity of the samples obtained after oxidized at 400°C are higher (almost 30 times) than the samples oxidized at 300°C. Broad peak at 561 cm^{-1} can be attributed to the E_1 (LO) mode of ZnO [21]. This mode could be caused by the defects of oxygen vacancy and Zn interstitial as Raman shift may vary with formation of excess Zn in the ZnO film [22].

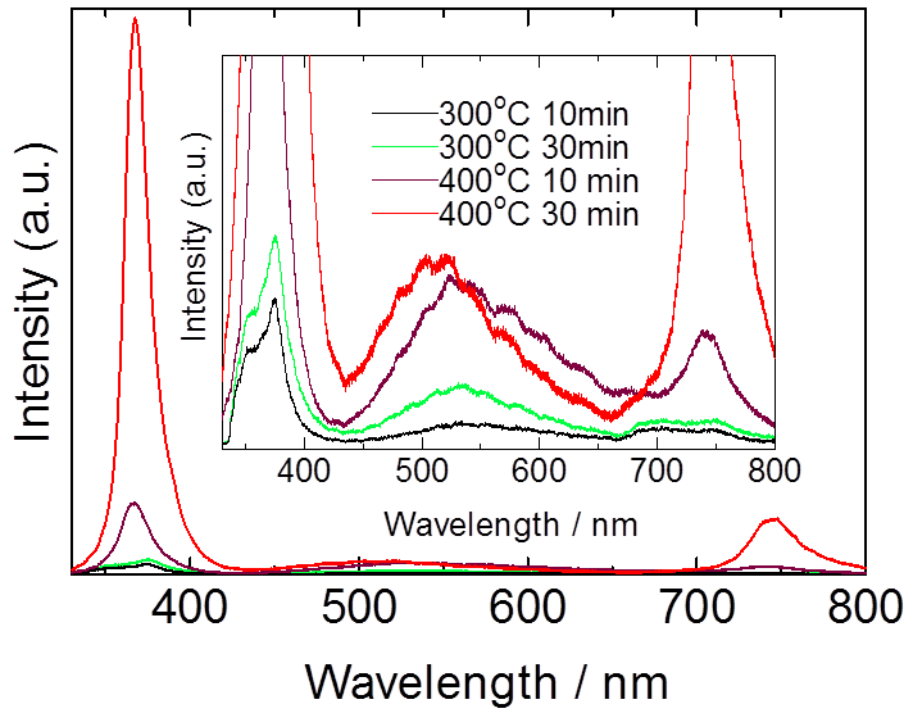


Fig. 8: Photoluminescence (PL) spectra for the samples oxidized in oxygenated environment at 300°C and 400°C for 10 and 30 min, with the magnified spectra (inset).

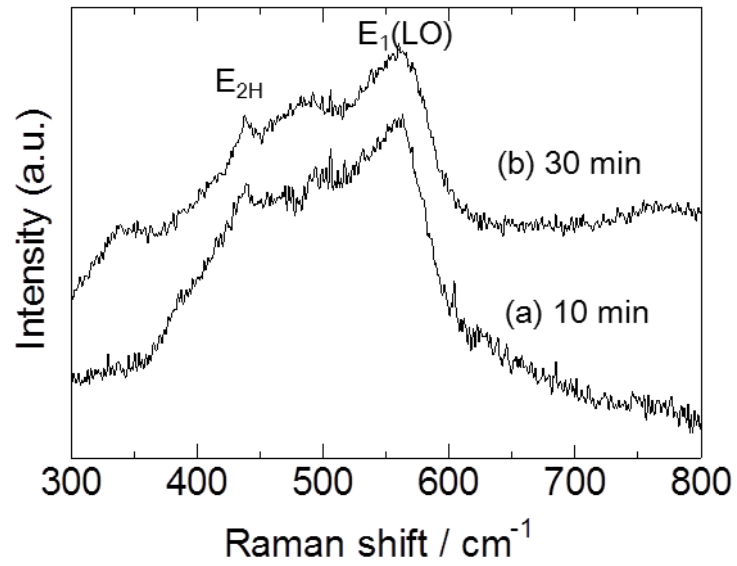


Fig. 9: Raman spectra of the Zn foils oxidized in the oxygenated condition at 400°C for (a) 10 min and (b) 30 min.

2.3.3 Photocatalytic properties

In order to investigate the photocatalytic properties of the nanosheets, methy orange (MO) has been used as the photocatalytic degradation dye. Fig. 10 shows the degradation rate of MO up to 5 h with UV-irradiation. The results show that all the samples exhibit photocatalytic behavior as the MO degraded with time. After 4 h of photo irradiation, almost 80 % of MO was degraded. Sample oxidized at 400°C for 10 min demonstrated slightly higher photocatalytic activity as it was the fastest to degrade 50 % of MO among all the samples after 2 h of photo irradiation. After 3 h, the degradation difference between all the samples began to reduce and the concentration of MO remaining in the solution was approximately 20 %. After 5 h, the photocatalytic activities reached a saturation point with approximately 5% of residual MO still remained in the solution. The photocatalytic activity of the ZnO nanosheets is compared to the commercially available P25 TiO₂ degradation of MO under UV irradiation reported by Zhan *et al.* [23]. It can be seen that the degradation of MO using TiO₂ P25 is approximately 80 % after 1 h of exposure whereby the degradation of ZnO nanosheets formed after oxidized at 400°C for 10 min is 35 %. This shows that the ZnO nanosheets obtained after rapid oxidation in oxygen for a short period exhibit good photocatalytic properties.

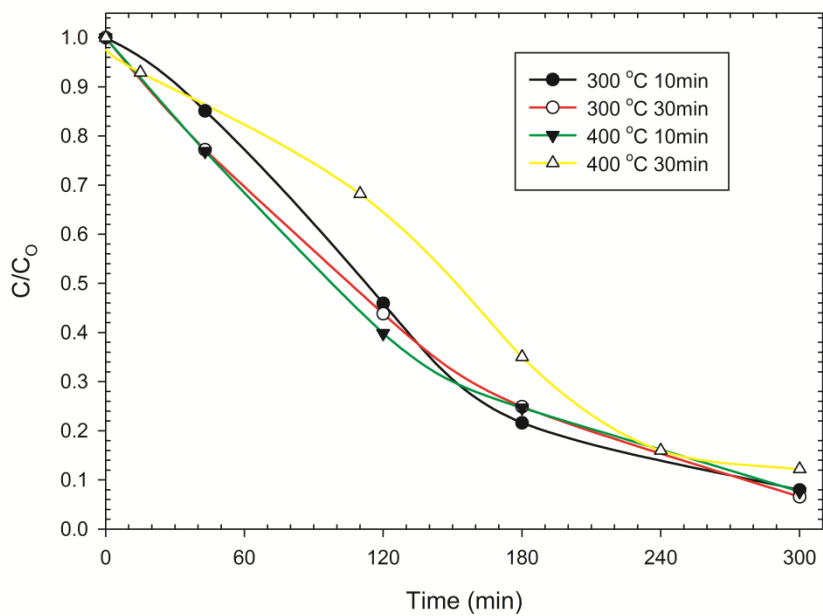


Fig. 10: Photocatalytic activity of as formed ZnO nanosheets after thermal oxidized in oxygen for 10 min and 30 min at 300°C and 400°C by degradation of methyl orange under UV-irradiation.

2.3.4 Formation mechanism of ZnO nanosheets

Thermal oxidation process involves transportation, diffusion and absorption of oxygen to the surface of the zinc substrate [8, 24]. The formation mechanism of the ZnO nanosheets by thermal oxidation in oxygen is illustrated in Fig. 11. Etching of Zn foil prior to oxidation would reveal the grain boundaries on the surface of the foil as shown in Fig. 11 (b). During rapid oxidation, the temperature was rapidly elevated from room temperature to the 300°C and 400°C in a short time. The rapid oxidation would result in the formation of nanosize metallic Zn vapor aero-sphere [3]. At the initial stage, the activation energy barrier is low as the interaction between the metal and the oxide layer is weak during the sublimation of Zn [16]. Subsequently, Zn ions would diffuse along the grain boundaries to grow preferentially at sites of the revealed grains (Fig. 11 (c)). As the melting point of Zn is 419°C, fast temperature elevation during rapid oxidation at 300°C and 400°C is believed to be adequate for the sublimation of Zn to occur and create a Zn vapor aero-sphere at the vicinity of the surface as shown in Fig. 11 (d) [13, 25]. The sublimed metallic Zn will then react with the oxygen to form the ZnO nuclei which then grow upon reaching supersaturation and agglomerate into larger particles before re-deposited onto the surface in the preferred hexagonal sheet-like structure of ZnO as shown in Fig. 11 (e). This can be seen from the images of the nanosheets formed after oxidized at 300°C for 10 min in Fig. 2(a), loosely bound ZnO particles forming sheet-like structure can be observed. At higher oxidation temperature of 400°C, the degree of sublimation is much greater as it is near the melting point of Zn (419°C), therefore the similar process took place at higher rate forming denser and ridge-like ZnO nanosheets as shown in Fig. 11 (f). Besides Zn sublimation, it is believed that oxidation of Zn on the surface would occur concurrently and could act as the seed layer for the subsequent re-deposition and growth of ZnO from the vapor source. As the oxidation duration increased from 10 min to 30 min, the intensity of the UV emission increased

dramatically. This is due to the improved crystals quality resulted from the restructuring of the ZnO nanosheet films. The excess Zn in the ZnO film will react with the oxygen to form improved stoichiometric ZnO structure that could reduce the non-radiative defects. However, the sample oxidized at 400°C for 10 min exhibit slightly better photocatalytic activity during the degradation of MO. This could be due the larger surface area of the sample as it has smaller particle size and higher surface area among all the samples oxidized at 400°C. Although the samples oxidized at 300°C possess even smaller particle size and thickness compared to those oxidized at 400°C, the photocatalytic activities were lower as oxidation at 300°C is believed to be insufficient to completely oxidize the Zn to form ZnO as reported by Zhang *et al.* [26].

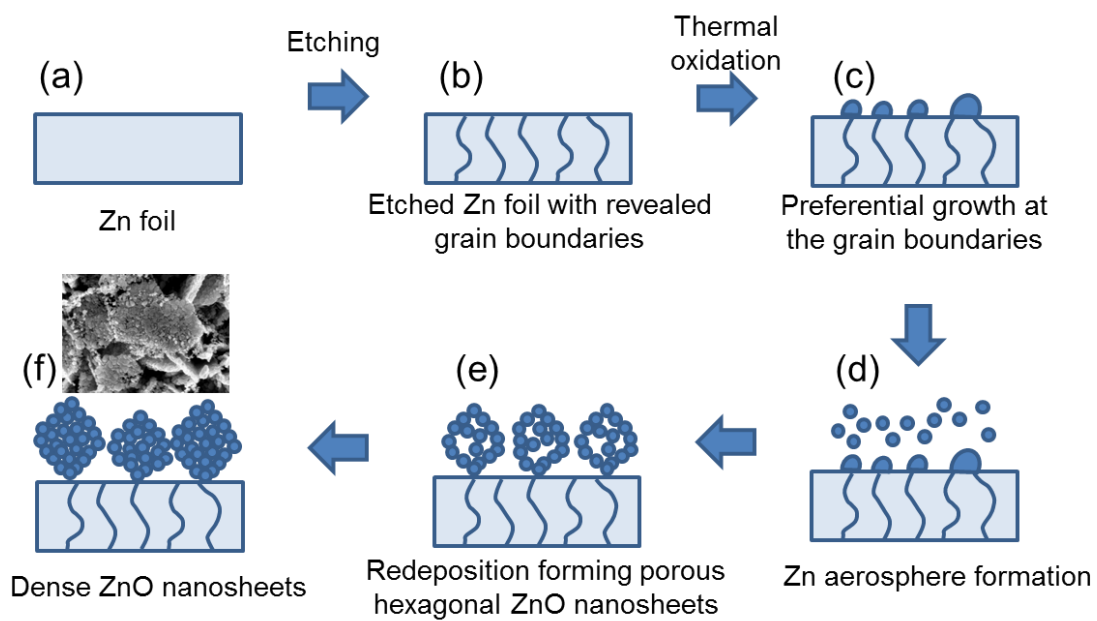


Fig. 11: Schematic of the ZnO nanosheets formation mechanism by rapid thermal oxidation with oxygen flow.

2.4 CONCLUSION

Crystalline 2D ZnO nanosheets films were formed by rapid thermal oxidation in oxygenated environment for short period of 10, 20 and 30 min. Photoluminescence of the thermally oxidized samples showed near band-edge UV and visible emission demonstrating good crystalline ZnO structure which was confirmed by HR-TEM and Raman scattering. All the ZnO nanosheets formed demonstrated photocatalytic activity by degradation of MO. Sample formed after thermally oxidized at 400°C for 10 min demonstrated slightly higher rate of MO degradation after 2 h of photo-irradiation. Approximately 90 % of MO degradation was observed all the samples after 5 h.

REFERENCES

- [1] K. Ariga, T. Mori, and J. P. Hill, *Adv. Mater.* 24, 158 (2012).
- [2] K. Ariga, Q. Ji, J. P. Hill, Y. Bando, and M. Aono, *NPG Asia Mater.* 4, e17 (2012).
- [3] Z.Y. Fan, J.G. Lu, *J. Nanosci. Nanotechnol.* 5, 1561 (2005).
- [4] C. Jagadish, S. Pearton, in *Zinc Oxide Bulk, Thin Films and Nanostructure Processing, Properties and Applications*, First ed., Elsevier (2006).
- [5] S. Xu and Z.L. Wang, *Nano Res.* 11, 1013 (2011).
- [6] O. Lupan and T. Pauporte, *J. Cryst. Growth*, 312, 2454 (2010).
- [7] M. Guo, P. Diao, X. Wang and S. Cai, *J. Solid State Chem.* 178, 3210 (2005).
- [8] W. Gao, Z.W. Li, R. Harikisun, and S.S. Chang, *Mater. Lett.* 57, 1435 (2003).

- [9] Z. Lockman, P.F. Yeo, W.K. Tan, K. Ibrahim, and K.A. Razak, *J. Alloys Compd.* 493, 699 (2010).
- [10] S.J. Lim, S. Kwon, and H. Kim, *Thin Solid Films*, 516, 1523 (2008).
- [11] S. Sreekantan, L.R. Gee, and Z. Lockman, *J. Alloys Compd.* 476, 513 (2009).
- [12] A.I. Inamdar, S.H. Mujawar, V. Ganesan, and P.S. Patil, *Nanotechnology*, 19, 325706 (2008) 325706.
- [13] W.K. Tan, K. Abdul Razak, K. Ibrahim and Z. Lockman, *J. Alloys Compd.* 509, 6806 (2011).
- [14] C.H. Xu, H.F. Lui, and C. Surya, *Mater. Lett.* 65, 27 (2011).
- [15] D. Yuvaraj, K. n. Rao, and K.K. Nanda, *J. Cryst. Growth* 311, 4329 (2009) 4329-4333.
- [16] R. Hong, L. Xu, H. Wen, J. Chen, J. Liao, and W. You, *Opt. Mater.* 34, 786 (2012).
- [17] Y. Masuda and K. Kato, *Cryst. Growth Des.* 8, 275 (2008).
- [18] W.K. Tan, K. Abdul Razak, K. Ibrahim and Z. Lockman, *J. Alloys Compd.* 509, 820 (2011).
- [19] Z.R.R. Tian, J.A. Voigt, J. Liu, B. McKenzie, M.J. McDermott, M.A. Rodriguez, H. Konishi, and H.F. Xu, *Nat. Mater.* 2, 821 (2003).
- [20] W. Bai, X. Zhu, Z. Zhu, and J. Chu, *Appl. Surf. Sci.* 6483 (2008).
- [21] W.K. Tan, K. Abdul Razak, Z. Lockman, G. Kawamura, H. Muto, A. Matsuda, *Mater. Lett.* 91, 111 (2013).
- [22] G.J Exarhos, and S.K Sharma, *Thin Solid films* 270, 27 (1995).

- [23] C. Zhan, F. Chen, H. Dai, J. Yang, M. Zhong, *Chem. Eng. J.* 225, 695 (2013).
- [24] M. Girtan, G.G. Rusu, S.S. Dabos, and M. Rusu, *Appl. Surf. Sci.* 254, 4179 (2008).
- [25] Y. Gui, C. Xie, Q. Zhang, M. Hu, J. Yu, and Z. Weng, *J. Cryst. Growth* 289,663 (2006).
- [26] D. Zhang, C. Wang, Y. Liu, Q. Shi, and W. Wang, *Opt. Laser Technol.* 44, 1136 (2012).

Chapter 3 FORMATION OF ZnO NANOSTRUCTURES VIA HOT-WATER TREATMENT

3. 1 HOT WATER TREATMENT OF METALLIC Zn FOILS

3.1.1 INTRODUCTION

The properties of ZnO nanostructures are highly dependent on their morphology [1]; therefore, controlling the dimensions of ZnO nanostructures has been the focus of many researchers, who have employed both physical and chemical methods. ZnO is an excellent material for ultraviolet (UV) laser applications due to its strong excitonic binding energy (~60meV) at room temperature [2], which enables intense UV luminescence to be obtained owing to the recombination of radiative excitons [3]. The high efficiency of the luminescent also enables the possibility to obtain laser effect with intensive optical pumping [4]. Furthermore, facile methods such as thermal oxidation of either metallic Zn foil [5] or Zn-coating on glass [6], silica [7] and sapphire [8] have been reported. In previous work, the evolution of the formation of ZnO nanostructures as a function of time and temperature during thermal oxidation was investigated [9]. Randomly oriented ZnO nanorods were formed upon oxidation beyond 400°C. Thermal oxidation of metallic Zn film is considered to be a simple and cost-effective method to form ZnO nanostructures on a large surface area. However, the crystallization temperature of Zn to form ZnO is about 300°C, which is relatively high considering the melting point of Zn is 419°C [6]. If crystalline ZnO nanostructures could be formed at lower temperatures, device fabrication on substrates with limited thermal stability, such as organic and polymeric materials, would become feasible. Xu *et al.* reported on the dry and wet oxidation of thermally evaporated Zn films on glass at 390°C and investigated the effects of water vapor and oxygen on the growth of ZnO nanostructures [10]. Chen et al. reported the formation of ZnO nanostructures using a wet-

oxidation process and demonstrated that water vapor plays an important role on the initial and final dimension of the ZnO nanostructures formation [3]. Matsuda *et al.* demonstrated the effect of hot-water treatment at a relatively low temperature of 90°C on the crystallization and formation of anatase nanocrystals on sol-gel derived SiO₂-TiO₂ coatings [11]. Niki *et al.* further investigated the formation and stabilization of crystalline sol-gel derived ZrO₂ by hot-water treatment under basic conditions [12]. Recently, Noothongkaew *et al.* reported that thermal oxidation of polycrystalline Zn foils at 90°C in ultra-high vacuum showed higher oxidation rates during the second stage of oxidation, compared with the rates obtained for samples oxidized at 25, 50 or 70°C [13].

Therefore, it is interesting to investigate the effect of surface oxidation of metallic Zn foils using hot-water treatment. To the best of the authors' knowledge, no recent work has been reported on this method of surface oxidation of Zn foils. In the present work, etched and unetched Zn foils were hot-water treated at 90°C for durations from 4 to 24 h. The optical properties of the ZnO nanostructures formed were investigated, and a plausible mechanism for formation of ZnO nanostructures proposed.

3.1.2 EXPERIMENTAL

The Zn (99.95%, Nilaco) foils used were 0.5 mm thick and were cut into 2×2 cm specimens. Prior to hot-water treatment, the Zn foils were ultrasonically cleaned using acetone for 5 min. They were then ground using ascending grit sizes SiC paper, polished with alumina powder and cleaned with acetone in an ultrasonic bath. Etching of Zn foils was performed using 5 % HCl in ethanol for 3 min. The etched and unetched Zn foils were then hot-water treated at 90°C for 4, 8, 12 or 24 h using deionized water obtained from water distillation apparatus (Advantec RFD 230NA) without stirring and dried at room temperature prior to characterization. The morphologies of the ZnO nanostructures formed were examined

using a field emission scanning electron microscope (Hitachi S-4800). X-ray diffraction (XRD) patterns of the ZnO layer were obtained using a high-voltage X-ray diffractometer (Rigaku RINT 2500) with CuK α radiation. Photoluminescence (PL) studies were performed using the monochromatic beam generated from a He-Cd laser at a wavelength of 325 nm and recorded using a monochromator (Nikon G250, Japan). Raman spectroscopy of the ZnO layers was performed at a laser wavelength of 532 nm, using a JASCO NSR-3100 Raman laser spectrometer. High-resolution transmission electron microscope observation was done using JEOL, JEM-2100F at an acceleration voltage of 200 kV to view the crystalline structure of the nanostructures formed.

3.1.3 RESULTS AND DISCUSSION OF HOT-WATER TREATED ETCHED Zn FOILS

3.1.3.1 Morphological observation

The surface morphologies and cross-sectional views of the etched Zn foils after hot-water treatment at 90°C for 4, 8, 12 or 24 h are shown in Fig. 1. The SEM images labelled (i) are observations of the surface morphologies, with higher magnification insets; cross-sectional views are labelled (ii). As shown in Fig. 1(a) (i), the average diameter of the ZnO nanowires generated after 4 h of hot water treatment was approximately 20 nm. A longer hot-water treatment time of 8 h resulted in the formation of flat-topped hexagonal ZnO nanorods, as demonstrated in Fig. 1(b) (i). The average diameter of the hexagonal ZnO nanorods increased to about 100 nm. The hexagonal morphology of the nanorods became less distinct upon longer hot-water treatment exposures of 12 h and 24 h as shown in Fig. 1(c) (i) and Fig. 1(d) (i), respectively. Tapered ZnO nanorods were observed after 12 h of hot-water treatment. Coarse surfaces were observed on the ZnO nanorods after a prolonged hot-water treatment time of 24 h; this may be as a result of dissolution of ZnO to form Zn²⁺ ions, followed by

subsequent re-deposition of Zn^{2+} ions as ZnO. The cross-sectional observation shows that the average length of the ZnO nanowire formed after hot-water treatment for 4 h was about 750 nm (Fig. 1(a) (ii)). The length of the nanorods increased to about 1 μm after 8 h of hot-water treatment (Fig. 1(b) (ii)). However, after 12 or 24 h of hot-water treatment, the average length of the nanorods reduced to about 800 nm. The reduction in the length of the ZnO nanorods was due to dissolution of the ZnO upon prolonged exposure to hot water. As seen in Fig. 1(d) (ii), the surface of the as-formed ZnO nanorods becomes rough and uneven after hot-water treatment for 24 h, because of the massive dissolution and re-deposition of ZnO. Coalescence of neighboring nanorods due to Ostwald ripening [14] could also be observed as highlighted in the inset of Fig.1 (d) (ii).

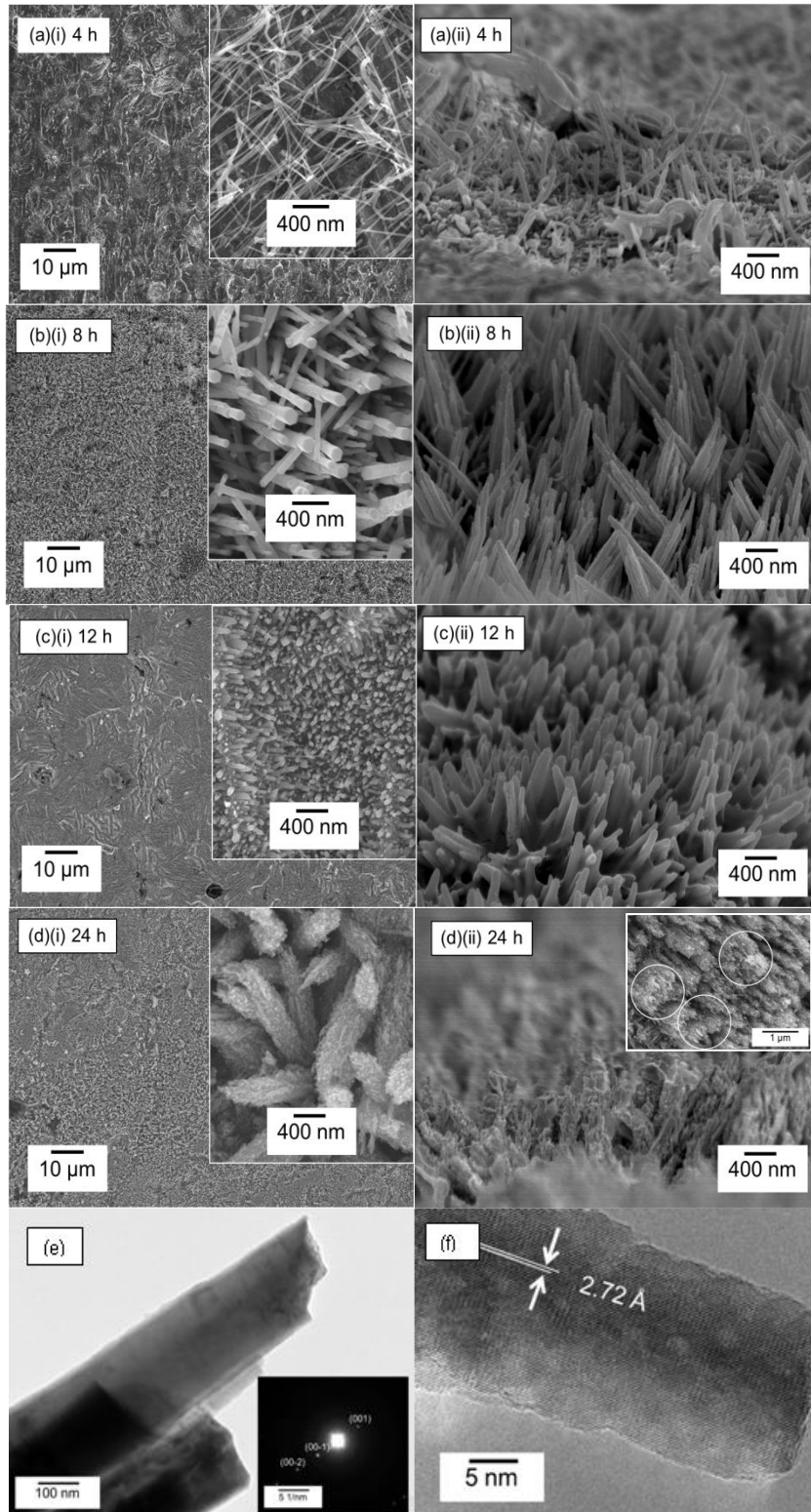


Fig. 1: SEM images of the etched Zn foils hot-water treated at 90°C for (a) 4 h, (b) 8 h, (c) 12 h and (d) 24 h. Images labelled with (i) and (ii) are the surfaces observed at higher magnification (inset) and cross-sectional views of the ZnO nanostructures, respectively. HR-TEM images of the nanorods formed after hot-water treatment for 8 h are shown in (e) low-magnification TEM image with selected area electron diffraction (SAED) (inset) and (f) high-resolution TEM image.

3.1.3.2 XRD

The XRD patterns for the Zn foils after hot-water treatment at 90°C for 4, 8, 12 and 24 h are shown in Fig. 2. Peaks are observed at 31.6, 34.4 and 36.2°, corresponding to the (100), (002), and (101) planes of ZnO (ICDD no: 00-035-1451). The peaks from the underlying metallic Zn substrate can also be observed at 36.2, 38.9 and 43.2° which correspond to the (002), (100), and (101) planes of Zn (ICDD no: 00-004-0831). Note that the (002) peak of Zn overlaps with the (101) ZnO peak, and, therefore, the peak at 36.2° could be attributed to both the underlying Zn layer and the ZnO nanostructures formed on the surface. The presence of the (002) ZnO peak in the XRD patterns shows that the ZnO nanostructures are preferentially orientated along the c-axis, which is consistent with the SEM images in Fig. 1.

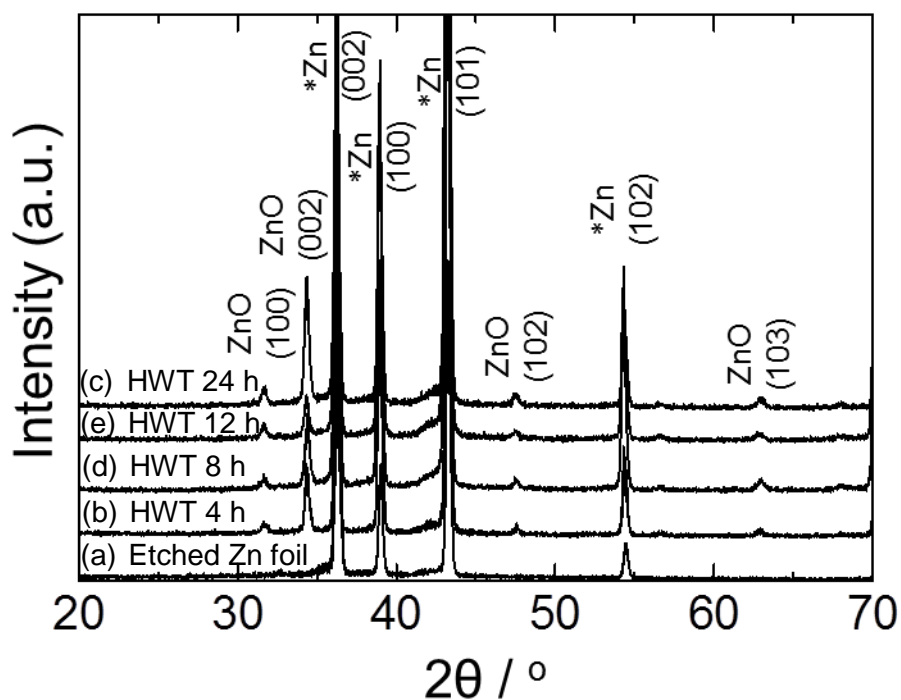


Fig. 2: XRD patterns of the etched Zn foils hot-water treated at 90°C for (a) 4 h, (b) 8 h, (c) 12 h and (d) 24 h.

3.1.3.3 Optical properties

Fig. 3 shows the room temperature PL spectra of the ZnO nanostructures formed on the Zn foils after hot-water treatment. All samples exhibit a UV emission at approximately 375 nm. However, the intensities of the UV emissions from specimens hot-water treated for 8, 12 or 24 h are relatively higher than that of the specimen which was hot-water treated for 4 h. The PL emission for the specimen hot-water treated for 4 h is shown in the inset of Fig. 3. The UV emissions obtained are attributed to the band to band emission of free excitons, and indicate the good crystallinity of the ZnO nanostructures obtained using hot-water treatment [15-17]. To demonstrate that the nanorods formed were indeed ZnO single crystals, HR-TEM images were obtained for a sample hot-water treated at 90°C for 8 h, and are shown in Fig. 1(e) and (f). The clear lattice fringes spaced at 0.272 nm confirm that the ZnO nanorods are single crystal ZnO with a hexagonal wurtzite structure. In addition, the selected area electron diffraction (SAED) pattern (inset) in Fig. 1(e) confirms the crystallinity of the nanorod [18].

Green photoluminescence peaks (wavelength 580–590 nm) were observed for the specimens hot-water treated for 4 h or 8 h. These peaks were attributed to the existence of oxygen vacancies because of deep-level or trap state emission [10, 15, 19]. A blue shift was observed after hot-water treatment for 12 h (the peak in the visible region shifted to approximately 520 nm compared with about 580 nm for the sample hot-water treated for 4 h). However, no emission peak within the green region was observed after hot-water treatment for 24 h. This may be because the crystal structure rearrangement during dissolution and recrystallization of the ZnO surface reduced the amount of oxygen vacancies available to contribute to the deep-level green emission [20].

Fig. 4 shows the Raman spectra for all the hot-water treated Zn foil specimens. The symmetry of the Raman active zone-center optical phonons is represented at the point of the Brillouin zone as follows:

$$\Gamma_{\text{opt}} = A_1 + 2B_1 + E_1 + 2E_2.$$

For all samples, the peak at 438 cm^{-1} that corresponds to the high- E_2 mode of the non-polar optical phonons can be attributed to the hexagonal wurtzite phase; this is further evidence that the ZnO nanostructures formed have good crystallinity [20, 21]. Furthermore, a broad peak at 561 cm^{-1} can be observed, which corresponds to the E_1 (LO) mode of ZnO, associated with oxygen deficiency [1]. The intensity of this peak decreased with increasing hot-water treatment time, indicating that oxygen deficiency was reduced at longer treatment times. The stronger E_2 mode and weaker E_1 (LO) phonon imply improved crystallinity structure in the hot-water treated samples. The Raman results were consistent with the PL results; both sets of results imply fewer internal defects in the ZnO nanostructures as the treatment time is increased [18].

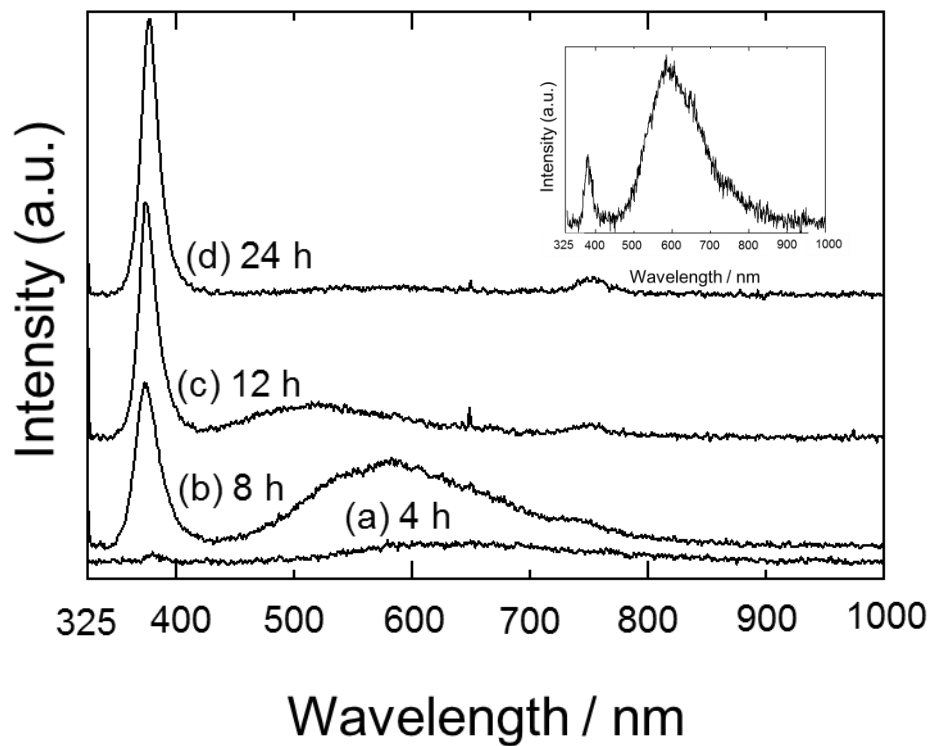


Fig. 3: Photoluminescence spectra of etched Zn foils hot-water treated at 90°C for (a) 4 h, (b) 8 h, (c) 12 h and (d) 24 h. Inset: Photoluminescence spectrum of the ZnO nanowires formed after hot-water treatment at 90°C for 4 h.

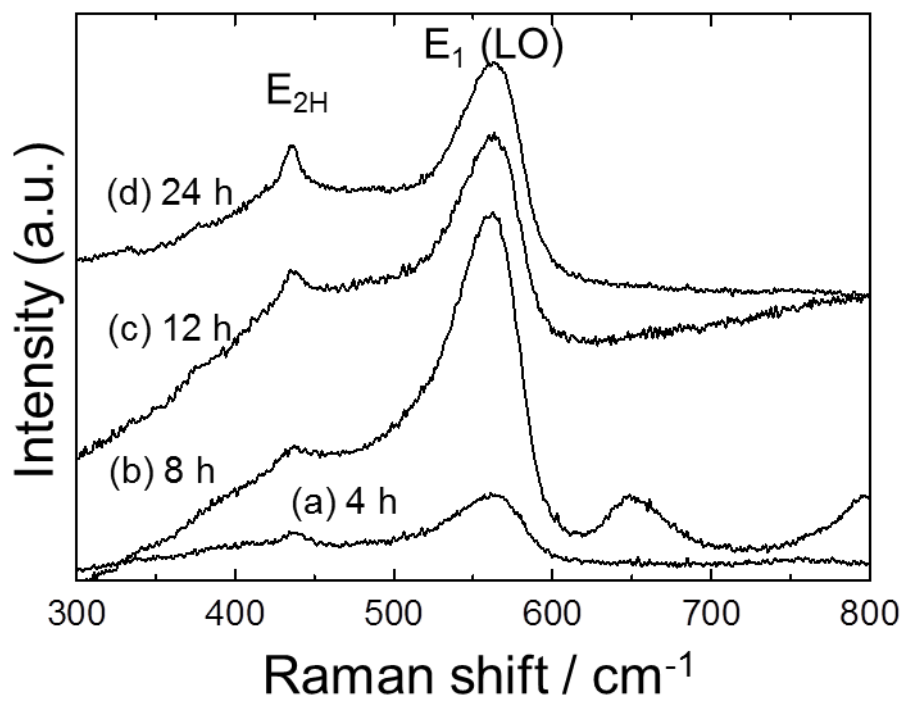


Fig. 4: Raman spectra of the ZnO nanostructures formed after hot-water treatment at 90°C for (a) 4 h, (b) 8 h, (c) 12 h and (d) 24 h.

3.1.4 RESULTS AND DISCUSSION OF HOT-WATER TREATED UNETCHED Zn FOILS

3.1.4.1 Morphological observation of ZnO nanosheets

The surface morphologies of unetched Zn foils after hot-water treatment at 90°C for 4, 8, 12 or 24 h are shown in Fig. 5. The SEM images labelled with (i) and (ii) are the surface morphologies observed at low and high magnifications, respectively. The corresponding cross sectional SEM images of the ZnO nanosheets are shown in the inset of images labelled (ii) in Fig. 5. As shown in Fig. 5(a) (ii), the average diameter and thickness of the ZnO nanosheets generated after 4 h of hot-water treatment are approximately 2 μm and 150 nm, respectively. No significant morphological change of the ZnO nanosheets is observed at prolonged hot-water treatment time of 8 and 12 h. However, after 24 h of hot-water treatment, some of the ZnO nanosheets with increased thickness resulted from the coalescence of neighbouring nanosheets by dissolution of the grain boundaries due to Ostwald ripening could also be observed as highlighted in the inset of Fig.5 (d) (i). From the high magnification images, it can be observed that the nanosheets formed appear to be interconnected, which could be beneficial for optoelectronic applications compared to non-integrated nanosheets [3]. The positions between two adjacent nanosheets or the nanosheets' edges have lower surface energy compare to the energy required to form a new nanostructure. Thus, the continuous growth of the nanosheets edges resulted in the formation of interconnected network of the nanosheets [3]. From the cross sectional SEM images shown in the inset of Fig.5 (ii), the films thickness of the ZnO nanosheets increased from approximately 1 μm to 2 μm after hot-water treated for 4 and 24 h, respectively.

In order to have further insight of the crystallinity of ZnO nanosheets, HR-TEM images were obtained for samples hot-water treated at 90°C for 8 and 24 h as shown in Fig. 6.

The selected area electron diffraction (SAED) patterns (inset) in Figs. 6(a)(ii) and (b)(ii) confirm that good crystallinity of ZnO nanosheets are obtained [21]. At high-resolution images in Figs.6 (a)(ii) and (b)(ii), clear lattice fringes spacing of 0.26 nm confirm that the ZnO nanosheets formed are single crystal ZnO with a hexagonal wurtzite structure [22]. In Fig. 6(b)(ii), a clear hexagonal nanosheet structure with a diameter approximately 25 nm can be observed. It is believed that the ZnO nanosheets were formed by arrangement of the smaller hexagonal ZnO nanosheet units at a preferred orientation forming larger sheet-like structure as observed in Fig. 5. Similar phenomenon of the hexagonal nanosheets formation was observed in our previous work where thermal evaporation of Zn onto polytetrafluoroethylene resulted in the formation of hexagonal ZnO grains that comprised of smaller hexagonal grains [23].

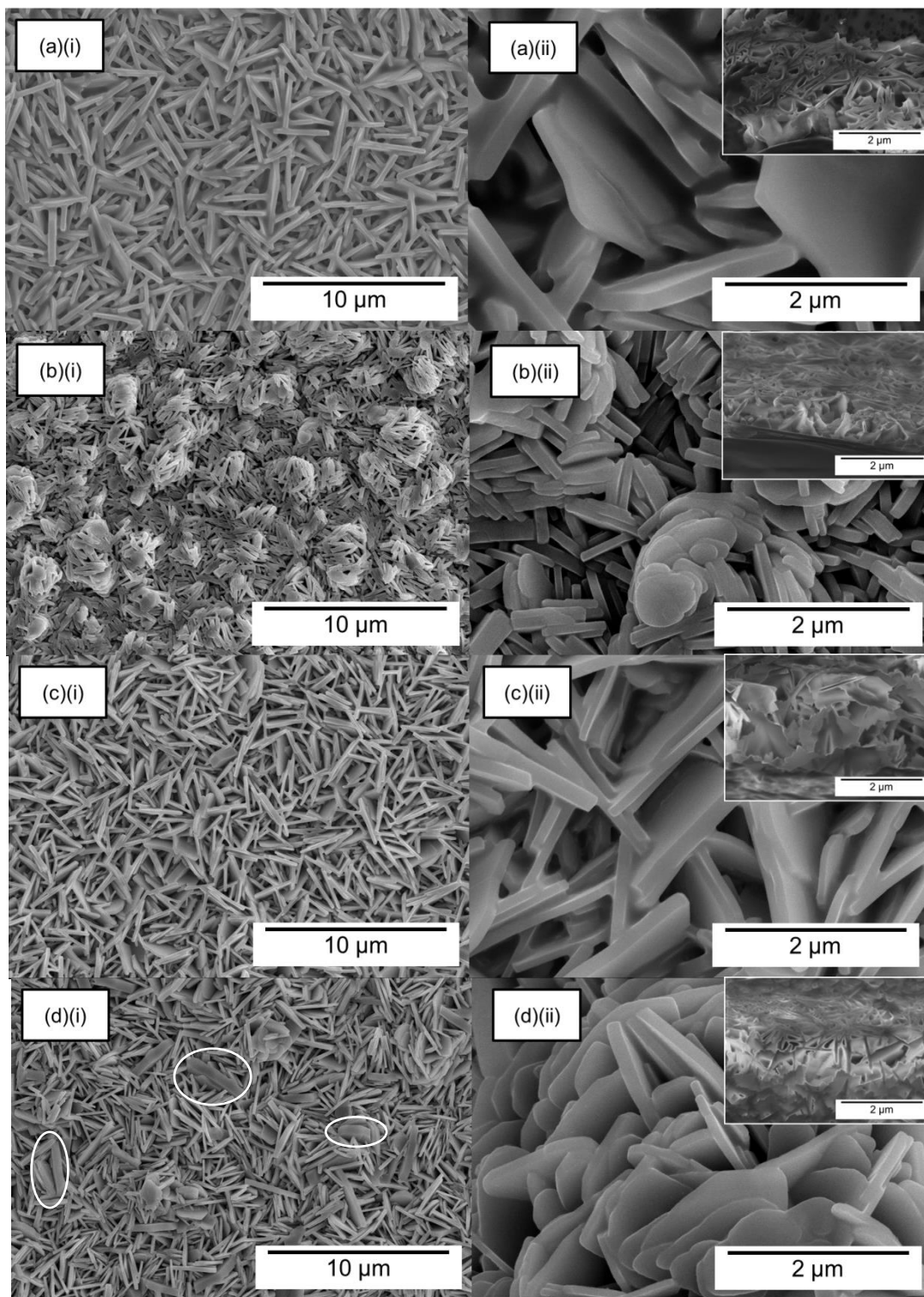


Fig. 5: SEM images of the ZnO nanosheets formed on the Zn foils after hot-water treatment at 90°C for (a) 4 h, (b) 8 h, (c) 12 h and (d) 24 h. Images labelled with (i) and (ii) are the surfaces observed at low and high magnifications, respectively. Cross-sectional SEM images of the ZnO nanosheets are shown as inset in (ii).

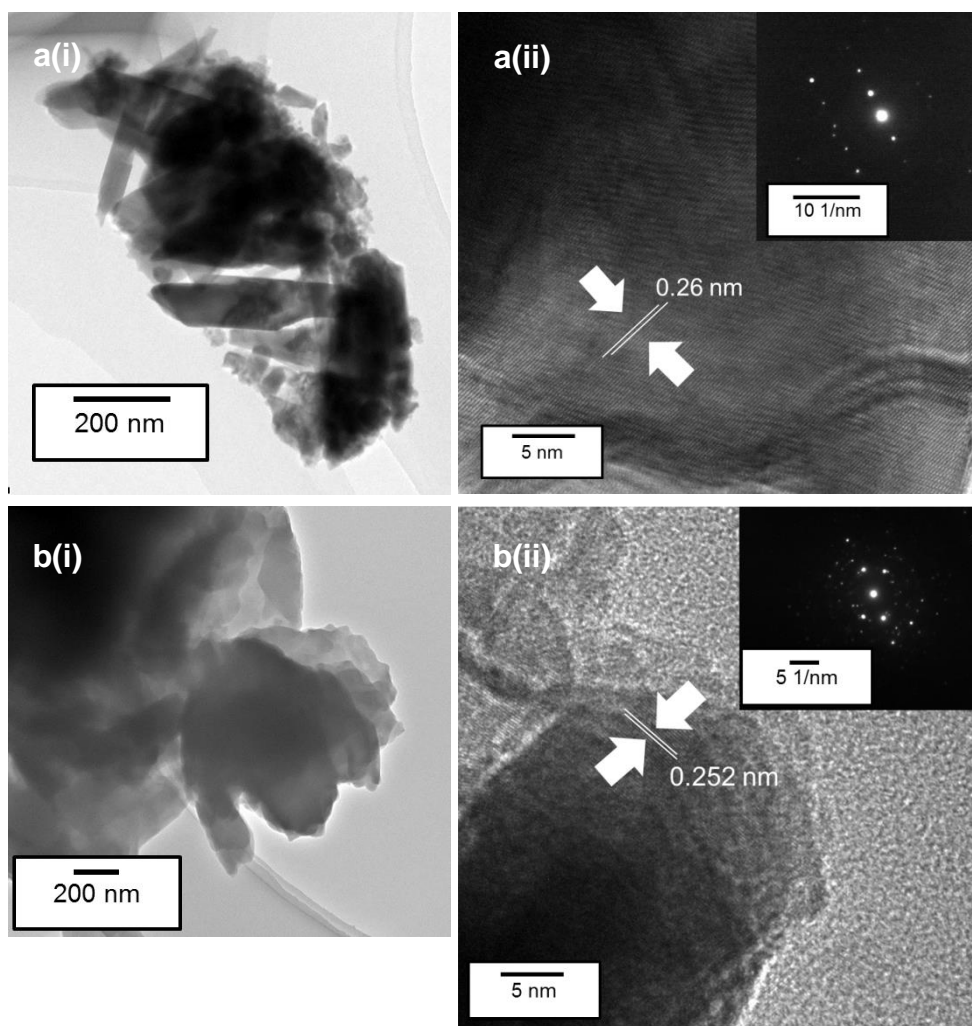


Fig. 6: HR-TEM images of the ZnO nanosheets formed after hot-water treatment for (a) 8 and (b) 24 h. Images labeled (i) and (ii) are the low and high-magnifications with selected area electron diffraction (SAED) (inset).

3.1.4.2 XRD

The XRD patterns for the Zn foils after hot-water treatment at 90°C for 4, 8, 12 and 24 h are shown in Fig. 7. Peaks are observed at 31.6°, 34.4° and 36.2°, corresponding to the (100), (002), and (101) planes of ZnO (ICDD no: 00-035-1451). The peaks from the underlying metallic Zn substrate can be also observed at 36.2°, 38.9° and 43.2° which correspond to the (002), (100), and (101) planes of Zn (ICDD no: 00-004-0831). As the (002) peak of Zn overlaps with the (101) ZnO peak, therefore, the peak at 36.2° could be attributed to both the underlying Zn layer and the ZnO nanostructures formed on the surface. The presence of the (002) ZnO peak in the XRD patterns shows that the ZnO nanosheets are preferentially orientated along the c-axis, which is consistent with the high-resolution HR-TEM images in Figs. 6(a)(ii) and (b)(ii).

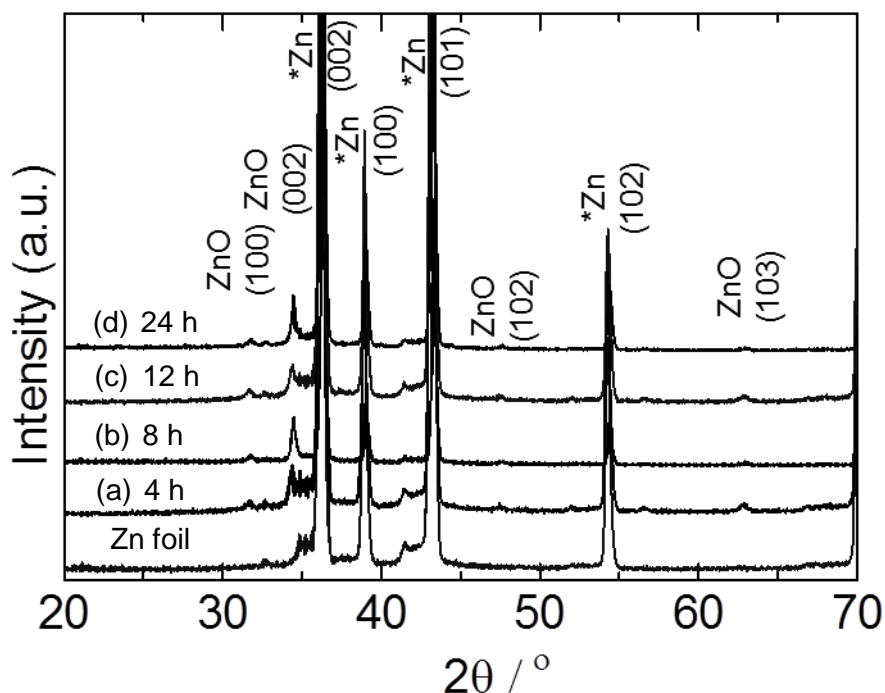


Fig. 7: XRD patterns of the ZnO nanosheets formed on Zn foils after hot-water treated at 90°C for (a) 4 h, (b) 8 h, (c) 12 h and (d) 24 h.

3.1.4.3 Optical properties

Fig. 8 shows the Raman spectra for all the hot-water treated Zn foil specimens. For all samples, the peak at 440 cm^{-1} that corresponds to the high- E_2 mode of the non-polar optical phonons can be attributed to the hexagonal wurtzite phase; this is further evidence that the ZnO nanostructures formed have good crystallinity [18, 24]. Furthermore, a broad peak at 568 cm^{-1} can be observed, which corresponds to the $E_1(\text{LO})$ mode of ZnO, associated with oxygen deficiency [26]. The shifts in the Raman scattering of high E_2 mode observed are due to the stress induced on the surface of the Zn foils after hot-water treatment [24]. With respect to high- E_2 mode of ZnO standard sample at 437 cm^{-1} , upshift of 3 cm^{-1} was observed in the hot-water treated specimens indicating compressive stress on the surface of the films [24, 26]. This could be resulted from the diagonal growth of the nanosheets along the surface of Zn foils generating compressive stress between the nanosheets.

The intensity of $E_1(\text{LO})$ increased with longer hot-water treatment time from 4 to 24 h, the rapid growth of the ZnO prolonged hot-water treatment time could lead to higher oxygen deficiency and Zn interstitials [24]. For the samples hot-water treated for 12 and 24 h, peaks at 335 cm^{-1} and 385 cm^{-1} which can be assigned to the $3E_{2\text{H}}-E_{2\text{L}}$ and $A_1(\text{TO})$ modes of ZnO, respectively, were observed.

Fig. 9 shows the PL spectra at room temperature of the ZnO nanosheets formed on the Zn foils after hot-water treatment. All samples exhibit a UV emission at approximately 378 nm. The UV emissions obtained are attributed to the band to band emission of free excitons, and indicate the good crystallinity of the ZnO nanostructures obtained using hot-water treatment [22].

Green photoluminescence peaks (wavelength 520–550 nm) were also observed for the all the specimens after hot-water treatment. These peaks were attributed to the existence of

oxygen vacancies because of deep-level or trap state emission [25]. The UV to visible ratio of approximately 4:1 indicates good optical properties of the ZnO nanosheets formed at relatively low-temperature of 90°C by wet oxidation of Zn foils by hot-water treatment.

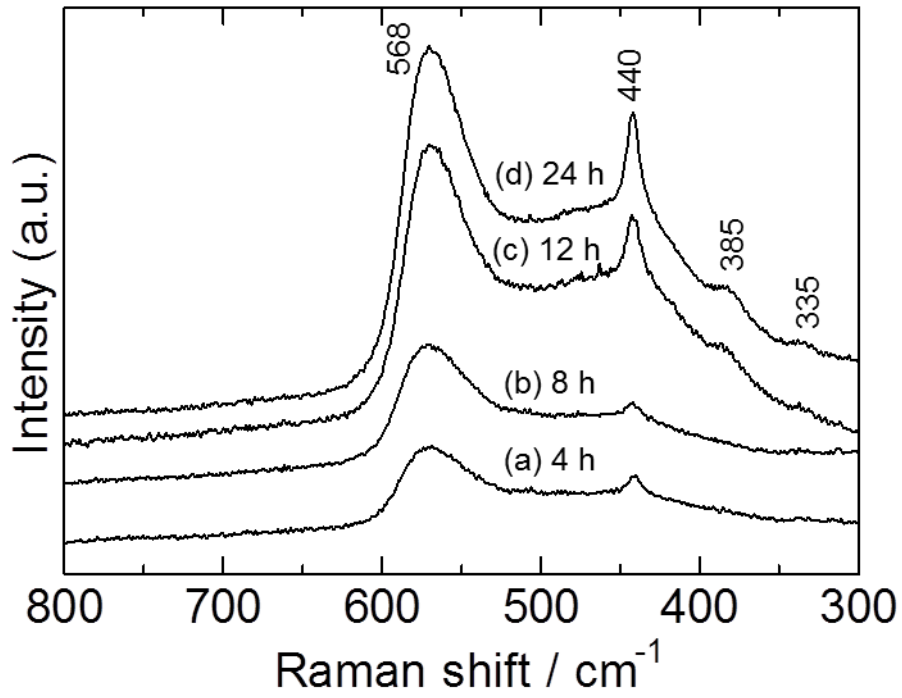


Fig. 8: Raman spectra of the ZnO nanosheets formed after hot-water treatment at 90°C for (a) 4 h, (b) 8 h, (c) 12 h and (d) 24 h.

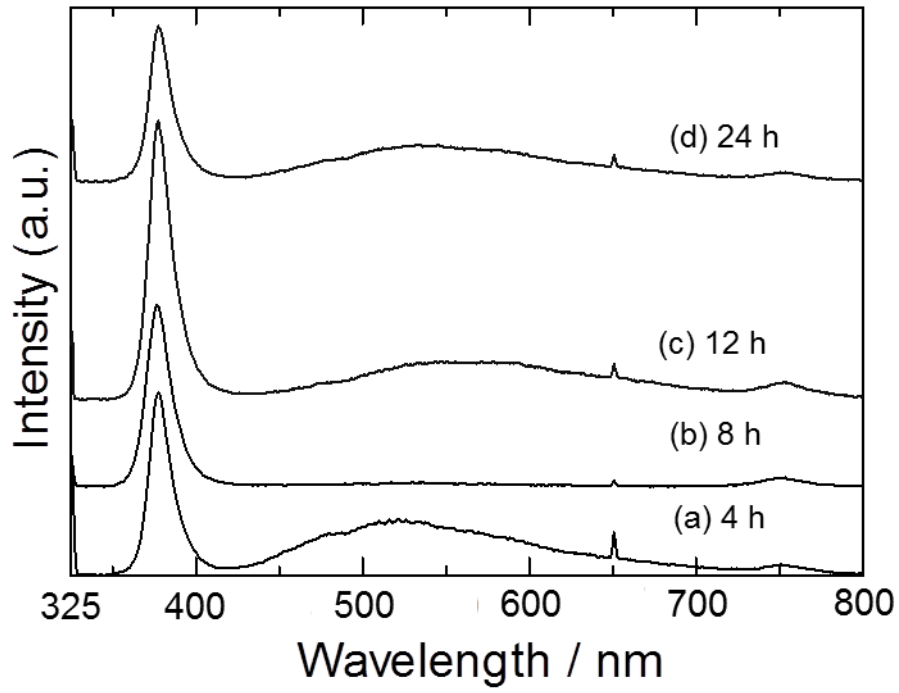


Fig. 9: Photoluminescence spectra of ZnO nanosheets formed on Zn foils after hot-water treatment at 90°C for (a) 4 h, (b) 8 h, (c) 12 h and (d) 24 h.

3.1.5 Formation mechanism of the ZnO nanostructures

Surface oxidation using hot water is a surface diffusion dominant process, which promotes non-planar growth perpendicular to the metallic Zn surface. For wet-oxidation processes, the growth of ZnO nanostructures requires nucleation sites. The etched Zn foils, the edges of the Zn grains acted as the nucleation sites. As water molecules are highly polar, with a negative partial charge on the O side, the water molecules are likely to be attracted by the Zn atoms, and adsorb onto the surface of the foil [3]. The fast adsorption and breakup of the water molecule on the Zn surface will accelerate the kinetics of oxidation to form ZnO nanocrystals that serve as a seed layer. More Zn ions then diffuse to the surface to react with water molecules and form ZnO nanostructures. The ZnO nanocrystals prefer a hexagonal structure. Polar faces with surface dipoles (Zn^{2+} or O^{2-}) are thermodynamically less stable than non-polar faces and tend to minimize their surface energy by undergoing rearrangement [27]. Interestingly, this resulted in the growth of ZnO nanowires and nanorods with an ideal hexagonal ZnO crystal structure. During the initial stage, ZnO nanowire growth occurred due to the diffusion of Zn ions to the tips of the ZnO nanostructures where they reacted with the water molecules to form ZnO crystals. When the ZnO nanowires became too long for diffusion to supply sufficient Zn ions to their tips, the formation mechanism changed. At this stage, the dissolution of ZnO resulted in the formation of hydroxide at the surface of the specimens. When the pH of water was 7 (neutral), $\text{Zn}(\text{OH})^+$ ionic species were formed. This polar hydroxide layer then subsequently dissolved into the hot-water bath as the surface of the oxide continued to be hydrolyzed [28]. After that, the solution near the surface eventually became supersaturated, and the dissolved hydroxide was re-deposited onto the surface, to form ZnO as shown in Equations (1–3). This phenomenon could be observed after a prolonged hot-water treatment time of 24 h when the re-deposition of ZnO onto the surface resulted in coarse nanorod formation.



As for the unetched Zn foils, the growth of ZnO nanosheets requires nucleation sites during the wet-oxidation process. Similarly, water molecules are likely to be attracted by the Zn atoms and adsorb onto the surface of the foil due to the polarity of water molecules [3]. The liquid phase epitaxial growth of the ZnO nanosheets can be divided into 2 stages; (1) the initial stage of ZnO buffer formation and (2) growth of the nanosheets by epitaxial diffusion as reported by Jia *et al.*[29]. No significant morphological change for all the hot-water treated samples from 4 to 24 h is observed due to the lower epitaxial diffusion rate of the Zn ions from the substrate to the surface compared to the higher diffusion of Zn ions along the grain boundaries of etched Zn foils. As there is no easy diffusion channel for the Zn ions for the unetched Zn foils compared to surface of etched Zn foils, the formation mechanism of the ZnO nanosheets is expected to follow epitaxial growth route [29]. The density of the oxide formed is dependent on the hot-water temperature and at 90°C; with higher oxidation rate during the second stage oxidation compared to those oxidized at lower temperatures [13], compact and dense Zn(OH)₂ is formed during the initial stage and finally converted to form ZnO as shown in Equations (1-3) above [30].

3.1.6 CONCLUSION

Crystallized ZnO nanorods and nanosheets were formed on etched and unetched metallic Zn foils, respectively by a hot-water treatment technique at a temperature of 90°C for 4, 8, 12 or 24 h. After 4 h of treatment of etched Zn foils, ZnO nanowires were observed. Furthermore, upon longer treatments, ZnO nanorods were obtained at 8, 12 and 24 h. Only ZnO nanosheets were observed for the hot-water treated of unetched Zn foils. Prolonged hot-water treatment for 24 h resulted in coalescence of some neighboring ZnO nanostructures. The photoluminescence spectra, Raman shifts, HR-TEM observations and SAED results from the ZnO nanostructures demonstrate that the samples possess good crystallinity. The optoelectronic properties of ZnO nanosheets can be exploited in devices that utilize flexible substrates with limited temperature stabilities, such as organic polymeric substrates

REFERENCES

- [1] S.J. Chen, Y.C. Liu, Y.M. Lu, J.Y. Zhang, D.Z. Shen, X.W. Fan, *J. Cryst. Growth* 289 (2006)55-58.
- [2] G. Deng, A. Ding, W. Cheng, Z. Zhen, P. Qiu, *Solid State Commun.* 134 (2005) 283-286.
- [3] R. Chen, C. Zou, X. Yan, A. Alyamani, W. Gao, *Thin Solid Films* 519 (2011) 1837-1844.
- [4] Y. Masuda, N. Kinoshita, K. Koumoto, *Electrochim. Acta* 53 (2007) 171-174
- [5] O. Koshy, M. Abdul Khadar, *J. Appl. Phys.* 109 (2011) 124315.
- [6] D. Zhang, C. Wang, Y. Liu, Q. Shi, W. Wang, *Opt. Laser Technol.* 44 (2012)1136-1140.
- [7] R. Hong, L. Xu, H. Wen, J. Chen, J. Liao, W. You, *Opt. Mater.* 34 (2011)786-789.
- [8] T. W. Kim, T. Kawazoe, S. Yamazaki, J. Lim, T. Yatsui, M. Ohtsu, *Solid State Commun.* 127 (2003)21-24.

- [9] W. K. Tan, K. Abdul Razak, K. Ibrahim, Z. Lockman, *J. Alloy and Compd.* 509 (2011) 6806-6811.
- [10] C.H. Xu, H. F. Lui, C. Surya, *Mater. Lett.* 65 (2011)27-30.
- [11] A. Matsuda, Y. Kotani, T. Kogure, M. Tatsumisago, T. Minami, *J. Am. Ceram. Soc.* 83 (2000) 229-231.
- [12] N. Prastomo, H. Muto, M. Sakai, A. Matsuda, *Mater. Sci. Eng., B* 173(2010) 99-104.
- [13] S. Noothongkaew, H. Nakajima, A.Tong-on, W. Meevasana, P. Songsiriritthigul, *Appl. Surf. Sci.* 258 (2012)1955-1957.
- [14] Z. Lockman, P. F.Yeo, W. K. Tan, K. Ibrahim, K. Abdul Razak, *J. Alloy and Compd.*493 (2010) 699-706.
- [15] M. Qiu, Z. Ye, J. Lu, H. He, J. Huang, L. Zhu, B. Zhao, *Appl. Surf. Sci.* 255 (2009) 3972-3976.
- [16] V. Gupta, P. Bhattacharya, Yuzuk, I. Yu, K. Sreenivas, R. S. Katiyar, *J. Cryst. Growth* 287 (2006)39-43.
- [17] W.I. Park, Y. H. Jun, S. W. Jung, G.-C. Yi, *Appl. Phys. Lett.* 82 (2003) 964-971.
- [18] O. Lupan, V. M. Guerin, I. M. Tiginyanu, V.V. Ursaki, L. Chow, H. Heinrich, T. Pauporte, *J. Photochem. Photobiol., A* 211(2010)65-73.
- [19] L. Z. Pei, H. S. Zhao, W. Tan, H. Y. Yu, Y. W. Chen, Q. F. Zhang, *Mater. Charact.* 60 (2009) 1063-1067.
- [20] O. Lupan, T. Pauporte, *J. Cryst. Growth* 312 (2010) 2454-2458.
- [21] R. Zhang, P. G. Yin, N. Wang, L. Guo, *Solid State Sci.* 11 (2009) 865-869.
- [22] W. K. Tan, K. A. Razak, Z. Lockman, G. Kawamura, H. Muto, A. Matsuda, *Mater. Lett.* 91 (2013) 111-114.
- [23] W. K. Tan, K. A. Razak, K. Ibrahim, Z. Lockman, *J. Alloy and Compd.* 509 (2011) 820-826.

- [24] R. Al Asmar, J. P. Atanas, M. Ajaka, Y. Zaatar, G. Ferblantier, J. L. Sauvajol, J. Jabbour, S. Juillaget, A. Foucaran, *J. Cryst. Growth* 27 (2005) 394-402.
- [25] S. J. Chen, Y. C. Liu, Y. M. Lu, J. Y. Zhang, D. Z. Shen, X. W. Fan XW, *J. Cryst. Growth* 289 (2006) 55-58.
- [26] G. J. Exarhos, S. K. Sharma, *Thin Solid Films* 270 (1995) 27-32.
- [27] A. Umar, A. Al-Hajry, Y. B. Hahn, D. H. Kim, *Electrochim. Acta* 54 (2009) 5358-5362.
- [28] A. Degen, M. Kosec, *J. Eur. Ceram. Soc.* 20: 667-673.
- [29] C. Jia, X. Zhang, Y. Chen, Y. Su, Q. Zhou, M. Xin, Y. Lv, W. Kong, *Appl. Surf. Sci.* 254 (2008) 2331-2335.
- [30] X. G. Zhang, *Corrosion and Electrochemistry of Zinc*, Plenum Press, New York and London, 1996.

3.2 HOT-WATER TREATMENT OF SOL-GEL DERIVED COATINGS

3.2.1 MORPHOLOGY-CONTROL OF CRYSTALLITES PRECIPITATED FROM ZnO GEL FILMS BY APPLYING ELECTRIC FIELD DURING HOT-WATER TREATMENT

3.2.1.1 INTRODUCTION

Zinc oxide nanostructures are used for many applications in semiconductor related fields such as solar cells [1], transparent conductive films, chemical sensors, and light emitting diodes because of its excellent electrical and optical properties [2, 3]. Ultraviolet laser emission using ZnO nanowires at room temperature has also been reported [4]. However, the controlled formation of ZnO nanostructures and dimension using low-temperature techniques has been the main focus of many researchers.

The control on the crystalline phase of ZnO thin film has been the major challenge faced by many researchers. Although controlled morphology using chemical vapor deposition (CVD) method was reported, high reaction temperature is required [5, 6]. Therefore, this method is inapplicable for substrates with low thermal stability. The feasibility of forming ZnO thin films with controlled morphology at low-temperature will not only reduce the production cost but also enable the utilization of substrates with low thermal stability such as organic substrates. Sol-gel method is one of the low-temperature approaches to produce ZnO thin films with large surface coverage [3]. However, heat treatment is usually required to induce the crystallization of the sol-gel coating (~ 300°C) which limits the usage of organic polymer and plastic substrates [7, 8]. On the other hand, the preparation of ZnO thin film can be performed by the liquid phase deposition at a low temperature below 100°C, by controlling the concentration of the additive and pH of the precursor solution. By using the liquid phase deposition method, zinc oxide crystal formations in the form of rods and wires

have been reported [9-12]. However, the low formation rate of the ZnO films varying from few hours to several days has been a major drawback of this technique. In previous work, the formation of ZnO nano and submicron rods by HWT of sol-gel coated layer at 60°C and 90°C for different duration from 30 min to 4 h was reported [13]. To the best of the authors' knowledge, the effect of induced electric field during hot-water treatment on the ZnO sol-gel film has not been reported.

Besides that, granular anatase nanocrystals on sol-gel derived SiO₂-TiO₂ coatings have been successfully formed using hot-water treatment at 90°C [14]. During HWT, special components in the materials dissolve into water and re-precipitation occurs, resulting in the formation of nanocrystals on the surface of the film. These reactions are generally influenced not only by thermodynamic and chemical conditions like temperature, pressure and pH of the solution but also by external stimuli such as vibrations and electric fields. Thus, HWT not only densified and crystallized the sol-gel coatings but also modified the surface morphology of the coatings by applying such external fields [15-17]. With the application of electric field during HWT, the shape of titania changed from round to ramiform precipitates and became more significant with higher applied potential [18].

Therefore, it is interesting to investigate the formation of ZnO nanostructures by using an electric field induced hot-water treatment (EF-HWT). The development of a feasible method to control the morphology of the ZnO crystal deposition at low-temperature with shorter process time by EF-HWT could be a useful technique for the semiconducting processing field. In this work, the control of ZnO crystals precipitates was demonstrated by applying the direct current (D.C.) EF-HWT.

3.2.1.2 EXPERIMENTAL

3.2.1.2.1 Preparation of sol-gel coating

A ZnO sol was prepared from zinc acetate dehydrate (ZnAc) (WAKO, 99%), and diethanolamine (DEA) (WAKO, 99%) using water (H₂O) and 2-propanol (2-PrOH) as the solvent. The molar ratio of ZnAc: DEA: H₂O: 2-PrOH was 1:1:1:20. Fluorine-doped tin oxide (FTO)/glass (Nippon Sheet Glass) and single crystal silicon with (100) orientation wafer (Sumitomo Mitsubishi) substrates (25 mm width, 50 mm height, 1 mm thickness) with sheet resistance of 10 Ωcm were dip-coated at room temperature using the ZnO sol at a down-speed of 5 mm/s, holding for 10 s, and then withdrawing with an up-speed of 0.5 mm/s in dry condition with the relative humidity of 40%. The ZnO-coated substrates were dried at room temperature and then placed in an oven at 90°C for 2 h. The thickness of as-prepared ZnO films was about 200 nm.

3.2.1.2.2 D.C. electric field induced hot-water treatment

The sol-gel coatings on FTO/glass and Si wafer substrates were hot-water treated at 50°C with D.C. electric field application as shown in schematic of Fig.1. The coated substrates were immersed in a Pyrex beaker filled with hot-water at 50°C. The D.C. electric field was supplied using a Nippon Eido type NC-1010 power supply. Deionized water with resistance of 0.06 ~ 0.07 μs used was obtained from water distillation equipment (RFD-230NA, ADVANTEC). A hot plate (RET basic C, IKA) was used to maintain the hot-water temperature and the distance between two substrates (positive and negative electrodes) was 1 cm. No stirring was performed during the HWT and water replenishment was done every 10 min in order to maintain the water volume as a result of water evaporation.

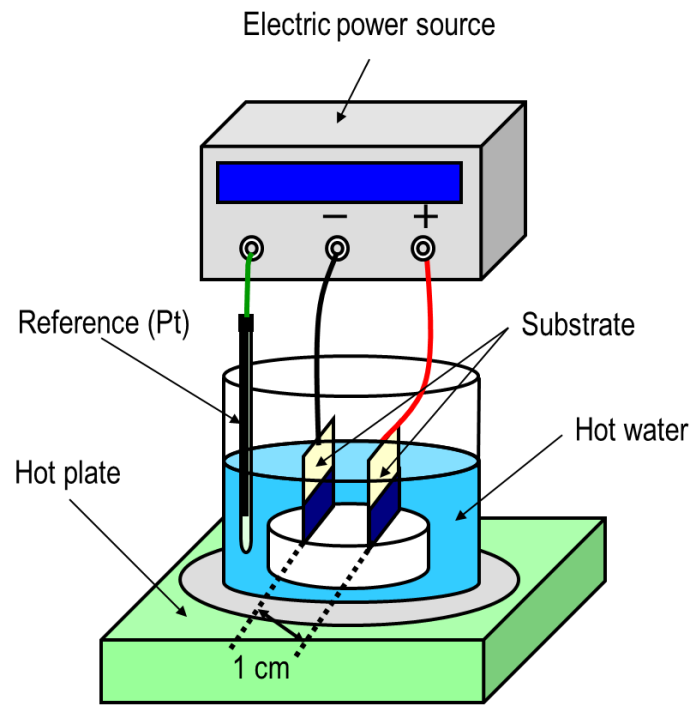


Fig. 1: Schematic of D.C. electric field hot-water treatment of the sol-gel coatings.

3.2.1.2.3 Characterizations

Surface morphologies of the ZnO nanostructures formed on FTO/glass substrates and Si wafers were viewed by using an S-4800 Field Emission Scanning Electron Microscope (Hitachi S-4800). Identification of the crystalline phases precipitated was obtained using an X-ray diffractometer (Rigaku RINT 2000) with $\text{CuK}\alpha$ radiation. UV visible absorption spectra of the samples were measured using UV-Visible spectrophotometer (Japan Spectroscopic V-560) with air set as the reference. Changes in weight of the ZnO film on an Au/quartz electrode during HWT was measured using a Quartz Microbalance (UQ-200, USI).

3.2.1.3 RESULTS AND DISCUSSION

3.2.1.3.1 Effect of electric field hot-water treatment on the morphological structures

The surface morphologies of the electric field hot-water treated ZnO gel films at 50°C for 5 h with an applied voltage of 10V/cm between the substrates are shown in Fig. 2. No precipitate was observed on the surface of the as-prepared sol-gel coating as in shown Fig.2 (a). The HWT of the sol-gel coating without an electric field resulted in the formation of ZnO particulate structure with the diameter of approximately 50 nm as shown in Fig.2 (b). As for the EF-HWT of the sol-gel coatings; on the positive electrode, the coatings dissolved into the hot-water bath and FTO surface was revealed, whereas hexagonal columnar precipitates were observed on the negative electrode as shown in Fig.2 (c) and (d), respectively. The average diameter of the precipitates formed on the negative electrode was approximately 200 nm. The dissolved gel film at the positive electrode was re-deposited onto the surface of the negative electrode during EF-HWT forming the hexagonal columnar ZnO crystals. From this finding, subsequent EF-HWTs were performed on the negative electrode only with bare

FTO/glass substrate on the positive electrode in order to avoid the re-deposition of the dissolve gel film from the positive electrode.

The crystallinity of the ZnO films was confirmed from the X-ray diffraction (XRD). The XRD patterns of the as-prepared, HWT, and EF-HWT ZnO films obtained are shown in Fig. 3. Only peaks from the underlying FTO/glass substrate are seen for the as-prepared ZnO films. Only ZnO peak at 36.2° that corresponds to ZnO (101) is seen for the HWT gel films without electric field. As for the D.C. EF-HWT ZnO films, peaks at 31.6° , 34.4° and 36.2° are observed which correspond to ZnO wurtzite (100), (002) and (101) planes, respectively (JCPDS card 36-1451).

As deionized water was used for HWT, so it is assumed that pH is near neutral (~ 7) and from the pH-potential diagram of Zn-H₂O system [19], dissolution of the ZnO gel film and would form Zn²⁺ and Zn(OH)₂ species. The re-deposition of the particulate ZnO crystal during HWT is believed due to dehydration-condensation process on the surface of Zn(OH)₂ based gel film similar to the HWT mechanism of our previous works [13-16]. Granular ZnO crystal is usually formed during homogeneous nucleation as the growth occurs in all crystallographic orientation, however, this phenomenon does not occur in the wet technique.

The formation of the hexagonal ZnO crystals is by heterogeneous nucleation instead of homogeneous nucleation as liquid phase deposition method is used in this work. During the precipitation of the hexagonal ZnO crystal at the negative electrode, electrolysis of water near the vicinity of the substrate would form a basic condition due to the formation of hydroxide ions. These hydroxide ions play an important role during the heterogeneous nucleation during the re-precipitation of the ZnO crystals onto the surface of the substrate. Therefore, the heterogeneous nucleation will promote the preferential growth c-axis (002) plane depending on the polarity of the terminating ions on the hexagonal ZnO columns [20].

Moreover, the electrolysis of water at positive electrode will generate the formation of hydrogen ions and therefore, the vicinity near the positive electrode is acidic, which causes dissolution of gel film on the positive electrode side during hot-water treatment.

The effect of EF-HWT time was investigated by varying the HWT time from 1 to 5 h. The surface morphologies of the ZnO gel film formed on FTO after EF-HWT at 50°C with D.C. 10 V/cm for 1 to 5 h are shown in Fig. 4. As the EF-HWT time increased from 1 to 3 h as shown in Fig. 4(a) - (c), the general distribution of the columnar ZnO precipitates on the surface of FTO increased. However, upon prolonged EF-HWT for 5 h (Fig. 4 (d)), the distribution of the hexagonal ZnO crystals formed reduced due to the dissolution of the ZnO precipitates. This shows that extensive dissolution of the ZnO films occurred beyond 3 h of EF-HWT.

The optical transmission spectra of the ZnO coatings formed on FTO after HWT for 1 to 3 h, with and without electric field induction are compared as shown in Figs. 5 and 6, respectively. The optical transmittance of the hot-water treated samples without electric field induction increased with HWT time. This is resulted by the dissolution of the ZnO films at prolonged HWT time. In contrast, with 10 V/cm EF-HWT, the optical transmission reduced with longer HWT time as a result of light scattering on the surface of the film due to higher amount of ZnO crystal precipitates formation as shown in Fig. 4. The optical transmission of the EF-HWT samples reduced significantly compared to the as-prepared ZnO films at shorter wavelength region due to light scattering. Longer EF-HWT time resulted in lower transmittance of the ZnO films.

The effect of electric field voltage during HWT was investigated. In Fig. 7, the surface morphologies of ZnO films obtained after HWT at 50°C for 3 h with 0, 5 10 and 20 V/cm of applied voltage are shown, respectively. Prominent hexagonal columnar ZnO crystal

structure was observed when the voltage of 10 V/cm was applied compared to 5 V/cm during HWT. The angular hexagonal structure diminished and metal Zn was formed when higher applied voltage of 20 V/cm was applied. This could be caused by the reduction at the surface of the ZnO nanostructures at the high applied potential as shown in Fig. 7 (d). XRD patterns from EF-HWT samples confirmed that the peaks attributed to ZnO wurzite (closed circles) were obtained while Zn metal (closed square) was also observed in the sample treated at 20 V/cm as shown in Fig. 8.

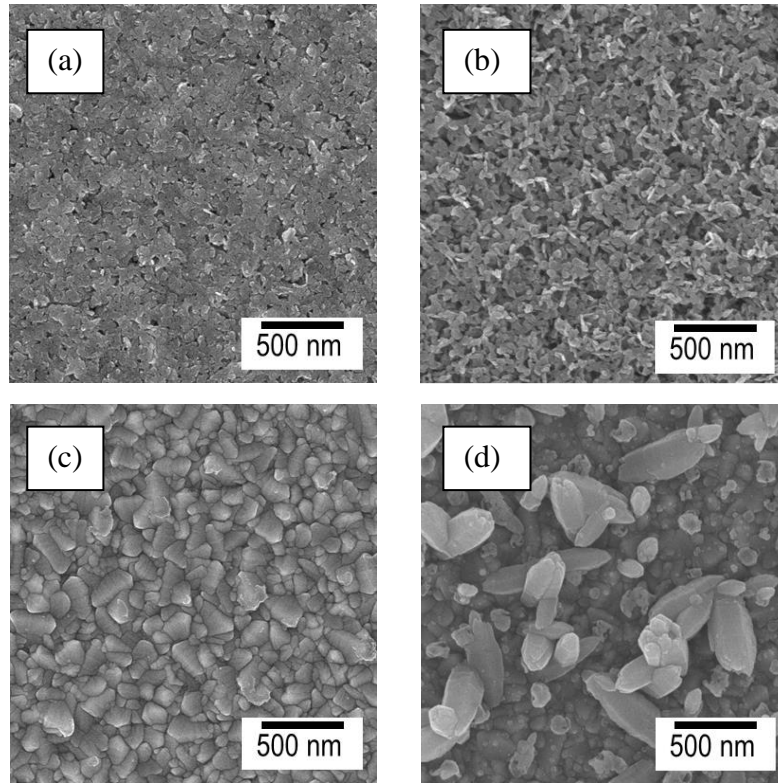


Fig.2: Surface morphology of the ZnO films on FTO after hot-water treated at 50°C for 5 h with 10 V/cm applied external field. (a) As prepared, (b) without electric field, (c) ZnO films formed on positive electrode and (d) ZnO films formed on negative electrode.

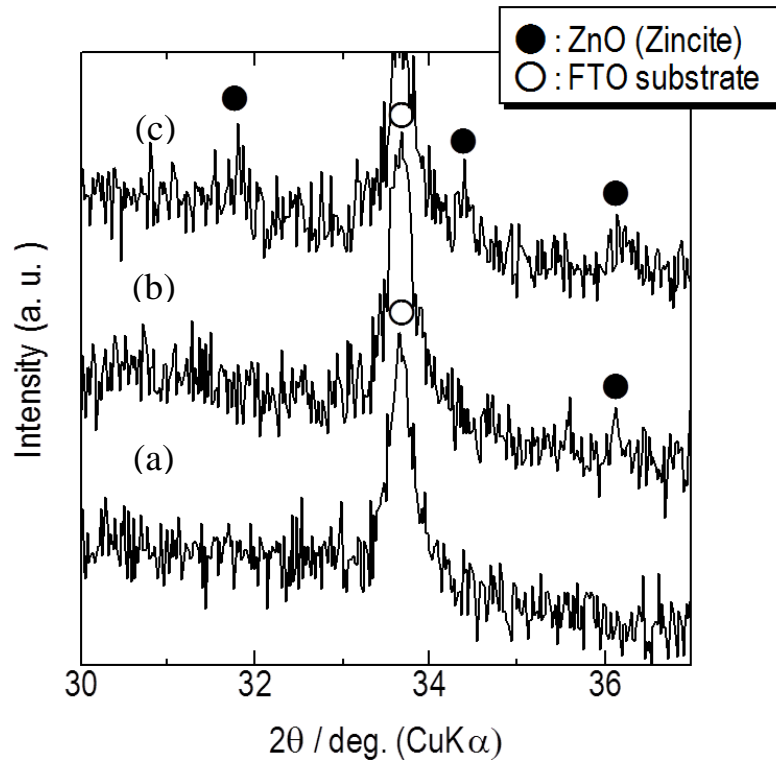


Fig. 3: XRD patterns of the ZnO film; (a) As prepared, (b) HWT without electric field at 50°C for 5 h and (c) EF-HWT at the negative electrode, at 50°C for 5 h with applied external field of 10 V/cm.

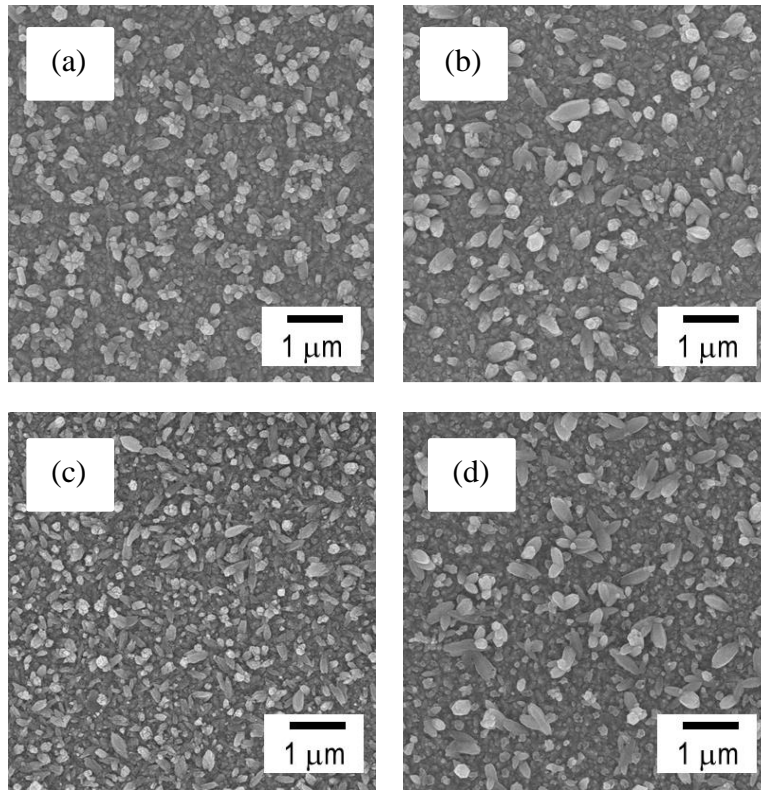


Fig. 4: Surface morphologies of the ZnO films formed on FTO after electric field hot-water treated at 50°C for (a) 1 h, (b) 2 h, (c) 3 h and (d) 5 h with applied voltage of 10V/cm on the negative electrode.

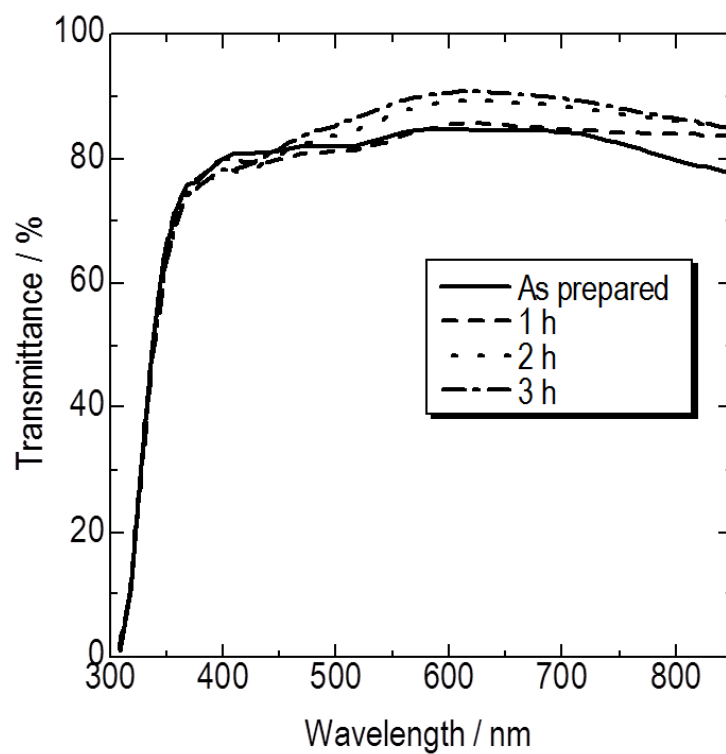


Fig. 5: Optical transmission spectra of the as prepared ZnO films and hot-water treated films at 50°C for 1 to 3 h.

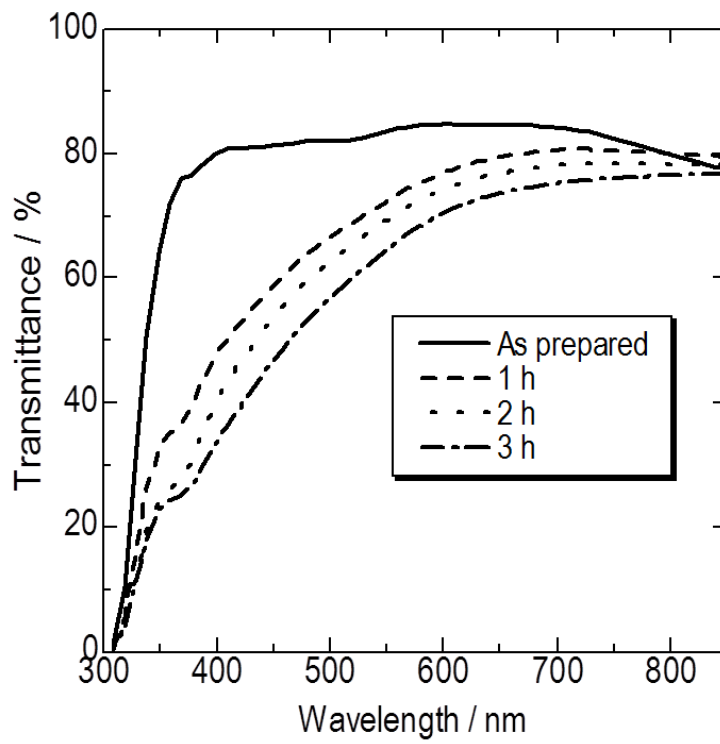


Fig. 6: Optical transmission spectra of the as prepared and electric field hot-water treated ZnO films at 50°C for 1 to 3 h at the negative electrode with applied voltage of 10 V/cm.

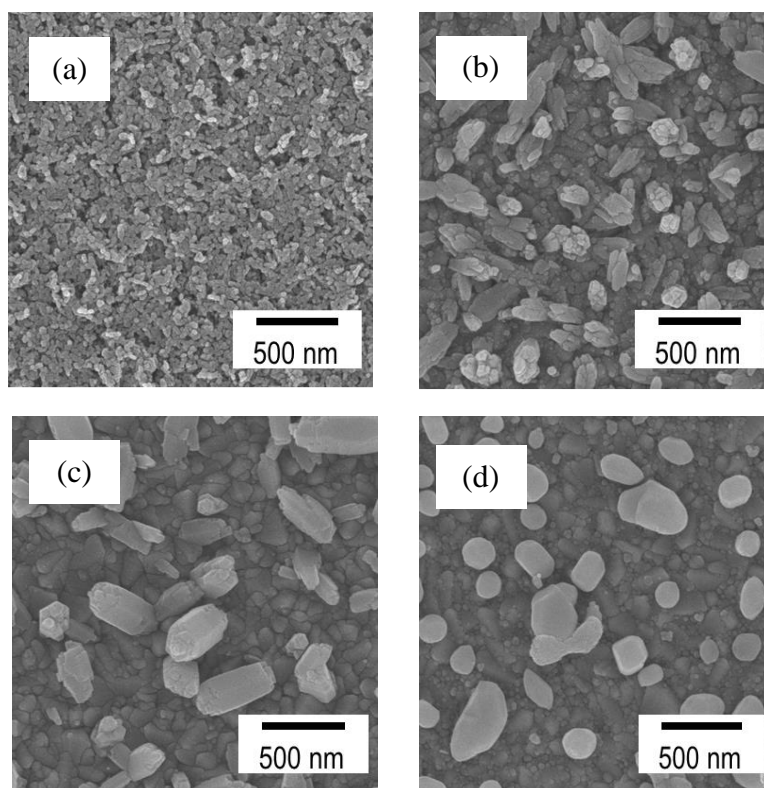


Fig. 7: Surface morphologies of the ZnO films hot-water treated at 50°C for 3 h with D.C. electric field of (a) 0 V/cm, (b) 5 V/cm, (c) 10 V/cm and (d) 20 V/cm at the negative electrode.

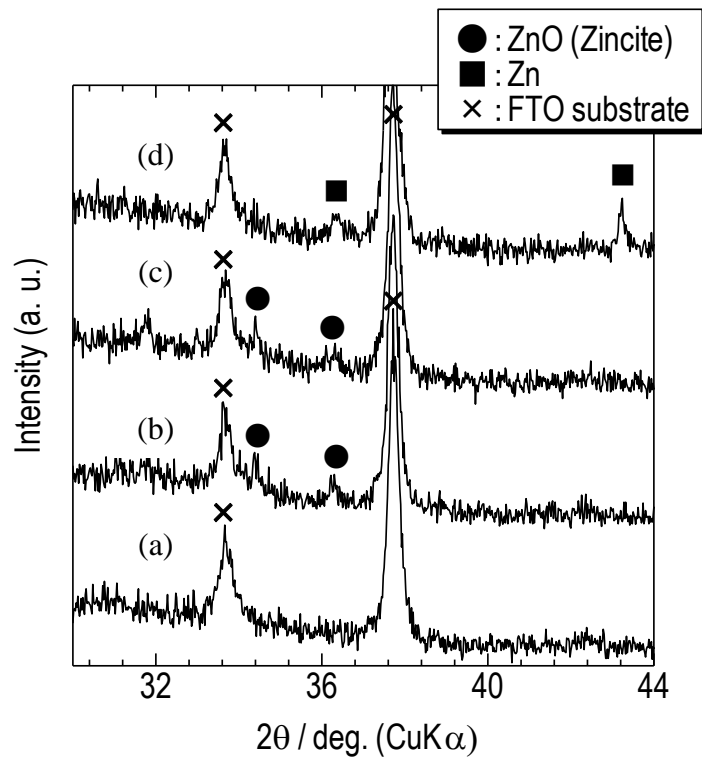


Fig. 8: XRD patterns of the ZnO films hot-water treated at 50°C for 3 h with D.C. electric field (a) 0 V/cm, (b) 5 V/cm, (c) 10 V/cm and (d) 20 V/cm at the negative electrode.

3.2.1.3.2 Effect of substrate on ZnO crystals formation

To study the effect of substrate during EF-HWT, comparison was made between the ZnO films formed on FTO/glass and Si wafer substrates after HWT with applied voltage of 10 V/cm for 3 h. The surface morphologies of the ZnO crystals formed on the surface of FTO/glass and Si wafer substrates with and without electric field during HWT are shown in Fig. 9. The applied voltage used during EF-HWT was 10 V/cm on the negative electrode. No significant change was observed in the surface morphologies of the HWT ZnO films without electric field on FTO/glass and Si wafer substrates as shown in Fig. 9 (a) and (c). On the other hand, significant flower-like ZnO crystals were obtained on the Si wafer substrate after EF-HWT compared to hexagonal columnar ZnO crystals formed on FTO. It is noteworthy that the type of substrate used during EF-HWT affects ZnO crystals formation of the ZnO gel films.

Fig. 10 shows the XRD patterns for the ZnO crystals formed on FTO/glass and Si wafer substrates with (10 V/cm) and without electric field during HWT. Strong (002) ZnO peak at 34.4° that correlates to the c-axis orientation can be seen for the EF-HWT ZnO film on the Si wafer substrate. The crystallinity of the ZnO coatings formed by HWT without electric field on FTO/glass and Si wafer substrates were poor compared to those obtained by EF-HWT.

In order to study the formation mechanism of the flower-like ZnO nanostructures on the Si substrate by EF-HWT, the applied voltage was varied during HWT. The ZnO crystals obtained after EF-HWT of the ZnO film on Si substrates with different applied electric field voltages of 0 - 20 V/cm are shown in Fig. 11. With applied potential of 5 V/cm, hexagonal columnar crystal precipitation with diameter of approximately 250 nm was observed similar to those obtained on FTO/glass substrates. At higher applied electric fields of 10 and 20 V/cm,

flower-like ZnO nanostructures were obtained as shown in Fig. 11 (c) and (d). The branching of the ZnO petal structures became more obvious when a stronger voltage was applied during HWT. This shows that external field applied during HWT of the ZnO films on the Si substrate would affect the concentration of the dissolved species forming different nucleation planes that led to the formation of flower-like structures. The lattice mismatch between the Si (100) and ZnO could promote the nucleation of branch columnar ZnO forming the flower-like structure during the crystal growth. With higher applied potential during EF-HWT, electrostatic repulsion between the hydrolysed species and negative electrode resulted in lower concentration of ZnO species on the surface coating [15]. However, EF-HWT of the coating on Si substrate with higher applied potential promoted higher degree of ZnO branching during crystal formation as the re-deposition tends to form at the surface with lower electrostatic repulsion. By using quartz crystal microbalance, the remaining ZnO coating on the substrates was measured. Approximately 30 % of the ZnO sol-gel coating remained on the substrate after HWT at 50°C for 3 h without an electric field.

The XRD patterns for the flower-like ZnO crystals formed on Si substrate after EF-HWTs at 5, 10 and 20 V/cm are shown in Fig. 12. The intensity of the ZnO (002) peak at 34.4° that correlates to the c-axis orientation increased when a stronger electric field was applied during HWT. Lattice mismatch between (001) plane of ZnO crystal and Si substrate with (100) orientation resulted in heteroepitaxy growth and promoted the formation of flower-like ZnO structure during EF-HWT. The degree of branching could be controlled changing the applied voltage during EF-HWT of the ZnO coating.

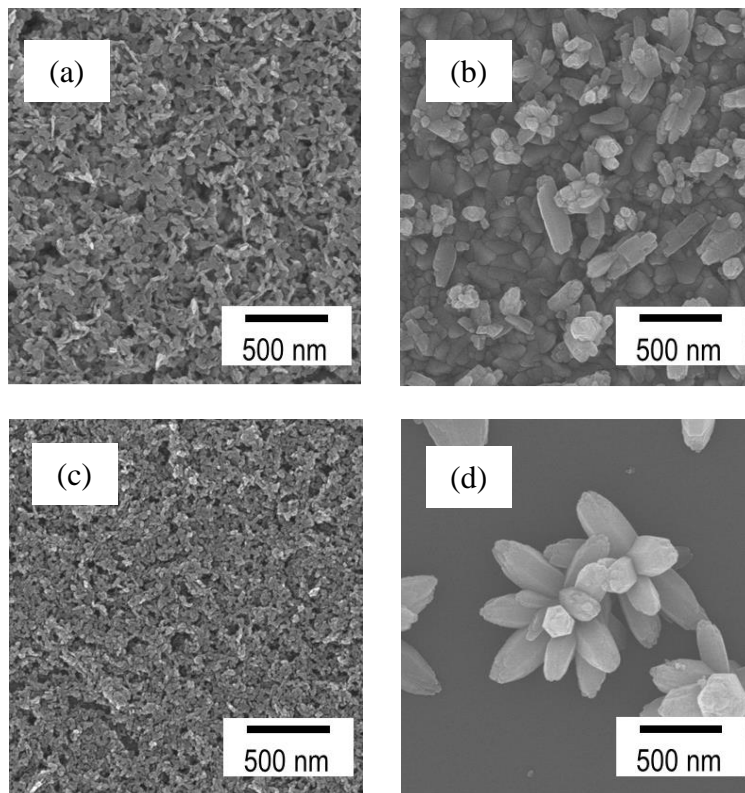


Fig. 9: Surface morphologies of the ZnO films formed after hot-water treated at 50°C for 3 h at the negative electrode with applied external field of 10 V/cm; (a) ZnO coatings on FTO without electric field, (b) ZnO coating on FTO with electric field, (c) ZnO coating on Si substrate without electric field, and (d) ZnO coating Si substrate with electric field.

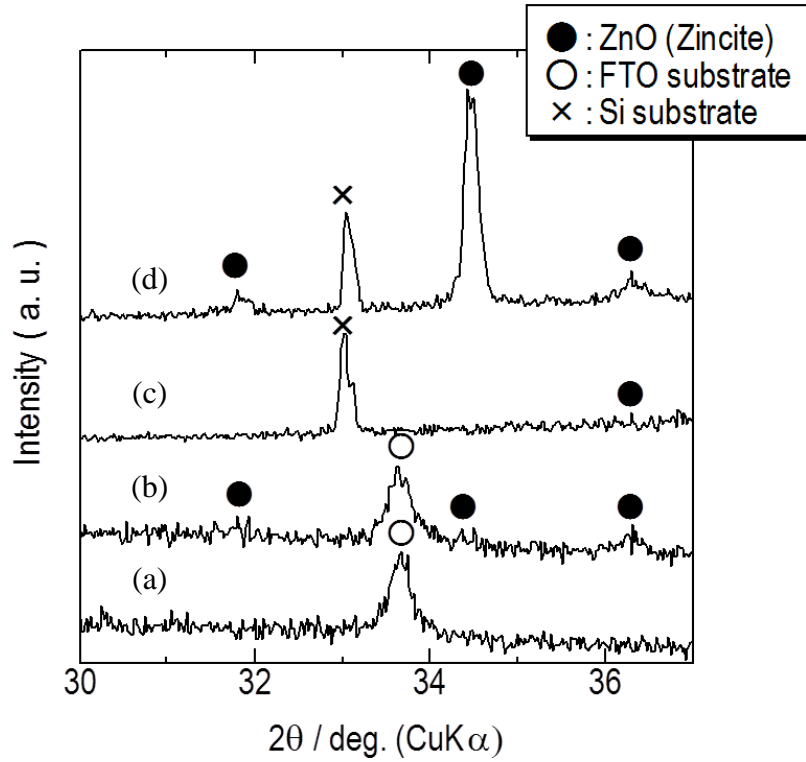


Fig. 10: XRD patterns of the ZnO films formed after hot-water treatment with and without external electric field induction on FTO and Si substrates;(a) Without electric field on FTO, (b) with applied external field of 10 V/cm at the negative electrode on FTO, (c) without electric field on Si substrates and (d) with applied external field of 10 V/cm at the negative electrode on Si substrate.

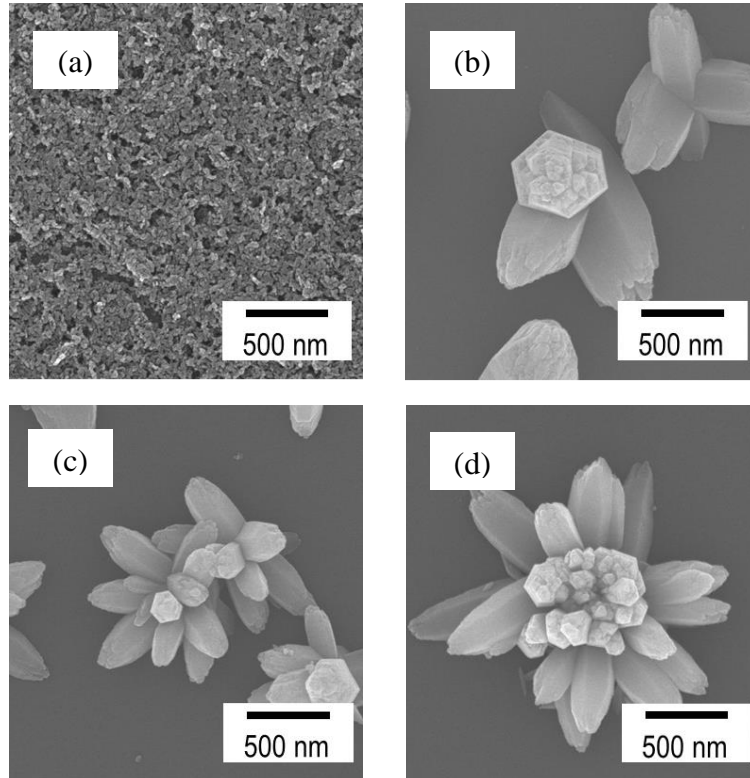


Fig. 11: Surface morphologies of the ZnO films formed on Si substrates after hot-water treated at 50°C for 3 h with applied external field of (a) 0 V/cm, (b) 5 V/cm, (c) 10 V/cm and (d) 20 V/cm at the negative electrode.

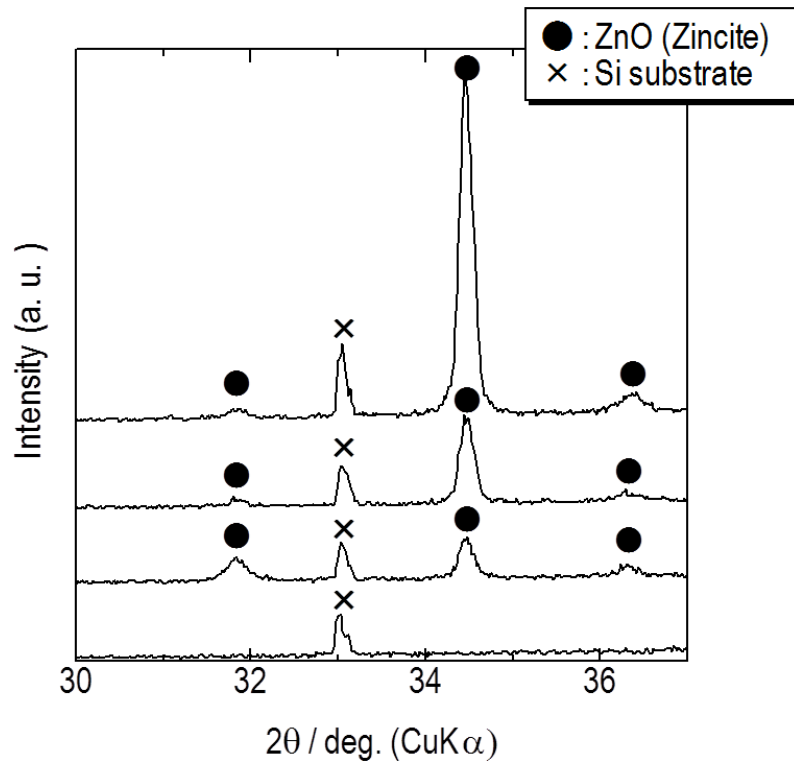


Fig. 12: XRD patterns of the ZnO films formed on Si substrates after hot-water treated at 50°C for 3 h with applied external field of (a) 0 V/cm, (b) 5 V/cm, (c) 10 V/cm and (d) 20 V/cm at the negative electrode.

3.2.1.4 CONCLUSION

ZnO nanostructures were successfully formed by EF-HWT of ZnO coatings prepared by sol-gel method at low-temperature of 50°C. Granular crystallites were precipitated on the surface of the sol-gel derived ZnO film on FTO during HWT, and the shape of the precipitates was changed to hexagonal column when the electric field was applied during HWT. The EF-HWT of ZnO gel films on Si wafer substrates influenced the morphology and orientation of the ZnO crystals formed; flower-like hexagonal ZnO crystals were obtained with the degree of branching increased with the applied voltage during HWT. The formation mechanism of the ZnO crystals during the electric field induced HWT is dissolution, nucleation and re-precipitation of the ZnO crystal onto the surface of the substrate.

REFERENCES

- [1] Y.J. Lee, D.S. Ruby, D.W. Peters, B.B. McKenzie, J.W.P. Hsu, ZnO nanostructures as efficient antireflection layers in solar cells, *Nano Lett.* 8 (2008) 1501-1505.
- [2] X. Qu, W. Wang, W. Liu, Z. Yang, X. Duan, D. Jia, The growth and optical property of ZnO rods evolved from layered basic zinc acetate in humid atmosphere, *Mater. Sci. Semicond. Process.* 14 (2011) 241-246.
- [3] C. Ravichandran, G. Srinivasan, Craig Lennon, S. Sivanathan, J. Kumar, Investigations on the structural and optical properties of Li, N, and (Li,N) co-doped ZnO thin films prepared by sol-gel technique, *Mater. Sci. Semicond. Process.* 13 (2010) 46-50.
- [4] M.H. Huang, S. Mao, H. Feick, H. Yan, Y. Wu, H. Kind, E. Weber, R. Russo, P. Yang, Room-temperature Ultraviolet Nanowire Nanolasers, *Science*, 292 (2001) 1897-1899.

- [5] J.L. Yang, S. J. An, W. I. Park, G. C. Y. Choi, Photocatalysis using ZnO Thin Films and Nanoneedles Grown by Metal-Organic Chemical Vapor Deposition, *Adv. Mater.*, 16 (2004) 1661-1664.
- [6] S.C. Lyu, Y. Zhang, C. J. Lee, H. Ruh, H. J. Lee, Low-temperature Growth of ZnO Nanowire Array by Simple Physical Vapor-Deposition Method, *Chem. Mater.*, 14 (2003) 3294-3299.
- [7] Y. Ohya, T. Ogata, T. Ban, Y. Takahashi, Microstructure of Sol-Gel ZnO Thin Films Fabricated Using Ethanolamine and Hydroxyketone Modifiers, *J. Ceram. Soc. Jpn.*, 113 (2005) 220-225.
- [8] S.M.H. Hejazi, F. Majidi, M.P. Tavandashti, M. Ranjbar, The effect of heat treatment process on structure and properties of ZnO nano layer produced by sol-gel method, *Mater. Sci. Semicond. Process.* 13 (2010) 267-271.
- [9] L. Vayssieres, Growth of Arrayed Nanorods and Nanowires of ZnO from Aqueous Solutions, *Adv. Mater.* 15 (2003) 464-466.
- [10] B. L., H. C. Zeng, Room Temperature Solution Synthesis of Monodispersed Single-Crystalline ZnO nanorods and Derived Hierarchical Nanostructures, *Langmuir* 20 (2004) 4196-4204.
- [11] S. Yamabi, H. Imai, Growth conditions for Wurtzite Zinc Oxide Films in Aqueous Solutions, *J. Mater. Chem.*, 12 (2002) 3773-3778.
- [12] H. Imai, S. Iwai, S. Yamabi, Phosphate-mediated ZnO nanosheets with a Mosaic structure, *Chem. Lett.*, 33 (2004) 768-769.

- [13] W. K. Tan, K. Abdul Razak, K. Ibrahim, G. Kawamura, J. Hamagami, A. Matsuda, Z. Lockman, *Malaysian Journal of Microscopy* 6 (2010) 58-63.
- [14] A. Matsuda, Y. Kotani, K. Kogure, M. Tatsumisago, T. Minami, Transparent Anatase Nanocomposite Films by the Sol-Gel Process at Low Temperatures, *J. Am. Ceram. Soc.*, 83 (2000) 229-231 (2000).
- [15] A. Matsuda, T. Matoda, T. Kogure, K. Tadanaga, T. Minami, M. Tatsumisago, Formation and Characterization of Titania Nanosheets-Precipitated Coatings via Sol-Gel Process with Hot-Water Treatment under Vibrations, *Chem. Mater.*, 17 (2005) 749-757.
- [16] N. Prastomo, K. Kimata, Y. Daiko, H. Muto, T. Kogure, M. Sakai, A. Matsuda, Effect of external fields applied during hot-water treatment on the aspect ratio of nanocrystallites formed on SiO₂-TiO₂ coatings derived from sol-gel techniques, *J. Sol-Gel Sci. Technol.* 56 (2010) 345-352.
- [17] M.T. Soo, N. Prastomo, A. Matsuda, G. Kawamura, H. Muto, A. F. M. Noor, Z. Lockman, K.Y. Cheong, Elaboration and characterization of sol-gel derived ZrO₂ thin films treated with hot-water, *Appl. Surf. Sci.* 258 (2012) 5250-5258.
- [18] A. Matsuda, K. Kobayashi, T. Kogure, M. Sakai, K. Tadanaga, T. Minami, M. Tatsumisago, Effects of Electric Field on the Formation of Titania Nanocrystals on SiO₂-TiO₂ Coatings during Hot Water Treatment, *J. Ceram. Soc. Jpn.*, 113 (2005) 333-335.
- [19] M. Pourbaix, *Atlas of Electrochemical Equilibria in Aqueous Solutions*, 2nd ed., National Association of Corrosion Engineers, Houston 406-413, 1974.
- [20] W. K. Tan, K. Abdul Razak, Z. Lockman, G. Kawamura, H. Muto, A. Matsuda, Formation of highly crystallized ZnO nanostructures by hot-water treatment of etched Zn foils, *Matt. Lett.* 91 (2013) 111-114.

3.2.2 PHOTOLUMINESCENCE PROPERTIES OF ROD-LIKE Ce-DOPED ZnO NANOSTRUCTURED FILMS FORMED BY HOT-WATER TREATMENT OF SOL-GEL DERIVED COATING

3.2.2.1 INTRODUCTION

ZnO has drawn widespread interest from researchers and been subjected to intensive investigation because it is known to possess the richest family of nanostructures [1]. ZnO exceptional properties such as direct band gap (3.3 eV at room temperature) and large exciton binding energy of 60 meV enable its usage in various applications [2]. There are many methods available to form ZnO nanostructures from either physical or chemical method. The fabrication costs of chemical route which include hydrothermal, chemical bath deposition and sol-gel method are lower than those of the physical route. The advantages of sol-gel method are large coating area and feasible to form various ZnO nanostructures with good photoluminescence properties [3]. In addition, the sol-gel method allows the hybridization of inorganic, organic and metallic materials at low-temperature [4].

The crystallization and densification of sol-gel derived oxide layer by low-temperature process has always been a subject of interest. Matsuda *et al.* has reported the formation anatase nanocrystals on sol-gel derived SiO₂-TiO₂ coatings by hot-water treatment at low-temperature of 90°C [5, 6]. The resultant hot-water treated coatings showed high photocatalytic properties and excellent wettability for water [7]. Masuda *et al.* demonstrated a novel site selective deposition and micropatterning to form crystalline ultra-violet (UV) and visible-light-emitting ZnO crystals in aqueous solution at low temperature of 50°C without any catalyst or annealing [8].

Metal ions doped into oxide semiconductors could trap photo-generated charge carriers temporarily and among all the rare earth metals, cerium has received much attention

due to its unique properties which include (1) redox couple $\text{Ce}^{3+}/\text{Ce}^{4+}$ that makes cerium oxide shift between CeO_2 and Ce_2O_3 under oxidizing and reducing conditions and (2) the easy formation of labile oxygen vacancies with the relatively high mobility of bulk oxygen species [9]. Therefore, the versatile properties of Ce-doped ZnO nanostructures have been explored for many applications such as photoluminescence, photoelectrochemical properties under visible light, and as well as chemical and gas sensors [10]. Yousefi *et al.* reported the increment of photocurrent density to almost double in photoelectrochemical water splitting reaction with the addition of Ce to the ZnO thin film.

To date, there are very limited reports on the formation Ce-doped ZnO nanostructured films. Moreover, most works reported the formation of Ce-doped thin film and nanostructures by annealing at 500 and 600°C to induce the crystallization of the thin films and nanostructures [9, 11-14]. In this work, thin film of Ce-doped ZnO films was formed by dip-coating of a sol-gel method and subsequently hot-water treated without stirring at 60°C for 30 min to induce the crystallization of Ce-doped ZnO film. For comparison, the undoped and Ce-doped ZnO sol-gel coatings were annealed at 500°C for 3 h and characterized as well. The optical properties of these nanostructured ZnO can be influenced by the defects induced by the doping as the electronic structure of the host might be changed [11]. The effects of Ce doping on the optical and structural properties of the ZnO nanostructured films formed after hot-water treatment were investigated in details.

3.2.2.2 EXPERIMENTAL

For undoped ZnO, the sol was prepared using zinc acetate dehydrate (ZnAc) (WAKO, 99%), diethanolamine (DEA) (WAKO, 99%), water (H₂O) and 2-propanol (2-PrOH) as the solvent. The molar ratio of ZnAc: DEA: H₂O: 2-PrOH was 1:1:1:20. To study the effect of Ce doping, cerium nitrate hexahydrate (Ce(NO₃)₃·6H₂O, 99.5%) was added into the sol with different molar ratios of Ce relative to ZnAc at 2, 5, 10 and 20 molar percentage. Non-alkaline glass substrates that were cleaned using RCA (H₂O: H₂O₂: NH₄OH=5:1:1 by volume) were dip-coated at room temperature in the Ce-doped ZnO sol at a down-speed of 5 mm/s, holding for 10 s, and then withdrawing at an up-speed of 2 mm/s. The ZnO-coated glass substrate was dried at room temperature and then placed in an oven at 100°C for 15 min and these steps were repeated twice. The ZnO-coated glasses were then immersed into pure, hot-water at 60°C for 30 min to induce the formation of the crystallized film as reported in our previous work [15]. Another set of experiments was conducted by annealing the ZnO-coated glasses at 500°C for 3 h to compare the optical properties of the as form ZnO films prepared by hot-water and heat treatments.

The surface morphologies of the ZnO layer on the glass substrate were viewed using a S-4800 Field Emission Scanning Electron Microscope (FE-SEM, Hitachi S-4800). X-ray diffraction (XRD) patterns of the ZnO layer were obtained using high-voltage X-ray diffractometer (Rigaku RINT 2500) with CuK α radiation. Photoluminescence (PL) studies were also performed using monochromatic beam generated from He-Cd laser with a wavelength of 325 nm and recorded using a monochromator (Nikon G250, Japan). X-ray photoelectron spectroscopy (XPS) was done using PHI Quantera SXM Scanning X-ray Microprobe (ULVAC-Phi, Inc.;Japan) with an Al cathode (h ν =1486.6 eV) under a base pressure of 5 x 10⁻⁹ Torr using an X-ray source with a power of 100 W, a pass energy of 260.0 eV, and take off angle of 45°. The binding energy values are all calibrated by fixing the

C (1s) core level line to 284.80 eV as a reference energy point. All the peaks were deconvoluted using Multipak software with 70% Gaussian-20% Lorentzian peak fitting.

3.2.2.3 RESULTS AND DISCUSSION

The XRD patterns of the undoped and Ce-doped ZnO sol-gel coated films after annealed at 500°C for 3 h and hot-water treated at 60°C for 30 min are shown in Fig. 1 and Fig. 2, respectively. As for the annealed samples shown in Fig. 1, peaks that correlate to the wurtzite ZnO (JCPDS=36-1451) at 31.77°, 34.48° and 36.50° that correlate to the ZnO (100), (002) and (101) planes, respectively, are observed. However, the intensity of the XRD peaks reduced as the concentration of Ce doping increased. The intensities of the peaks decreased gradually and broadening of the peaks with the higher Ce doping imply smaller Ce-doped ZnO crystallites were formed. As for the hot-water treated samples, only peaks at 2θ of 31.77° and 36.50° relating to (100) and (101) planes are observed. No diffraction peaks of Ce-related oxides or other impurity phases were observed, indicating that Zn²⁺ sites or the interstitial sites in the ZnO lattice were uniformly substituted with Ce³⁺ ions [13]. The diffraction peak at (002) was not observed for the samples treated with hot-water, which shows that the Ce-doped and undoped ZnO nanostructures formed do not exhibit preferential growth perpendicular to the substrate surface. ZnO (100) diffraction peak indicates that the rod-like ZnO nanostructures formed were laid parallel onto the surface of the films [16].

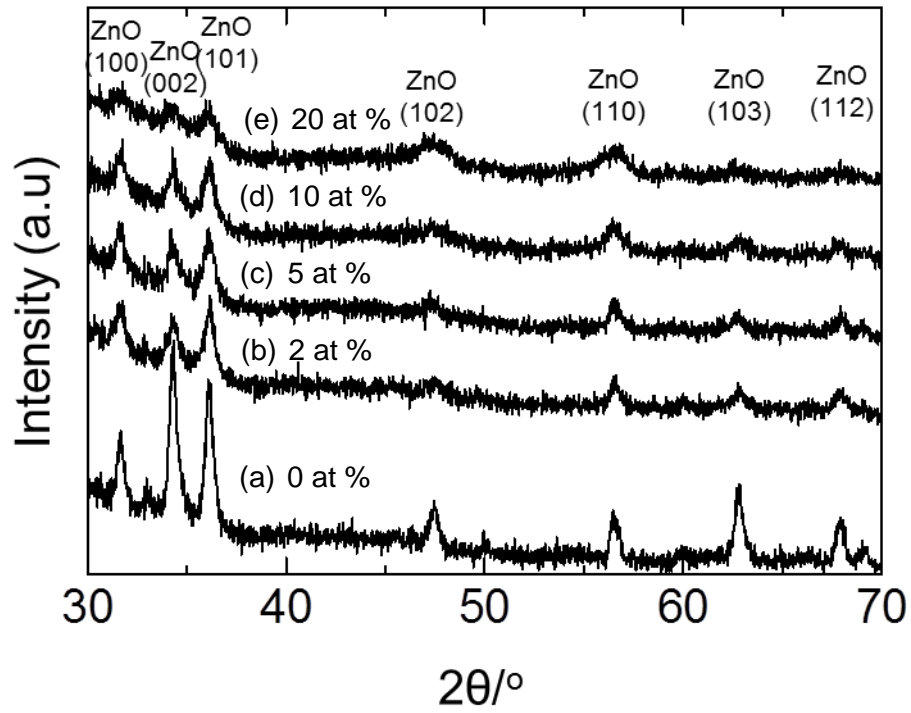


Fig. 1: XRD patterns of the undoped and Ce-doped ZnO films at (a) 0 at%, (b) 2 at%, (c) 5 at%, (d) 10 at% and (e) 20 at% after annealed at 500°C for 3 h.

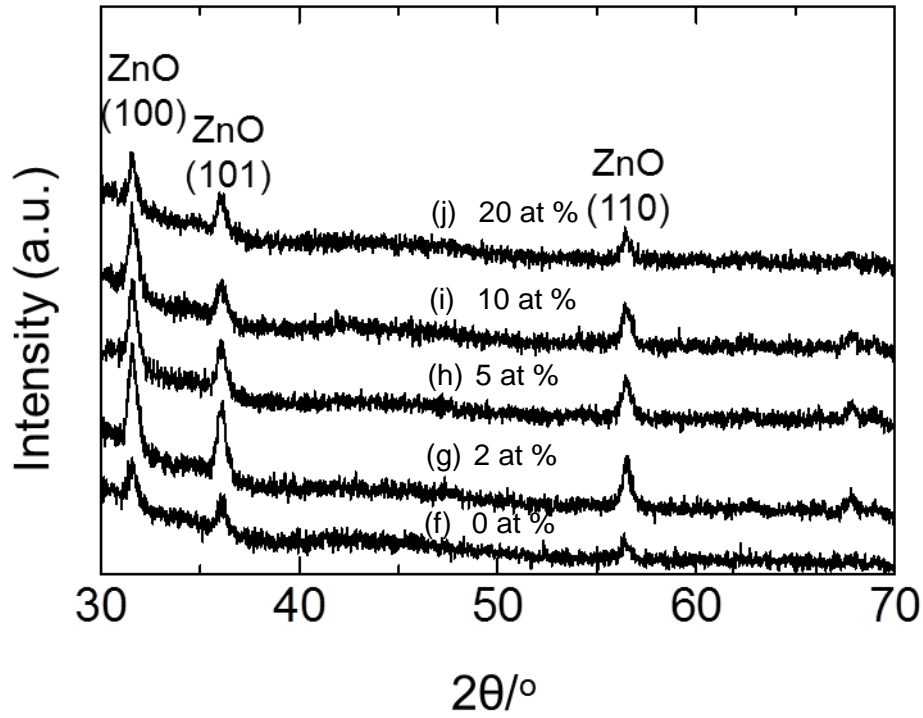


Fig. 2: XRD patterns of the undoped and Ce-doped ZnO sol-gel films at (a) 0 at%, (b) 2 at%, (c) 5 at%, (d) 10 at% and (e) 20 at% after hot-water treatment at 60°C for 30 min.

The surface morphologies of the annealed and hot-water treated samples are shown in Fig. 3 and Fig. 4, respectively. The inset images are the high magnification of the SEM images obtained. From Fig. 3, it can be observed that the grain size of the annealed Ce-doped surface reduced with the increment of Ce doping concentration of the precursor film from 2 to 20 at %. The average grain size for the undoped ZnO is around 70 nm. After doping with Ce, the grain size reduced to 26 nm, 17 nm, and 8 nm, for the samples doped with 2, 5, and 10 at % of Ce in the precursor films, respectively. Yousefi *et al.* also reported that the average crystallite size decreased with increasing Ce concentration as the Ce^{3+} and Ce^{4+} ions are more likely to form complex with the surface oxygen of ZnO and decrease the growth of ZnO crystallite due to the larger ionic radii of Ce^{3+} and Ce^{4+} compared to that of Zn^{2+} [9]. As for the hot-water treated samples, the undoped ZnO films formed after hot-water treatment at 60°C for 30 min is shown in Fig. 4(a). The rod-like ZnO nanostructures were formed by the dissolution and re-precipitation process of the sol-gel derived layer. Upon exposure to hot-water, the upper layer of the gel dissolves due to the agitation from the hot-water bath. Then, this layer crystallized and acts as the seed layer for the subsequent re-deposition. $\text{Zn}(\text{OH})_2$ precipitated on the seed layer to form ZnO upon reaching supersaturation due to the increased Zn ions concentration in the solution from the dissolution of the sol-gel layer [15]. From the FESEM images obtained, the nanostructures formed appear to have rod-like structures with pointed ends. Uniform and well distributed rod-like undoped and Ce-doped ZnO films can be observed for all the samples from the low magnification images shown in Fig. 4. This shows that hot-water treatment of the sol-gel derived layer enables the formation of even and uniform crystalline ZnO nanostructures. No significant morphological changes were seen for all the hot-water treated Ce-doped samples at low magnification observation. However, upon higher magnification observation as shown in inset of the images in Fig. 4, the surface roughness of the ZnO nanostructures changes with the concentration of Ce doping in the

precursor films. The surfaces of the ZnO nanostructures appear to consist of smaller spherical grains as the concentration of Ce doping in the precursor film increases. This could be caused by the larger Ce^{3+} and Ce^{4+} ionic radii that make it difficult for these ions to substitute the Zn^{2+} in ZnO lattice similar to the annealed Ce-doped ZnO films mentioned earlier. Cross sectional views of the undoped and Ce-doped ZnO films after HWT are shown in Fig.5. The thickness of the films after HWT varied approximately from 800 nm to 1000 nm. The rod-like nanostructure of the films can be seen from the cross sectional views which tally with the surface morphologies shown in Fig. 4.

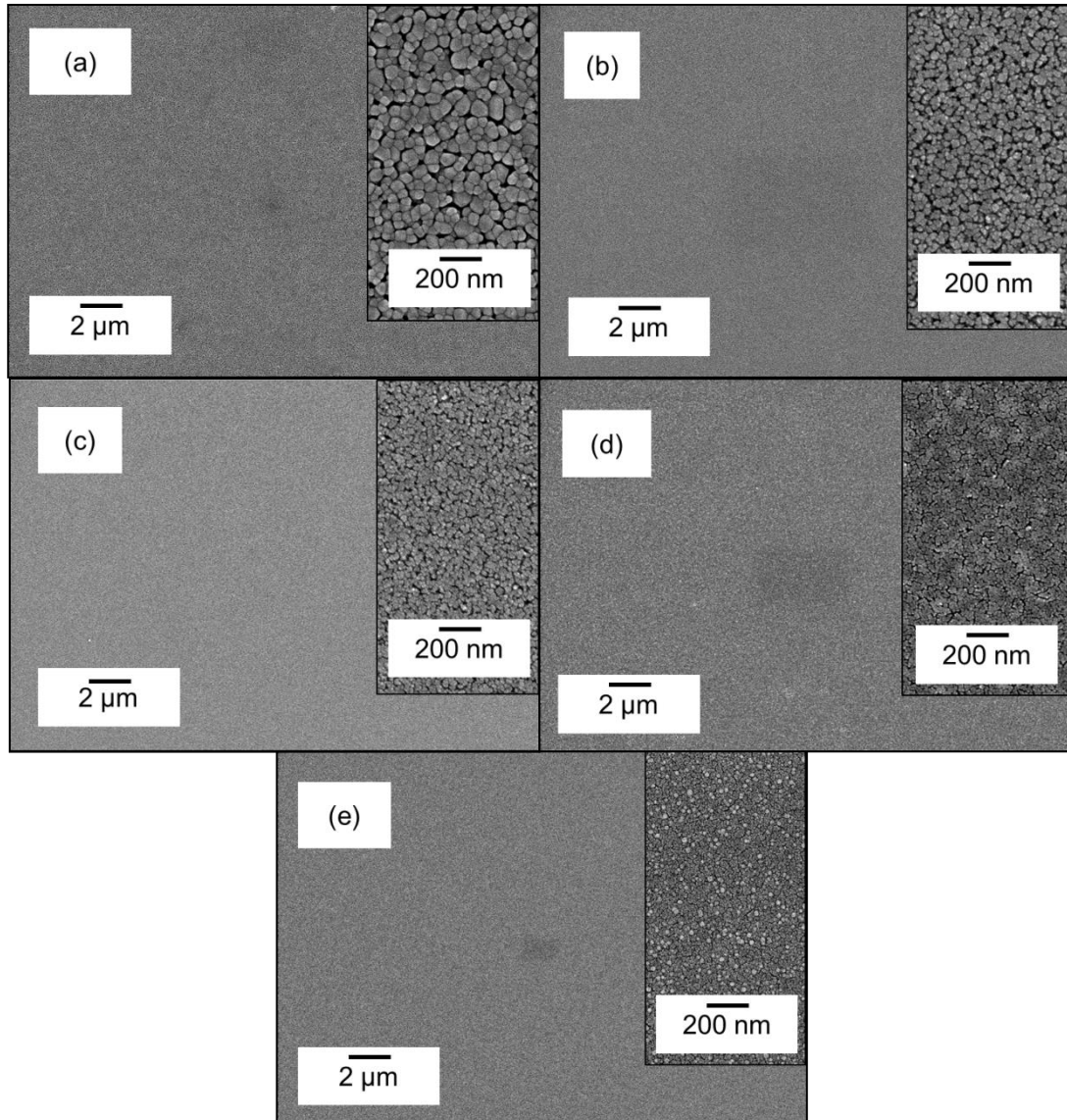


Fig. 3: SEM images of surface morphologies of the Ce-doped ZnO sol-gel coated layer after annealed at 500°C for 3 h with Ce concentrations of (a) 0 at %, (b) 2 at %, (c) 5 at %, (d) 10 at % and (e) 20 at %.

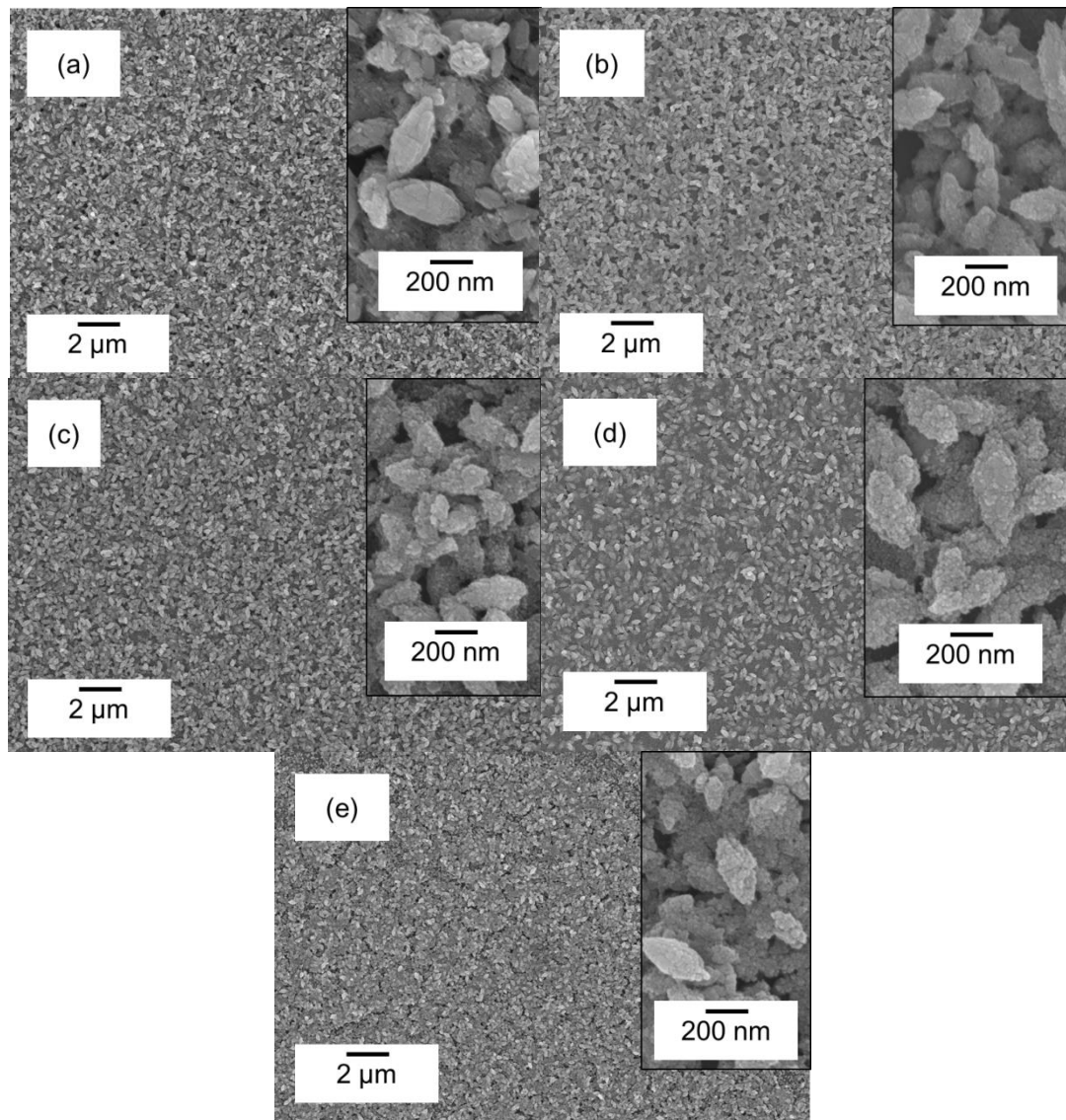


Fig. 4: SEM surface morphologies images of the Ce-doped ZnO films after hot-water treated at 60°C for 30 min with Ce concentrations of (a) 0 at %, (b) 2 at %, (c) 5 at %, (d) 10 at % and (e) 20 at %.

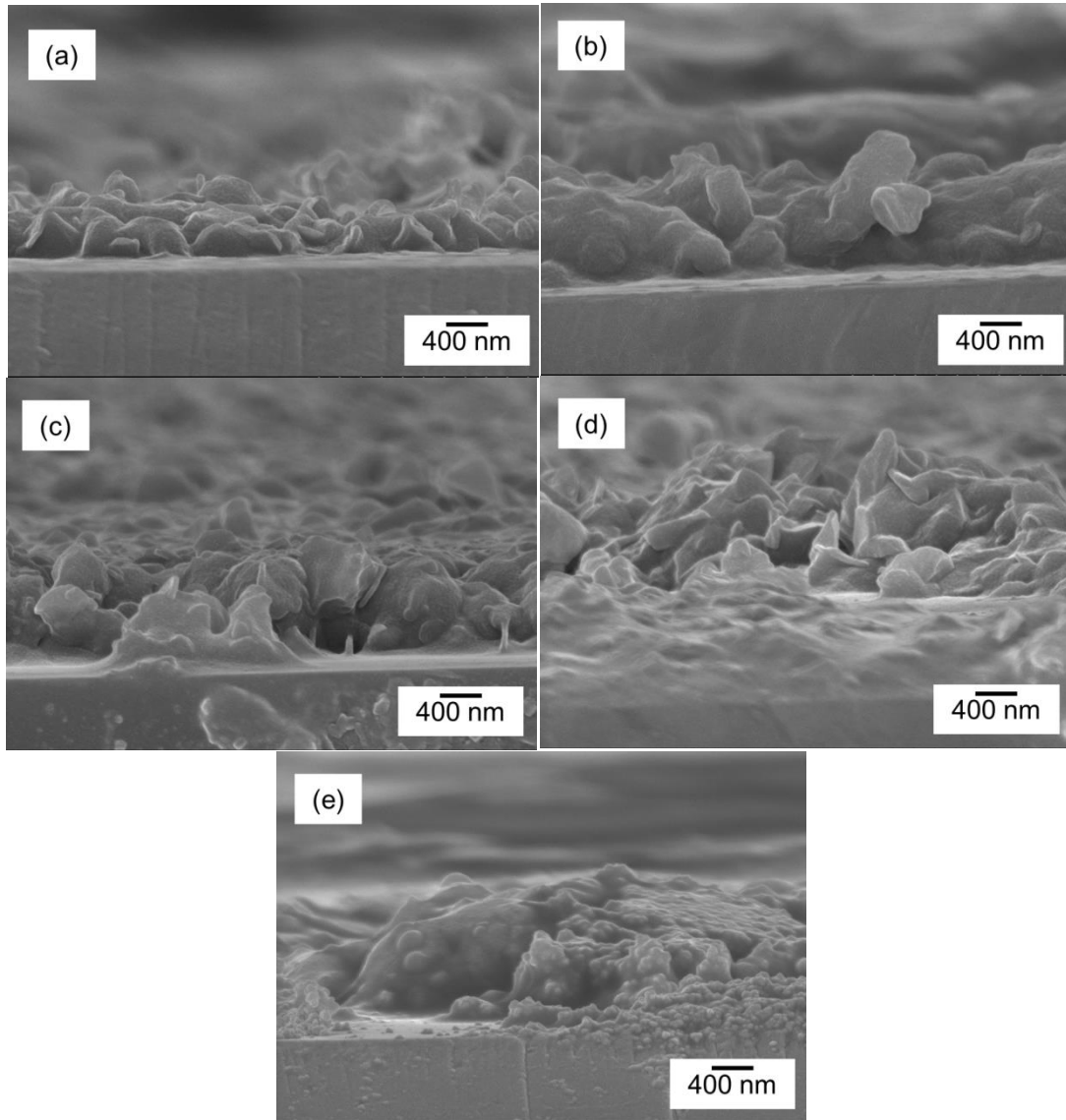


Fig. 5: Cross-sectional SEM images of the undoped and Ce-doped ZnO films after hot-water treated at 60°C for 30 min with Ce concentrations of (a) 0 at %, (b) 2 at %, (c) 5 at %, (d) 10 at % and (e) 20 at %.

The qualities and the incorporation of Ce ions in the ZnO lattice and their vibration states were further determined by XPS. Fig. 6 shows the XPS spectra for the 10 at % of Ce-doped ZnO precursor film formed after hot-water treatment. The general surface scan XPS spectrum is shown in Fig. 6(a). The high-resolution scans Zn 2p, Ce 3d, and O1s are shown in Fig. 6 (b), (c) and (d), respectively. The Zn 2p peaks located at 1021 and 1044 eV are attributed to Zn 2p_{3/2} and Zn 2p_{1/2} [13]. Fig. 6(c) clearly shows 8 de-convoluted peaks for the measurement of Ce 3d at higher scan resolution. From the de-convoluted peaks, two sets of spin-orbital corresponding to Ce (3d_{3/2}) and Ce (3d_{5/2}) are observed. Peaks at 887.00 and 903.70 eV are attributed to the final states of Ce(IV), which consist of a mixing of Ce(3d⁹4f²)O(2p⁴) and Ce(3d⁹4f¹)O(2p⁵). Meanwhile, the peak located at 898.40 eV corresponds to Ce (3d⁹4f⁰)O(2p⁶) of Ce(IV) final state. As for Ce(III) state, the peaks located at 881.80 and 885.20 eV are correlated to Ce(3d⁹4f²)O(2p⁵) and Ce(3d⁹4f¹)O(2p⁶), respectively. As for the peaks at 900.50 and 905.90 eV, similar assignation can be made for the Ce (3d_{3/2}) levels. Therefore, these results show that there is co-existence of Ce³⁺ and Ce⁴⁺, which is also reported by other researchers [9, 17]. In the O1s region shown in Fig. 6 (d), two distinct de-convoluted peaks are observed for lower energy component at 529.5 eV and higher energy component at 531.5 eV which correspond to Ce-O and Zn-O bonding, respectively. However, there is no compound related to CeO₂ was observed from the XRD patterns in Fig. 2, indicating that the CeO₂ compound might be amorphous or had very low concentration in the films.

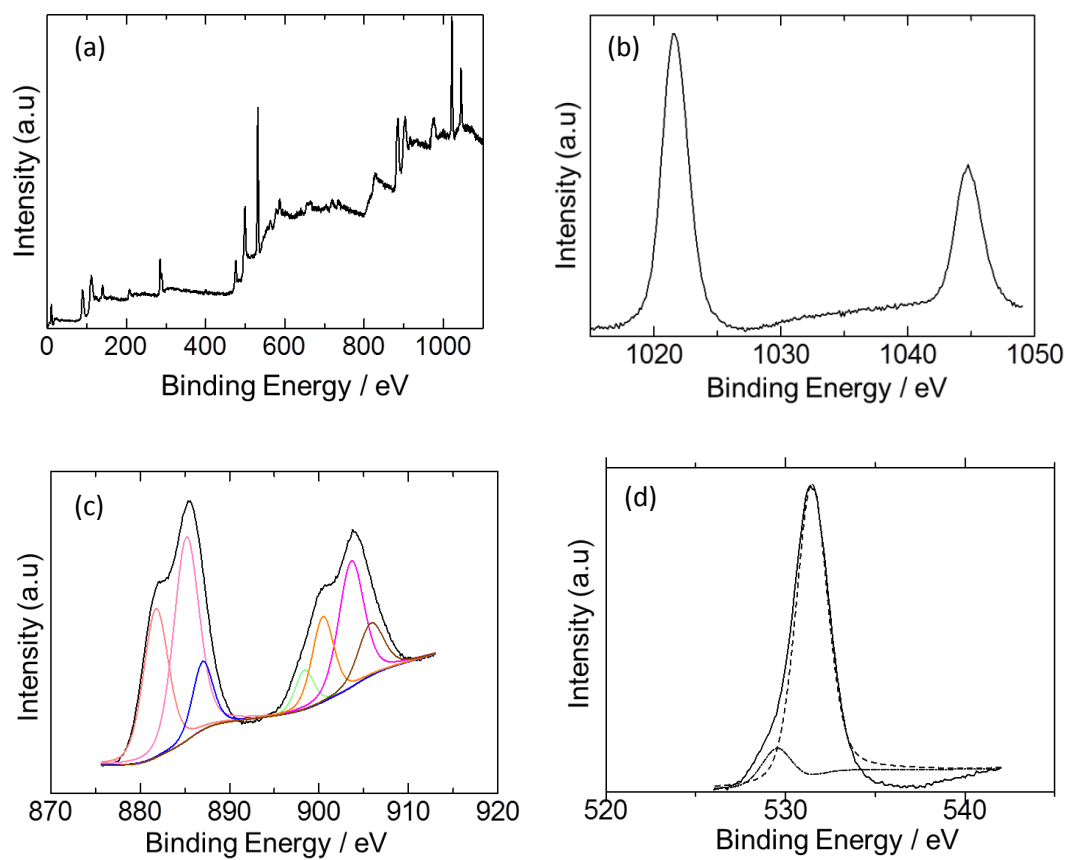


Fig. 6: XPS spectra of the 10 at % Ce-doped ZnO precursor films after hot-water treated at 60°C for 30 min. (a) Surface scan, (b) Zn (2p_{3/2}), (c) Ce (3d) and (d) O (1S).

The luminescence properties of all the samples were investigated using room temperature photoluminescence. The PL spectra of the coated sol-gel films that were annealed at 500°C for 3 h are shown in Fig. 7. The undoped ZnO thin film exhibits strong UV emission at 378 nm, blue emission at 440 nm and weak red emission at 754 nm. The UV emission is associated with the excitonic recombination corresponding to the near band edge emission of ZnO [8, 13] while the visible emissions are commonly attributed to the deep level emission due to Zn and oxygen vacancies as well as Zn interstitials [16, 18]. As for the Ce-doped ZnO films annealed in the same condition, no UV emission is observed while only blue emission peak around 436 nm is detected. The blue emission exhibits blue shift compared to the undoped ZnO films [11, 13]. No UV emission is observed for the Ce-doped ZnO films due to the increase of non-radiative defects and the reduction of the ZnO grain size [13].

As for the hot-water treated samples, the photoluminescence spectra of the undoped and Ce-doped samples are shown in Fig. 8. The PL spectra of all the samples showed UV, blue and green emission. The blue emissions at 440 nm of the Ce-doped ZnO samples are suppressed compare to the undoped ZnO sample. On the contrary, the green emission increased gradually with Ce doping concentration in the precursor films as shown in Fig. 8, which could attributed to the existence of Ce impurities in ZnO films that might induce the formation of new defects such as Ce vacancies [12]. The stronger and broader green emission of the Ce-doped films compared to the undoped films is resulted from the multi-emission centre formation due to the incorporation of Ce ions into ZnO and act as the donor [11]. The emission of the donors as well as the intrinsic transition of Ce^{3+} ions could lead to broad green emission.

There is gradual blue shift observed for the UV emission with the increasing Ce doping concentration in the precursor film. At 20 at % doping of Ce in the precursor film,

blue shift in the UV emission from 375 nm to 368 nm is observed which is also reported by other researchers as more electrons contributed by cerium dopants that would absorb the energy levels located at the bottom of the conduction band. Upon excitation using laser with wavelength of 325 nm, the excitons take up higher energy levels at the bottom of the conduction band and the radiative recombinations of these excitons led to the blue shift and broaden of UV emission peak [11, 13]. The intensity of the UV emission reduced with the Ce doping concentration due to surface bound states that act as defects leading to higher non-radiative relaxation [19].

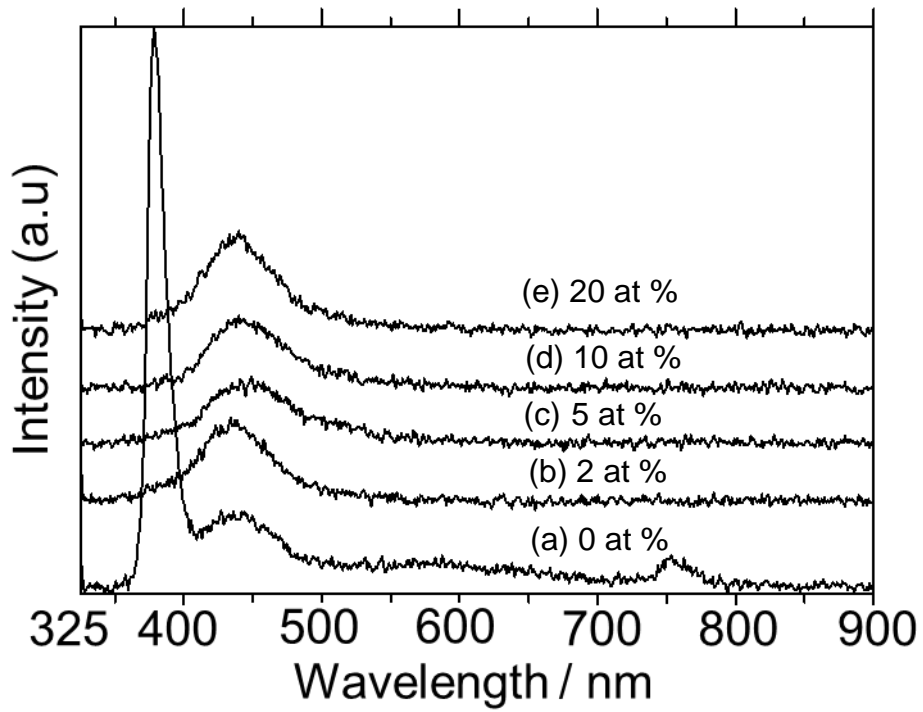


Fig. 7: Photoluminescence of undoped and Ce-doped ZnO films at (a) 0 at% (b) 2 at%, (c) 5 at%, (d) 10 at% and (e) 20 at% after annealed at 500°C for 3 h.

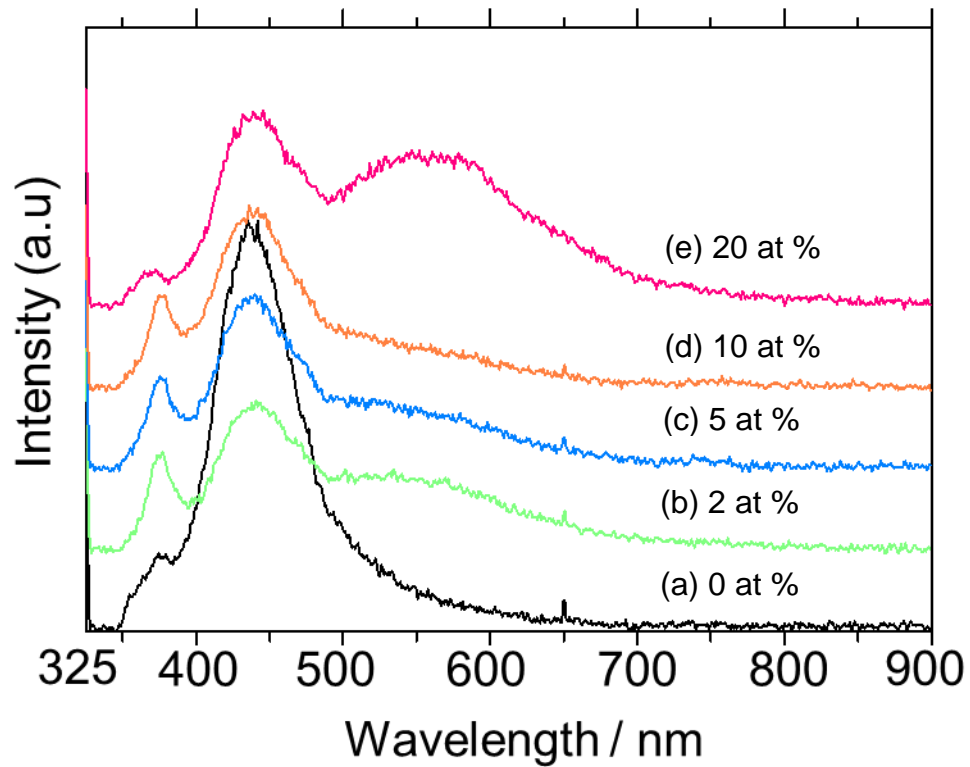


Fig. 8: Photoluminescence of undoped and Ce-doped ZnO films at (a) 0 at %, (b) 2 at %, (c) 5 at %, (d) 10 at % and (e) 20 at % after hot-water treated at 60°C for 30 min.

3.2.2.4 CONCLUSION

Rod-like undoped and Ce-doped ZnO nanostructured films were formed by hot-water treatment of undoped and Ce-doped sol-gel derived coatings at low temperature of 60°C for 30 min. Effect of Ce-doping in the precursor films to the optical properties of hot-water treated ZnO films showed suppressed blue emission and slight blue shift of UV emission with increasing Ce concentration in the precursor films especially at 20 at %. Photoluminescence results show UV and visible emission which indicated good crystalline Ce-doped ZnO films formation. For samples annealed at 500°C for 3 h, strong UV emission was obtained for the undoped ZnO while Ce-doped ZnO films only exhibit blue emissions. The formation mechanism of the rod-like ZnO nanostructured films involves the dissolution and re-precipitation of the sol-gel derived ZnO layer during the hot-water treatment. Hot-water treatment method is proven to be able to form crystalline ZnO and Ce-doped ZnO nanostructured films at low temperature. This feasible formation of Ce-doped ZnO nanostructured films with good optical properties using hot-water treatment method can be applied on substrates with limited thermal stabilities such as polymeric substrates for fabrication of flexible optoelectronic devices.

REFERENCES

- [1] R. Wahab, S.G. Ansari, Y.S. Kim, H.K. Seo, G.S. Kim, G. Khang, H.S. Shin, Low-temperature solution synthesis and characterization of ZnO nanoflowers. *Mater. Res. Bull.* 42 (2007) 1640-1648.
- [2] Y. Masuda, K. Kato, Aqueous synthesis of ZnO rod arrays for molecular sensor. *Cryst. Growth Des.* 9 (2009) 3083-3088.

- [3] Z.Chen, X.X. Li, N. Chen, H. Wang, G. P. Du, Andy Y. M. Suen. Effect of annealing on photoluminescence of blue-emitting ZnO nanoparticles by sol-gel method. *J. Sol-Gel Sci. Technol.* 62 (2012) 252-258.
- [4] N. Prastomo, H. Muto, M. Sakai, A. Matsuda, Formation and stabilization of tetragonal phase in sol-gel derived ZrO₂ treated with base-hot-water. *Mater. Sci. Eng., B* (2010) 173:99-104.
- [5] A. Matsuda, Y. Kotani, T. Kogure, M. Tatsumisago, T. Minami, Transparent anatase nanocomposite films by sol-gel process at low temperature. *J. Am. Ceram. Soc.* 83 (2000) 229-231.
- [6] Y. Kotani, A. Matsuda, M. Tatsumisago, T. Minami, T. Kogure, Formation of anatase nanocrystals in sol-gel derived TiO₂-SiO₂ thin films with hot water treatment. *J. Sol-Gel Sci. Technol.* 19 (2001) 585-588.
- [7] A. Matsuda, Y. Kotani, T. Kogure, M. Tatsumisago, T. Minami, Photocatalytic decomposition of acetaldehyde with anatase nanocrystals-dispersed silica films prepared by the sol-gel process with hot water treatment. *J. Sol-Gel Sci. Technol.* 22 (2001) 41-46.
- [8] Y. Masuda, N. Kinoshita, F. Sato, K. Koumoto, Site-selective deposition and morphology control of UV- and visible-light-emitting ZnO crystals. *Cryst. Growth Des.* 6 (2006) 75-78.
- [9] M. Yousefi, M. Amiri, R. Azimirad, A.Z. Moshfegh, Enhanced photoelectrochemical activity of Ce doped ZnO nanocomposite thin films under visible light. *J. Electroanal. Chem.* 661 (2011) 106-112.
- [10] G. N. Dar, A. Umar, S. A. Zaidi, A. A. Ibrahim, M. Abaker, S. Baskoutas, M. S. Al-Assiri, Ce-doped ZnO nanorods for detection of hazardous chemical. *Sens. Actuators, B* (2012) 72-78.

- [11] W.E. Mahmoud, Synthesis and optical properties of Ce-doped ZnO hexagonal nanoplatelets. *J. Cryst. Growth* 312 (2010) 3075-3079.
- [12] H.C. Gong, J.F. Zhong, S.M. Zhou, B. Zhang, Z.H. Li, Z.L. Du, Ce-induced single crystalline hierarchical zinc oxide nanobrushes. *Superlattices Microstruct.* 44 (2008) 183-190.
- [13] J. Yang, M. Gao, L. Yang, Y. Zhang, J. Lang, D. Wang, Y. Wang, H. Liu, H. Fan, Low-temperature growth and optical properties of Ce-doped ZnO nanorods. *Appl. Surf. Sci.* 255 (2008) 2546-2650.
- [14] F. Du, N. Wang, D. Zhang, Y. Shen, Preparation, characterization and infrared emissivity study of Ce-doped ZnO films. *J. Rare Earths*, (2010) 391.
- [15] W.K. Tan, K. Abdul Razak, K. Ibrahim, G. Kawamura, J. Hamagami, A. Matsuda, Z. Lockman, Formation of ZnO nano and sub-micron-rods by chemical process on hot-water treated and non-treated sol-gel coating. *Malaysian Journal of Microscopy* 6 (2010) 58-63.
- [16] Y. Masuda, N. Kinoshita, K. Koumoto, Hexagonal symmetry radial whiskers of ZnO crystallized in aqueous solution. *J. Nanosci. Nanotechnol.* 9 (2009) 522-526.
- [17] C. Liu, X. Tang, C. Mo, Z. Qiang, Characterization and activity of visible-light-driven TiO₂ photocatalyst codoped with nitrogen and cerium. *J. Solid State Chem.* 181 (2008) 913-919.
- [18] M. El Jouad, M. Alaoui Lamrani, Z. Sofiani, M. Addou, T. El Habbani, N. Fellahi, K. Bahedi, L. Dghoughi, A. Monteil, B. Sahraoui, S. Dabos, N. Gaumer, Roughness effect on photoluminescence of cerium doped zinc oxide thin films. *Opt. Mater.* 31 (2009) 1357-1361.

[19] A. George, S.K. Sharma, S. Chawla, M.M Malik, M.S. Qureshi, Detailed of X-ray diffraction and photoluminescence studies of Ce doped ZnO nanocrystals. *J. Alloys Compd.* 509 (2011) 5942-5946.

Chapter 4 HYDROTHERMAL GROWTH OF ZnO NANOSTRUCTURES

4.1 ENHANCE DYE-SENSITIZED SOLAR CELLS PERFORMANCE OF ZnO NANOROD ARRAYS GROWN BY LOW-TEMPERATURE HYDROTHERMAL REACTION

4.1.1 INTRODUCTION

The development of clean energy is imperative due to the increasing global energy demand and heightened environmental awareness. Dye-sensitized solar cells (DSSCs) are a well-known renewable and clean solar-to-electricity conversion system with huge development potential for achieving sustainable energy supply in the future. A DSSC comprises of a large bandgap nanostructured semiconductor which was fabricated on a transparent conductive oxide (TCO) sandwiched with dye, a platinum counter electrode, and an electrolyte solution between the two electrodes. The energy conversion efficiency is interdependent on the dimension and properties of the nanostructured semiconductor.

Zinc oxide (ZnO) is an n-type wide-gap semi-conductive TCO with optical transparency in the visible range [1]. ZnO can be prepared in nanostructures with varying dimensions and shapes. These unique properties allow it to be used as a photocatalyst [2], and DSSCs [3-20]. Vast advantages of DSSC such as low fabrication cost and good efficiency have prompted many researches in this category. ZnO is a promising candidate as an alternative electrode material due to its almost similar bandgap and higher electronic mobility compared to TiO₂ [12, 21]. Moreover, the higher flat band potential of ZnO compared to TiO₂ is beneficial for enhancing the cell's open circuit photovoltage [22, 23]. By using ruthenium complex as a sensitizer, efficiency of about 11 % was reported [24]. Guo *et al.* investigated the effect of hydrothermal growth temperature on the ZnO nanorods formed on indium tin oxide (ITO) coatings and reported the solar-to-electricity conversion efficiency of

2.4% at 95°C [25]. However, the effect of hydrothermal growth time of the ZnO nanorod arrays on the DSSC performance is rarely reported. Yengantiwar *et al.* reported the effect of growth time on ZnO nanorods by aqueous solution deposition with continuous stirring up to 8 h. The reagent solution was replaced every hour and the maximum efficiency yield was 0.71% after 8 h of growth. Therefore, it is interesting to investigate the effect of hydrothermal growth time on the structural, optical and conversion efficiency of ZnO nanorod arrays grown using a single reactive bath for prolonged growth time.

In this study, we fabricated dense and well-aligned ZnO nanorod arrays by two-step methods on ITO/glass substrates. Firstly, the seed layer was coated onto the substrates via sol-gel dip-coating. Due to the advantage in large coating area and low cost consumption, the sol-gel method is favourable to form the seed layer [26]. Besides that, sol-gel method could induce the growth of high-quality orientated ZnO films [27], which is crucial for the subsequent growth of ZnO nanorods. Although physical methods such as sputtering [28] and pulsed laser deposition have better control on the morphologies formation, however, complicated and thus expensive equipment is required. Chemical methods such as sol-gel [29] and hydrothermal [30] are cost effective and also large scale productions using these methods are easily accessible, which prompts intensive research in this category. Then, in this study, hydrothermal growth of the seed layer was performed at low-temperature of 80°C using the similar conditions reported in our previous works to induce the growth of the ZnO nanorods [31, 32]. The ZnO nanorod arrays obtained after hydrothermal growth of 4, 8, 12, 24 h were produced in order to systematically investigate the effect of prolonged growth time on the structural, crystallinity, optical and the conversion efficiency of the DSSCs. The formation mechanism of the ZnO nanorod arrays as the function of time and the effect of the prolonged growth time on the performance of DSSC are discussed in details.

4.1.2 EXPERIMENTAL

4.1.2.1 Preparation of ZnO seed-coated substrate

Indium-tin oxide (ITO)-coated glass substrates (ITO-glass, 10 Ω /sq) were cleaned with RCA solution (H_2O : H_2O_2 : NH_4OH =5:1:1 by volume). The ITO substrates were rinsed with deionized water and dried using nitrogen gas flow. The cleaned ITO substrates were coated with ZnO sol which was prepared using zinc acetate dehydrate (ZnAc) (WAKO, 99%), and diethanolamine (DEA) (WAKO, 99%), water (H_2O) and 2-propanol (2-PrOH) as solvent. The molar ratio of ZnAc: DEA: H_2O : 2-PrOH was 1:1:1:20. Dip-coating was carried out at room temperature using down-speed of 5 mm/s, holding for 10 s, and then withdrawing with an up-speed of 2 mm/s. Dip-coated substrates were dried at room temperature followed by in an oven at 100°C for 15 min. These steps were repeated twice and then the sample was heated at 300°C for 10 min to induce densification and phase transformation.

4.1.2.2 Hydrothermal growth of ZnO nanorod arrays by low-temperature hydrothermal reaction

The ZnO-coated ITO substrate was then immersed into a hydrothermal reactive bath in a Teflon-lined pressure vessel. The bath containing of zinc nitrate hexahydrate (ZnN) (Sigma-Aldrich, 99%) and hexamethylenetetramine (HMT) (Sigma-Aldrich, 98%) with a ZnN:HMT molar ratio of 1:1. The pressure vessel was placed in an oven at 80°C for 4, 8, 12 or 24 h, similar to the conditions reported in previous works [31, 32]. After that, the samples were removed from the vessel and rinsed vigorously with deionised water before characterization.

4.1.2.3 Characterizations

The surface morphologies of the ZnO layer on the ITO-glass substrate were observed using a field emission scanning electron microscope (FE-SEM, Hitachi S-4800). X-ray diffraction (XRD) patterns of the ZnO layer were obtained using an X-ray diffractometer (Rigaku RINT 2500) with CuK α radiation. Photoluminescence (PL) studies were performed using monochromatic beam generated from He-Cd laser with a wavelength of 325 nm and recorded using a monochromator (Nikon G250, Japan). Raman spectroscopy was performed using a Raman laser spectrometer (Jasco NSR-3100). High-resolution transmission electron microscope observation was done using JEOL, JEM-2100F at an acceleration voltage of 200 kV to view the crystalline structure of the nanorods formed.

4.1.2.4 DSSCs assembly

The ZnO nanorod arrays formed on ITO substrate were sensitized in an ethanolic solution of 3×10^{-4} M N719 dye (Dyesol Ltd.) for 2 h. A Pt-sputtered (approximately 100 nm), ITO-coated glass plate was used as the counter electrode. The solar cells were then sealed with a thermal adhesive film prior to solar simulation. The electrolyte solution composed of 0.05 M iodine, 0.1 M lithium iodide, 0.6 M 1,2-di-methyl-3-propylimidazolium iodide, 0.5 M 4-tert-butylpyridine and acetonitrile as the solvent was injected into the cell through one of the small holes drilled in the counter electrode. Then, these small holes were sealed using polytetrafluoroethylene (PTFE) polymer sealant to prevent leakage of the electrolyte. The current-voltage curves were measured under illumination of AM 1.5 solar simulator combining a potentiostat/galvanostat (OTENTO-SUN, Bunkoukeiki Co., Ltd). A metal mask with opening window of 1 cm^2 was placed onto the cell to limit active area for the solar simulator measurement.

4.1.3 RESULTS AND DISCUSSION

4.1.3.1 Morphology and the structure of the hydrothermally-derived ZnO nanorod arrays.

The surface and cross-sectional images of the hydrothermally grown ZnO nanorod arrays on ITO substrates using the reactive solution consisting of Zn ions and HMT (ratio 1:1) for 4, 8, 12 and 24 h are shown in Figure 1. The images labelled (i) are the cross-sectional view of the ZnO nanorods. After 4 h of hydrothermal exposure, hexagonal flat-top ZnO nanorods were observed from the surface morphology as shown in Figure 1(a). The average diameter of the ZnO nanorods was approximately 100 nm and the average length was at 150 nm. After 8 h of hydrothermal reaction, the average diameter of the nanorods increased to 230 nm with an average length of approximately 1 μm . From the cross sectional view shown in Figure 1(b)(i), it can be observed that the nanorods have slightly tapered blunt tips. As the hydrothermal time increased to 12 h, the blunt tips structure diminished as shown in Figure 1(c)(i). The average diameter of the nanorods remains at 230 nm after 12 h of exposure time but the length increased to about 1.5 μm . At 24 h, the nanorods were 2 μm long with an average diameter of 250 nm.

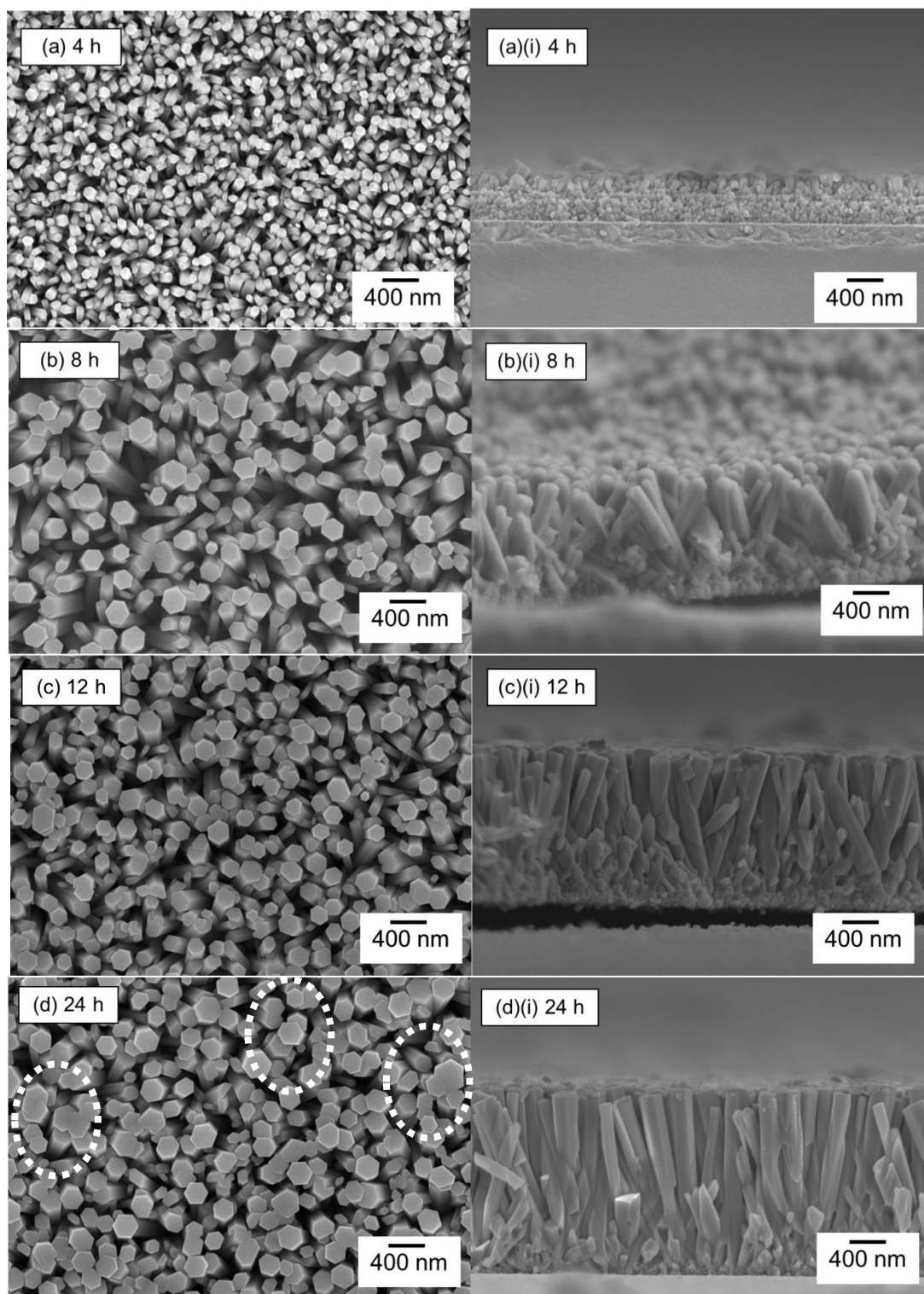


Figure 1: Surface morphologies and cross-sectional views (labelled (i)) of the ZnO nanorod arrays formed on seeded ITO after hydrothermally grown at 80°C for (a) 4 h, (b) 8 h, (c) 12 h, and (d) 24 h.

4.1.3.2 XRD and HR-TEM observation

In Figure 2, XRD peaks attributed to ZnO can be detected at 2θ of 31.77° , 34.42° , and 36.25° relating to (100), (002), and (101) (JCPDS=36-1451) planes of ZnO for all the samples, which can be indexed to hexagonal wurtzite structure. Predominant ZnO peak at (002) plane indicates that the ZnO nanorod arrays formed along c-axis were aligned perpendicularly to the surface of the substrates. The intensity of the peak at ZnO (002) plane increased with the hydrothermal exposure time from 4 to 24 h. From the SEM images in Figure 1, the improved alignment of the ZnO nanorods can be observed, which corresponds to the XRD results for the nanorods formation along the [0001] direction. This could be induced by a steric effect that suppressed the oblique growth and only allowed vertical growth of the nanorods due to the presence of dense nuclei formed on the surface of ITO using sol-gel method [17]. Peaks from the underlying ITO substrate are also observed and denoted with the symbol (*). The preferential directional growth of the ZnO nanorods is further confirmed by the HR-TEM images shown in Figure 3. Low-magnification image of the general distribution for the ZnO nanorods formed is shown in Figure 3(a) and at high resolution TEM shown in Figure 3(c), the inter-planar spacing of about 0.52 nm can be seen clearly, which indicates single crystal ZnO wurtzite structure with interplanar spacing of (0001) grown preferentially along c-axis. No stacking fault or dislocation was observed in the uniform structure.

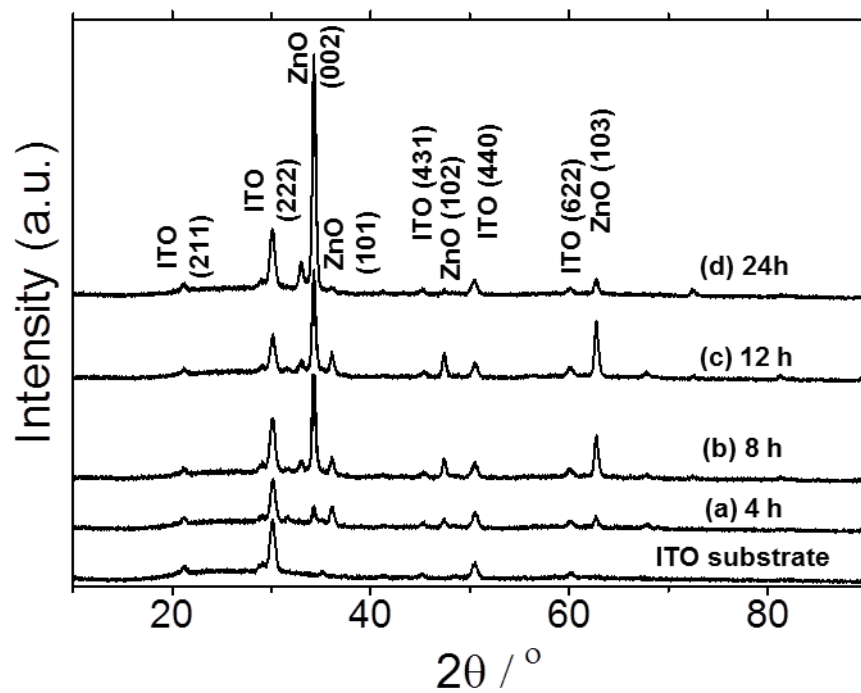


Figure 2: XRD patterns of the bare ITO substrate and ZnO nanorod arrays formed on seeded ITO after hydrothermally grown at 80°C for (a) 4 h, (b) 8 h, (c) 12 h and (d) 24 h.

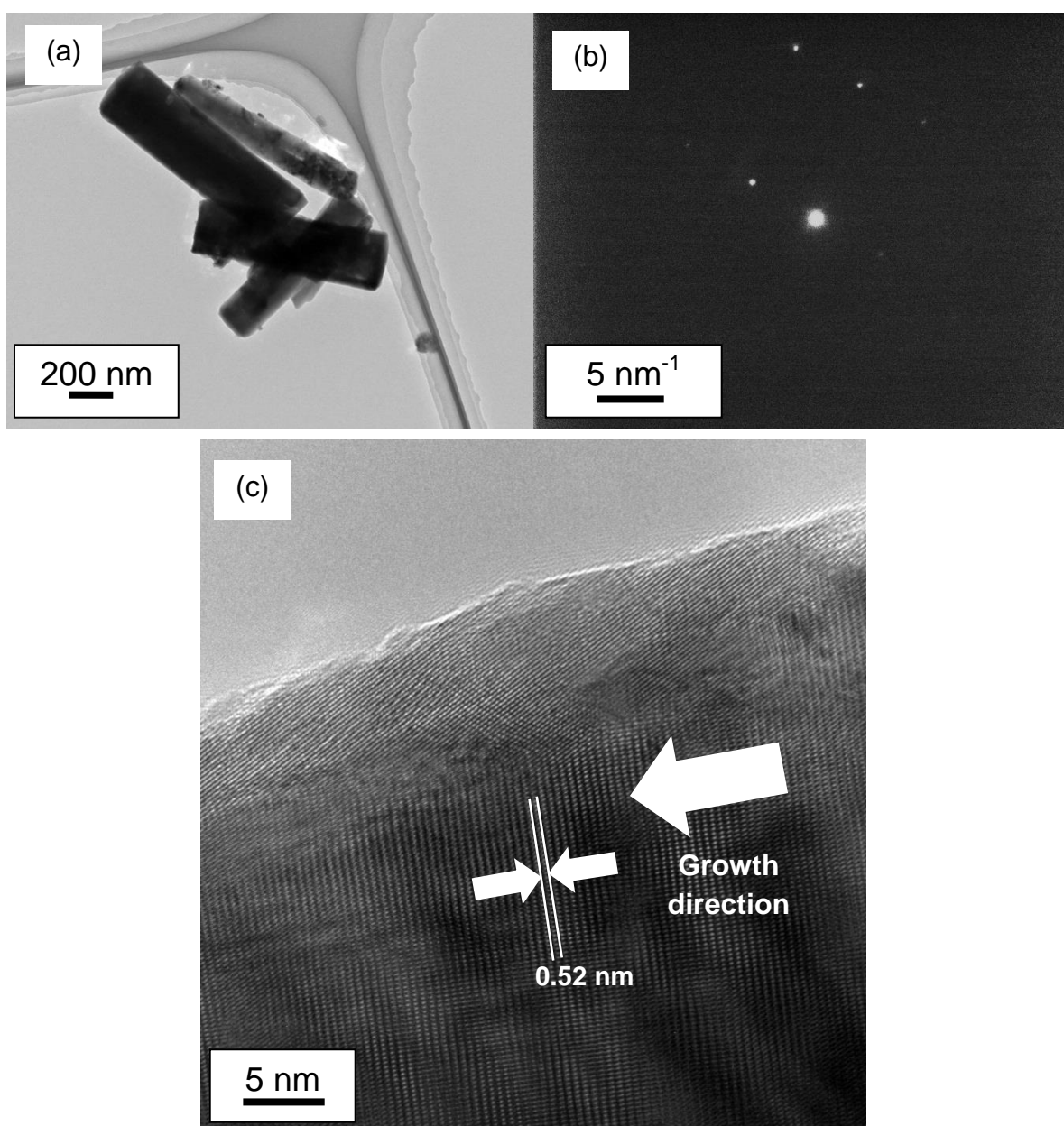


Figure 3: (a) Low magnification, (b) Selected area electron diffraction (SAED) and (c) high-resolution TEM images of the ZnO nanorods obtained after 24 h of hydrothermal growth at 80°C .

4.1.3.3 Optical properties of the ZnO nanorod arrays

Figure 4 is the photoluminescence spectra of the ZnO nanorods formed after 4, 8, 12 and 24 h of hydrothermal exposure. For all samples, a strong UV emission peak was obtained at 380 nm (~3.3 eV). The UV emission peak was attributed to the recombination of free excitons via band to band recombination [33-35]. This result also shows that the ZnO nanorods formed possessed good crystallinity. However, a peak associated to green emission was also observed at approximately 540 nm for all samples. This emission was attributed to the existence of oxygen vacancies referred to as deep-level or trap-state emission. Deep level emission is a phenomenon where non-radiative recombination of electrons and holes in which an electron is trapped into a deep level near the middle of an energy gap associated with a lattice defect. The emission peak could also be attributed to the excess presence of Zn ions in the rods [33, 34].

Raman scattering spectra of the all the ZnO nanorod arrays obtained after 4, 8, 12 and 24 h are shown in Figure 5. Generally, the symmetry of Raman active zone-centre optical phonons is represented at the point of the Brillouin zone as follows:

$$\Gamma_{\text{opt}} = A_1 + 2B_1 + E_1 + 2E_2.$$

Both A_1 and E_1 modes are polar phonons and can be divided into transverse (TO) and longitudinal (LO) optical phonons. Non-polar phonon modes with symmetry E_2 have two frequencies, E_2 (H) that is associated with oxygen atoms, and E_2 (L) that is associated with the Zn sublattice. Among the optical modes, only A_1 , E_1 and E_2 modes are Raman active for ZnO single crystalline materials [35-38]. A sharp band at 438 cm^{-1} which belongs to the high- E_2 mode of non-polar optical phonons is observed for all samples. This shows that the samples obtained possess the characteristic band of the hexagonal wurtzite phase and further confirms that the nanorods formed are of good crystal quality [31, 36-38]. The intensity of

the high- E_2 increased with the exposure time, which indicated the improved crystalline structure at longer hydrothermal growth time. Meanwhile, bands at 331 and 384 cm^{-1} can be associated with the $3E_{2H}$ - E_{2L} and $A_1(\text{TO})$ modes of ZnO, respectively [36]. The broad band at approximately 561 cm^{-1} corresponds to the $E_1(\text{LO})$ mode of ZnO associated with oxygen deficiency. The lower intensity of the band at $E_1(\text{LO})$ shows that oxygen deficiency was reduced with longer hydrothermal growth time from 4 to 24 h. Stronger $E_2(\text{H})$ mode and weaker $E_1(\text{LO})$ mode imply improved crystallinity of the ZnO nanorods formed with prolonged hydrothermal growth time [39].

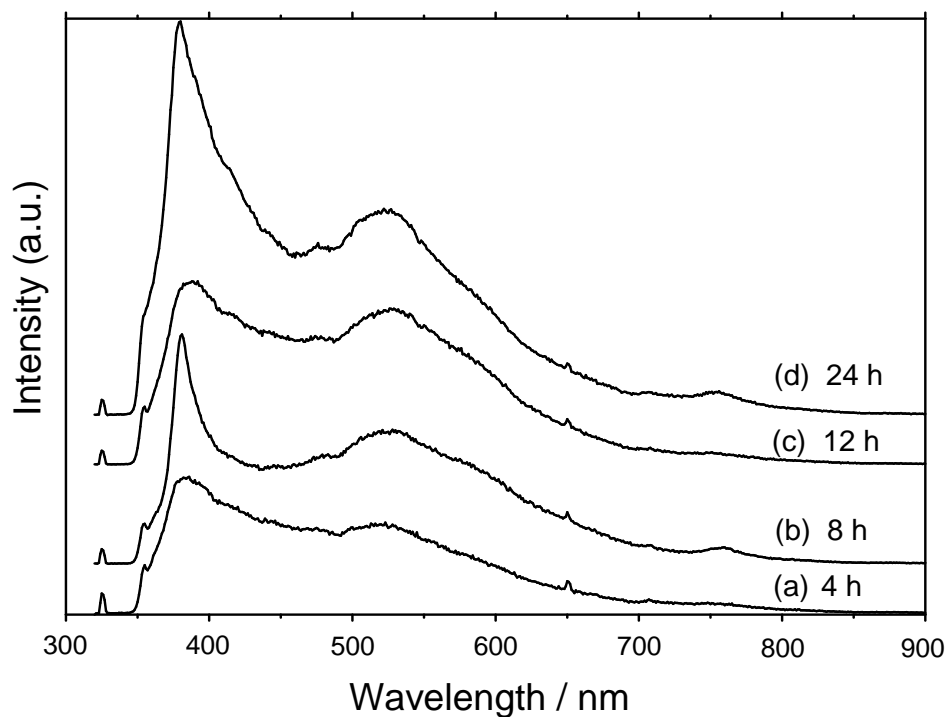


Figure 4: PL spectra for ZnO nanorod arrays formed on seeded ITO by hydrothermal growth at 80°C for (a) 4 h, (b) 8 h, (c) 12 h, and (d) 24 h.

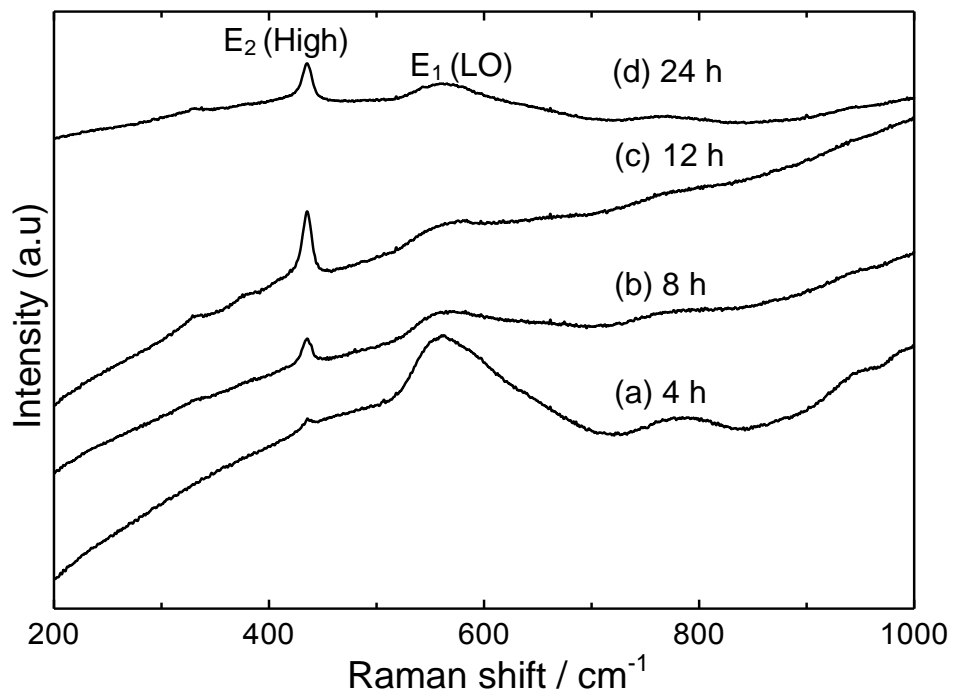


Figure 5: Raman spectra of the hydrothermally grown ZnO nanorod arrays on seeded ITO at 80°C for (a) 4 h, (b) 8 h, (c) 12 h and (d) 24 h.

4.1.3.4 DSSC efficiency measurement

The current density voltage (J-V) characteristics for the dye-sensitized solar cell fabricated using well-aligned ZnO nanorods on ITO for 4, 8, 12, and 24 h are shown in Figure 6. The solar cell conversion efficiency is given as $\eta = (J_{SC} \times V_{OC} / P_{in}) \times FF$ where J_{SC} is the short-circuit current density, V_{OC} is the open circuit voltage, FF is the fill factor and P_{in} is the incident light power. Table 1 summarizes the conversion efficiency obtained. As seen from Table 1, the conversion efficiency increased with hydrothermal exposure time from 4, 8, 12 and 24 h with the value of 0.065, 0.133 0.186 and 0.221%, respectively. This is influenced by the increment of the current density as shown in Table 1 from 0.42, 0.56 0.81 and 0.86 mA/cm² for the nanorods formed after 4, 8, 12 and 24 h, respectively. The improved crystallinity of the ZnO nanorods formed at longer hydrothermal time proven earlier also led to higher fill factor [22]. As the hydrothermal exposure time increased from 4 to 8 h, the average diameter of the ZnO nanorods doubled from 100 nm to 230 nm. At the initial process, HMT decomposed to produce hydroxyl ions and in later stages, HMT serves as the non-polar chelating agent that retards the radial growth of the nanorods. Therefore, diameter maintained after 12 h and increased slightly to 250 nm after prolong hydrothermal exposure of 24 h. Therefore, the increment in length of the nanorods with longer hydrothermal exposure provides higher adsorption surface area and offers a better and more effective pathway for the electron transportation throughout the photoelectrode [8]. The conversion efficiency of the dye-sensitized solar cell can be improved by controlling the length of the ZnO nanorods that serve as the photo electrode [3]. Gao *et al.* compared the conversion efficiency of well-aligned ZnO nanorods formed by a one-step continuous growth for 10 h to a discrete multi-step route for 48 h where fresh solution was introduced every 6 h and obtained conversion efficiency of 0.08 % and 0.32 %, respectively [8]. Relatively, the conversion efficiency we obtained was higher (0.13 % at 80°C for 8 h) compared to the one-step continuous growth

reported by Gao *et al.* (0.08 % at 140°C for 10 h). Our results showed that prolonged hydrothermal reaction time could enhance the conversion efficiency using a single reactive bath at low-temperature.

Deposition time (h)	J _{sc} (mA/cm ²)	I _{sc} (mA)	V _{oc} (mV)	FF (%)	PCE, η (%)
4	0.42	0.42	0.70	0.22	0.065
8	0.56	0.56	0.77	0.31	0.133
12	0.81	0.81	0.75	0.31	0.186
24	0.86	0.86	0.69	0.37	0.221

Table 1: Photovoltaic efficiency of the dye sensitized ZnO nanorod arrays as the photoelectrodes at different hydrothermal exposure time at 80°C on ITO.

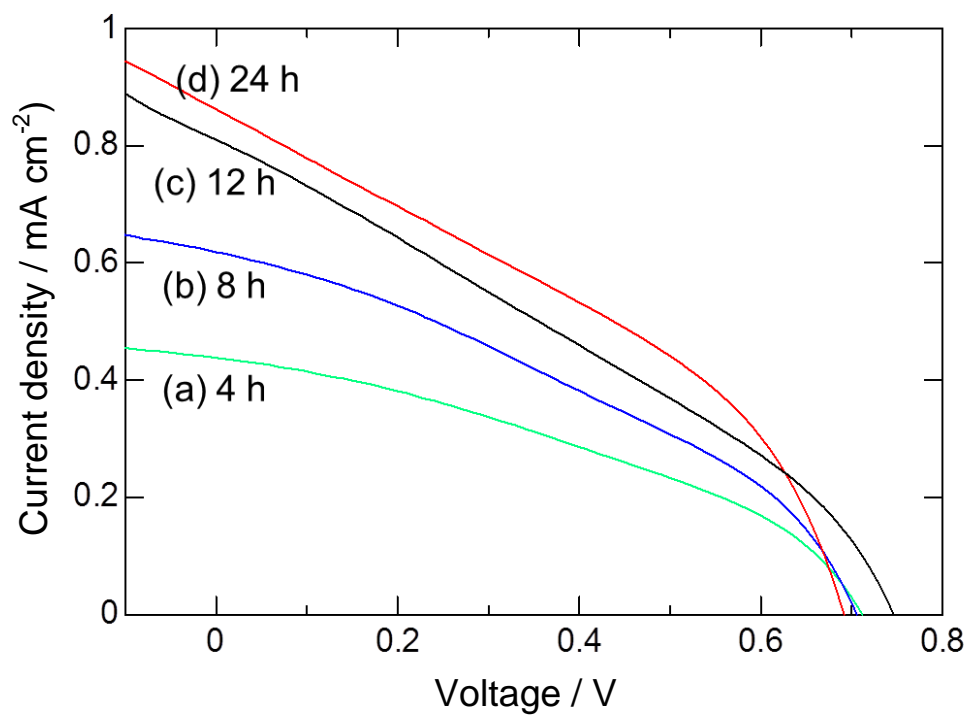


Figure 6: DSSCs conversion efficiency for ZnO nanorod arrays hydrothermally grown on seeded ITO at 80°C for (a) 4 h, (b) 8 h, (c) 12 h and (d) 24 h.

4.1.3.5 ZnO nanorods growth mechanism

During the hydrothermal reaction, the presence of HMT, a non-ionic ligand, promotes the oriented growth of ZnO nanorod arrays. HMT adherence to the six prismatic side planes of wurtzite ZnO crystals hinders the radial growth and allows growth along the c-axis, thus a rod-like structure is formed [40]. The HMT chelated to the non-polar surfaces of the nanorods prevented radial growth by inhibiting the absorption of Zn^{2+} ions. The temperature adopted for the hydrothermal reaction must be high enough to allow decomposition of HMT to supply hydroxyl ions for the formation of ZnO as described equations (1) and (2), and 80°C is adequate for the mentioned reaction to take place. When a sufficient amount of OH^- presence, the hydrothermal solution reaches supersaturation and Zn ions will react with OH^- to form ZnO as shown in equations (3) and (4).



The formation of ZnO nanocrystals during the early stage of the process is also crucial to provide heterogeneous nucleation sites for ZnO formation. Therefore, seed layers play an important role for the subsequent growth of ZnO nanorod arrays. Because ZnO is a polar crystal, each Zn atom is tetrahedrally coordinated to four O atoms, and vice versa. The alternating arrangement of Zn^{2+} and O^{2-} ions along the c-axis gives either positive or negative charges depending on the terminating ions. The electrostatic charges attract the ions of opposite charge and lead to the accumulation of $\text{Zn}(\text{OH})_2$ or $\text{Zn}(\text{OH})_2(\text{NH}_3)_4$ on the existing grains. From the comparison between the ZnO nanorods formed after 4 and 8 h of hydrothermal exposure, short nanorods of about 150 nm are observed compared to the length of 1 μm after 8 h. This shows that adequate time is required for the decomposition of HMT to

supply sufficient OH^- ions to react with the Zn ions presence in the solution [31, 41]. However, at prolonged exposure time of 24 h, recrystallization and the consumption of the smaller rods to form larger rods by Ostwald ripening phenomenon will occur as highlighted in circles in Figure 1(d). The continuous dissolution-recrystallization process that takes place during the hydrothermal process improves the crystallinity of the ZnO nanorods at prolonged hydrothermal reaction time, which leads to better electron transport and higher conversion energy.

Generally, in the fabrication of DSSC, the dye sensitization plays a crucial role in order to obtain good solar conversion efficiency. Most of the dye solutions used for DSSC application are catered for TiO_2 and are done by immersing the film into a typical ethanolic dye solution. The carboxyl groups function as anchoring group for the dye molecules onto the TiO_2 surface and favor monolayer formation. However, the sensitization process for ZnO is more complex due to the dissolution of the ZnO surface caused by the proton from the acidic carboxyl groups, which subsequently leads to the formation of Zn^{2+} /dye complex in the nanostructured film. The dissolution of ZnO and Zn^{2+} /dye complex formation could cause the filter effect that reduces the conversion efficiency of the DSSC [42].

4.1.4 CONCLUSION

Well-aligned, oriented single crystal ZnO nanorod arrays were formed on ITO by hydrothermal reaction at a low temperature of 80°C at different exposure of 4, 8, 12 and 24 h. The effect of prolonged hydrothermal growth time on the ZnO nanorods was investigated systematically. PL measurements of the nanorods showed two major bands in the UV and green regions. XRD, HR-TEM and SAED analyses indicated that the ZnO nanorods possessed a single crystal wurtzite structure with a preferred (0001) growth plane. Prolonged hydrothermal growth time led to longer ZnO nanorods with improved crystallinity, which

directly influenced the conversion efficiency of the DSSCs fabricated. The maximum conversion efficiency of 0.22% was obtained for the ZnO nanorods formed after 24 h of exposure using single a reactive bath. The lower conversion efficiency for ZnO based DSSC obtained compared to TiO₂ is caused by the dye sensitization mechanism. The acidic condition of the dye solution resulted in the dissolution of the ZnO interface and formation of Zn²⁺/dye complexes. The conversion efficiency can be further improved by researching on the new type of anchoring group and controlling the reaction at the oxide/dye/electrolyte interface.

REFERENCES

- [1] Natsume Y, Sakata H. Zinc oxide prepared by sol-gel spin-coating. *Thin Solid Films* 2000; 372: 30-36.
- [2] Xie J, Wang Hu, Duan M, Zhang L. Synthesis and photocatalysis properties of ZnO structures with different morphologies via hydrothermal method. *Applied Surface Science* 2011; 257: 6358-6363.
- [3] Kumar RS, Sudhagar P, Matheswaran P, Sathyamoorthy R, Kang YS. Influence of seed layer treatment on ZnO growth morphology and their device performance in dye-sensitized solar cells. *Materials Science and Engineering B* 2010; 172: 283-288.
- [4] Hames Y, Alpaslan Z, Kosemen A, San SE, Yerli Y. Electrochemically grown ZnO nanorods for hybrid solar cell applications. *Solar Energy* 2010; 84: 426-431.
- [5] Uthirakumar P, Kang JH, Senthilarasu S, Hong CH. The different types of ZnO materials on the performance of dye-sensitized solar cells. *Physica E* 2011; 43:1746-1750.
- [6] Lee YM, Yang HW. Optimization of processing parameters on the controlled growth of ZnO nanorod arrays for the performance improvement of solid-state dye-sensitized solar cells. *Journal of Solid State Chemistry* 2011; 184:615-623.

- [7] Mou J, Zhang W, Fan J, Deng H, Chen W. Facile synthesis of ZnO nanobullets/nanoflakes and their applications to dye-sensitized solar cells. *Journal of Alloys and Compounds* 2011; 509: 961-965.
- [8] Fu YS, Sun J, Xie Y, Liu J, Wang LH, Du XW. ZnO hierarchical nanostructures and application on high-efficiency dye-sensitized solar cells. *Materials Science and Engineering B* 2010; 166:196-202.
- [9] Gao H, Fang G, Wang M, Liu N, Yuan L, Li C, Ai L, Zhang J, Zhou C, Wu S, Zhao X. The effect of growth conditions on the properties of ZnO nanorod dye-sensitized solar cells. *Materials Research Bulletin* 2008; 43:3345-3351.
- [10] Suh DI, Lee SY, Kim TH, Chun JM, Suh EK, Yang OB, Lee SK. The fabrication and characterization of dye-sensitized solar cells with a branched structure of ZnO nanowires. *Chemical Physics Letters* 2007; 442:348-353.
- [11] Umar A, Al-Hajry A, Hahn YB, Kim DH. Rapid synthesis and dye-sensitized solar cell applications of hexagonal shaped ZnO nanorods. *Electrochimica Acta* 2009; 54:5358-5362.
- [12] Al-Hajry A, Umar A, Hahn YB, Kim DH. Growth, properties and dye-sensitized solar cells-application of ZnO nanorods grown by low-temperature solution process. *Superlattices and Microstructures* 2009; 45:529-534.
- [13] Yuan K, Yin X, Li J, Wu J, Wang Y, Huang F. Preparation and DSC application of size-tuned ZnO nanoarrays. *Journal of Alloys and Compounds* 2010; 486:694-699.
- [14] Lupan O, Guerin VM, Tiginyanu IM, Ursaki VV, Chow L, Heinrich H, Paupore T. Well-aligned arrays of vertically oriented ZnO nanowires electrodeposited on ITO-coated glass and their integration in dye sensitized solar cells. *Journal of Photochemistry and Photobiology A* 2010; 211:65-73.

- [15] Karst N, Rey G, Doisneau B, Roussel H, Deshayes R, Consonni V, Ternon C, Bellet D. Fabrication and characterization of a composite ZnO semiconductor as electron transporting layer in dye-sensitized solar cells. *Materials Science and Engineering B* 2011; 176:653-659.
- [16] Qiu J, Guo M, Feng Y, Wang X. Electrochemical deposition of branched hierarchical ZnO nanowire array and its photoelectrochemical properties. *Electrochimica Acta* 2011; 56:5776-5782.
- [17] Huang Q, Fang L, Chen X, Saleem M. Effect of polyethyleneimine on the growth of ZnO nanorod arrays and their application in dye-sensitized solar cells. *Journal of Alloys and Compounds* 2011; 509:9456-9459.
- [18] Gonzales-Valls I, Yu Y, Ballesteros B, Oro J, Lira-Cantu M. Synthesis conditions, light intensity and temperature effect on the performance of ZnO nanorods-based dye sensitized solar cells. *Journal of Power Sources* 2011; 196:6609-6621.
- [19] Rani S, Suri P, Shishodia PK, Mehra RM. Synthesis of nanocrystalline ZnO powder via sol-gel route for dye-sensitized solar cells. *Solar Energy Materials and Solar Cells* 2008; 92:1639-1645.
- [20] Masuda Y, Kato K. Aqueous Synthesis of ZnO Rod Arrays for Molecular Sensor. *Crystal Growth & Design* 2009; 9:3083-3088.
- [21] Wang B, Kerr LL. Dye sensitized solar cells on paper substrates. *Solar Energy Materials & Solar Cells* 2011; 95:2531-2535.
- [22] Chung J, Lee J, Lim S. Annealing effects on ZnO nanorods on dye-sensitized solar cell efficiency. *Physica B* 2010; 405:2593-2598.
- [23] Lu L, Li R, Fan K, Peng T. Effects of annealing conditions on the photoelectrochemical properties of dye-sensitized solar cells made with ZnO nanoparticles. *Solar Energy*; 84:844-853.

- [24] Chen J, Li C, Song JL, Sun XW, Lei W, Deng WQ. Bilayer ZnO nanostructure fabricated by chemical bath and its application in quantum dot sensitized solar cell. *Applied Surface Science* 2009; 255: 7508-7511.
- [25] Guo M, Diao P, Wang X, Cai S. The effect of hydrothermal growth temperature on preparation and photoelectrochemical performance of ZnO nanorod arrays. *Journal of Solid State Chemistry* 2005; 178:3210-3215.
- [26] Santos AMP, Santos EJP. High quality c-axis orientated thin ZnO film obtained at very low pre-heating temperature. *Materials Letters* 2007; 61:3432-3435.
- [27] Zhang CY, Li XM, Zhang X, Yu WD, Zhao JL. Seed-layer induced growth of high quality orientated ZnO films by a sol-gel process. *Journal of Crystal Growth* 2006; 290: 67-72.
- [28] Teki R, Parker TC, Li H, Koratkar N, Lu TM, Lee S. Low temperature synthesis of single crystalline ZnO nanorods by oblique angle deposition. *Thin Solid Films* 2008; 516: 4993-4996.
- [29] Ting CC, Li CH, Kuo CY, Hsu CC, Wang HC, Yang MH. Compact and vertically-aligned ZnO nanorod thin films by low-temperature solution method. *Thin Solid Films* 2010; 518:4156-4162.
- [30] Song J, Baek S, Lim S. Effect of hydrothermal reaction conditions and optical properties of ZnO nanorods. *Physica B* 2008; 403:1960-1963.
- [31] Lockman Z, Yeo PF, Tan WK, Ibrahim K, Abdul Razak K. Formation of self-aligned ZnO nanorods in aqueous solution. *Journal of Alloys and Compounds* 2010; 493:699-706.
- [32] Tan WK, Abdul Razak K, Ibrahim K, Lockman Z. Formation of ZnO nanorod arrays on polytetrafluoroethylene (PTFE) via a seeded growth low-temperature hydrothermal reaction. *Journal of Alloys and Compounds* 2011; 509:820-826.

- [33] Pei LZ, Zhao HS, Tan W, Yu HY, Chen YW, Zhang QF. Single crystalline ZnO nanorods grown by simple hydrothermal process. *Materials Characterization* 2009; 60: 1063-1067.
- [34] Qiu M, Ye Z, Lu J, He H, Huang J, Zhu L, Zhao B. Growth and properties of ZnO nanorods and nanonails by thermal evaporation. *Applied Surface Science* 2009;255:3972-3976
- [35] Gupta V, Bhattacharya P, Yuzuk, Yu I, Sreenivas K, Katiyar RS. Optical phonon modes in ZnO nanorods on Si prepared by pulsed laser deposition. *Journal of Crystal Growth* 2006; 287:39-43.
- [36] Park WI, Jun YH, Jung SW, Yi G-C. Exciton emissions observed in ZnO single crystal nanorods. *Applied Physics Letters* 2003; 82:964-971.
- [37] Zhang R, Yin PG, Wang N, Guo L. Photoluminescence and Raman scattering of ZnO nanorods. *Solid State Sciences* 2009; 11:865-869.
- [38] Lupan O, Pauporte T. Hydrothermal treatment for the marked structural and optical quality improvement of ZnO nanowire arrays deposited on lightweight flexible substrates. *Journal of Crystal Growth* 2010; 312:2454-2458.
- [39] Tan WK, Abdul Razak K, Lockman Z, Kawamura G, Muto H, Matsuda A. Formation of highly crystallized ZnO nanostructures by hot-water treatment of etched Zn foils. *Materials Letters* 2013; 91:111-114.
- [40] Sugunan A, Hemant C, Boman M, Dutta J. Zinc oxide nanowires in chemical bath on seeded substrates: Role of hexamine. *Journal of Sol-Gel Science and Technology* 2006;39:49-56.
- [41] Hu X, Masuda Y, Ohji T, Kato K. Micropatterning of ZnO Nanoarrays by Forced Hydrolysis of Anhydrous Zinc Acetate. *Langmuir* 2008; 24:7614-7617.

[42] Boschloo G, Edvinsson T, Hagfeldt A. Dye-sensitized Nanostructured ZnO Electrodes for Solar Cell Applications. Nanostructured Materials for Solar Energy Conversion: Elsevier B.V.; 2006.

4.2 SYNTHESIS OF ZnO NANOROD-NANOSHEET COMPOSITE VIA FACILE HYDROTHERMAL METHOD AND THEIR PHOTOCATALYTIC ACTIVITIES UNDER VISIBLE LIGHT IRRADIATION

4.2.1 INTRODUCTION

Zinc oxide (ZnO) can be prepared in nanostructures with varying dimensions and shapes. This oxide ceramic has unique properties which allow it to be used as a transparent conducting ceramic oxide for photocatalyst [1], field emitters [2] and dye-sensitized solar cells [3]. Various one-dimensional (1D), two-dimensional (2D) and three-dimensional (3D) ZnO nanostructures have drawn widespread interest from researchers because of their multi-functional properties, leading to possible applications in existing and emerging electronic and optoelectronic industries [4]. For example, in the form of 1D nanorod arrays, ZnO can be used as active layers in emission devices, and as electrodes in dye sensitized solar cells and photovoltaic solid state solar cells. These structures have improved optical absorption properties, and their excellent crystallinity enhances electronic transportation. ZnO in the form of nanotubes, nanorods or nanowires can be produced by various physical [5] and chemical methods, including sol-gel and hydrothermal processes [6-12]. Hierarchical ZnO nanostructures with multi-scale configurations consisting of ZnO nanosheets and nanorods were demonstrated by Qiu *et al.* with the aim of achieving a higher internal surface area for photoelectrodes [13]. Besides that, ZnO ability to effectively degrade various waste water organic compounds by simple oxidation and reduction reactions has been explored for photocatalytic applications under solar irradiation in UV-visible region [1, 14-17].

Despite the successful formation of the desired aligned nanostructures, research efforts continue to focus on the formation of ZnO nanorods and on mixtures of nanostructures, like nanorods and nanosheets, through viable, cost-effective and near-room temperature

processes. The enrichment of the surface region of the 1D nanostructure is important, because the hierarchical and complex ZnO nanoarchitecture has stimulated considerable interest in the 2D structures. When the two structures can be made to co-exist on the same substrate, it is expected that unique properties that cannot be found in mono-morphological structures could be obtained [18]. ZnO nanosheets with larger surface areas could enhance the electronic and photocatalytic properties of the structures [19]. Simultaneous formation of ZnO nanorod arrays and nanosheets by hydrothermal processes has rarely been reported. In our work, ZnO crystallites in the forms of both nanorods and nanosheets were produced on glass substrates. The formation of these nanostructures was explored, focusing on the effects of the time of development for both nanosheets and nanorods. To the authors' knowledge, this is the first work to report on the simultaneous formation of ZnO nanorod arrays and nanosheets using a hydrothermal process. The ZnO nanorod array and nanosheet structures obtained were single crystalline and polycrystalline, respectively, and were formed without any post-annealing treatment. The crystal structures, optical properties, mechanism and the photocatalytic activity of the nanostructures obtained were also investigated.

4.2.2 EXPERIMENTAL

A ZnO sol was prepared from zinc acetate dihydrate (ZnAc) (Wako, 99%) and diethanolamine (DEA) (Wako, 99%) using water (H₂O) and 2-propanol (2-PrOH) as the solvent. The molar ratio of ZnAc:DEA:H₂O:2-PrOH was 1:1:1:20. Non-alkaline glass substrates were dip-coated at room temperature in the ZnO sol by inserting with a down-speed of 5 mm/s, holding for 10 s, and then withdrawing with an up-speed of 2 mm/s. The ZnO-coated glass substrate was dried at room temperature and was then placed in an oven at 100°C for 15 min. These steps were repeated twice and the slide was then heated at 300°C for

10 min to induce a phase transformation. The glass substrate with the seed layer was then placed in a stainless steel Teflon-lined vessel containing a hydrothermal bath. The bath consisted of zinc nitrate (ZnN) (Sigma-Aldrich, 99%) and hexamethylenetetramine (HMTA) (Sigma-Aldrich, 98%) with a ZnN:HMTA molar ratio of 1:1, as described in previously reported work [20,21]. The vessel was placed in an oven at 80°C for 4 h, 12 h or 24 h.

After cleaning, the surface morphologies of the ZnO layer on the glass substrate were viewed using a field emission scanning electron microscope (FE-SEM, Hitachi S-4800). X-ray diffraction (XRD) patterns of the ZnO layer were obtained using an X-ray diffractometer (Rigaku RINT 2500) with CuK α radiation. The ZnO nanostructures produced were investigated with a high-resolution transmission electron microscope (HR-TEM, JEOL JEM-2100F) at an acceleration voltage of 200 kV. Photoluminescence (PL) studies were performed using monochromatic beam generated from He-Cd laser with a wavelength of 325 nm and recorded using a monochromator (Nikon G250, Japan), and Raman spectroscopy measurements were performed using a Raman laser spectrometer (Jasco NSR-3100) with a laser wavelength of 532 nm. The photocatalytic activity was examined by the exposure of ZnO nanorods and nanosheets composite structure with 1cm² surface area to 50 mL methylene blue solution (MB, Wako, Japan) under visible-light irradiation with ~50 mW cm⁻² intensity (Hayashi Me-180, Japan) for 1 to 5 h. Optical filters were used to limit visible-light region within the wavelength of 480-800 nm during the photo-degradation test. Samples that consisted of only ZnO nanorods formed by hydrothermal of the sol-gel seeded layer in inverse position were compared. The residue concentration of the MB was determined by measuring its absorbance at ~ 663 nm using V-560 ultraviolet/visible spectrometer (UV/Vis, Jasco, Japan). The photocatalytic degradation (PD) was evaluated from expression: PD= {1-(C/C₀)} x 100%, where C₀ is the concentration of pristine MB (~20 ppm) and C is the concentration of MB after irradiation.

4.2.3 RESULTS AND DISCUSSION

4.2.3.1 Sol-gel seed layer

Prior to hydrothermal growth, nanoscale crystalline seed layers were coated as they are indispensable for the growth of well-oriented ZnO nanorods by hydrothermal reaction [10, 21-24]. SEM images of the sol-gel derived ZnO seed layer after heat treatment at 300°C for 10 min are presented in Fig. 1. The surface of the ZnO seed layer appears homogenous at low magnification, while the ZnO grains are resolved at higher magnification (inset). The XRD pattern of the seed layer indicated c-axis orientation in the (002) plane, as shown in Fig. 2, where the peak at 34.42° that correlates to the ZnO (002) reflection can be observed. The average grain size of the seed layers after heat treatment is approximately 40 nm. The grain size of the ZnO seed layer affects the subsequent growth of the ZnO nanorod arrays; larger grains induce the formation of larger ZnO nanorods [11, 22, 25]. The sol-gel coating thickness is approximately 1.5 μm, as shown in Fig. 1(b).

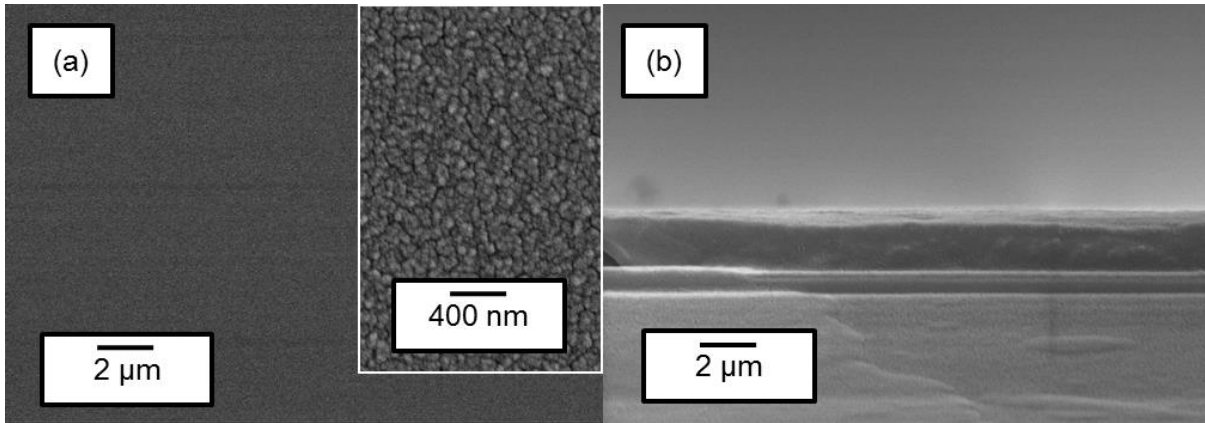


Fig. 1: FE-SEM morphology images of (a) the surface at low and high (inset) magnifications, and (b) a cross-sectional view of the sol-gel dip-coated layer on non-alkaline glass after heat treatment at 300°C for 10 min.

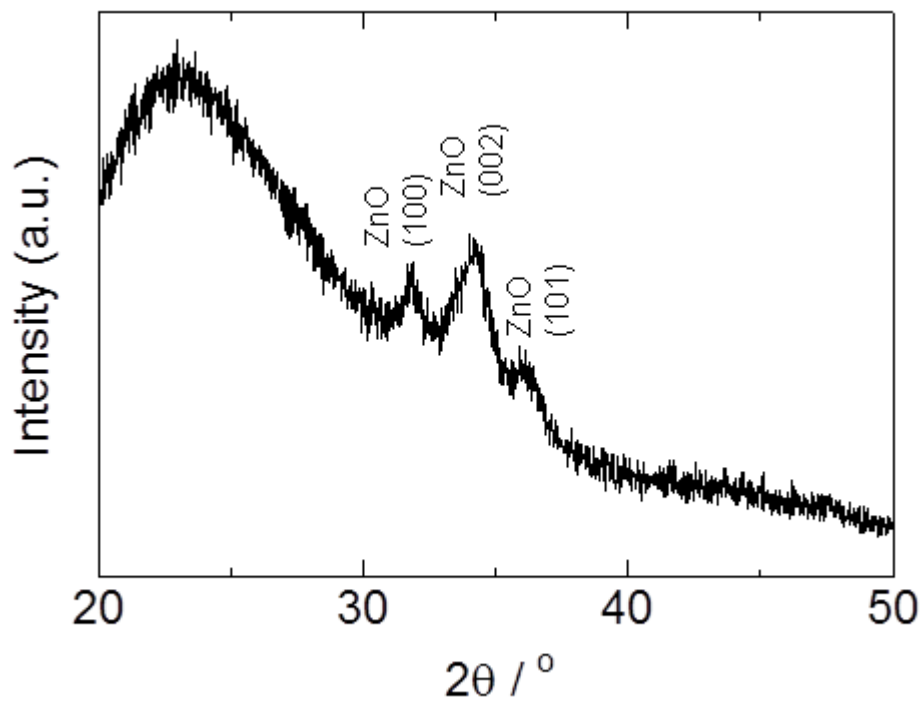


Fig. 2: XRD pattern of the ZnO sol-gel derived seed layer after heat treatment at 300°C for 10 min.

4.2.3.2 Morphology and structure of hydrothermally-derived ZnO composite films

Hexagonal ZnO nanorods with diameter of approximately 50 nm and nanosheets could be observed on all of the specimens after hydrothermal growth. The width and density of the nanosheets increased with the hydrothermal exposure time, while the diameter of the ZnO nanorod arrays remained constant at approximately 50 nm. After hydrothermal exposure for 4 h, thin and almost translucent layers of nanosheets (Fig. 3(a)) are seen on the surfaces of the nanorods. When the hydrothermal exposure time was increased to 12 h and 24 h, the density of the nanosheets formed increased, as shown in Fig. 3(b) and (c).

Cross-sectional views of the ZnO nanorod array-nanosheet composite films after hydrothermal reaction for 4, 12 and 24 h are shown in Fig. 4(a), (b) and (c), respectively. The SEM images on the left marked with the symbol (i) and on the right marked with the symbol (ii) are the low and high magnification images. Hexagonal, flat-topped ZnO nanorod arrays are observed after 4 h, indicating rapid ZnO crystal growth along the c-axis. The length of the ZnO nanorods increased from 200 nm after 4 h to 350 nm after 24 h of hydrothermal exposure. The length of the ZnO nanorods is obviously dependent on the duration of the hydrothermal growth process. Meanwhile, the width of the nanosheets increased from about 300 nm after 4 h to approximately 1~2 μm after 24 h. The nanosheet thickness is approximately 11 nm after 24 h of hydrothermal exposure. The density and structure of the nanosheets appear to consolidate with longer hydrothermal exposure times.

The XRD patterns of the ZnO composite films presented in Fig. 5 showed strong peaks at 2θ of 34.42° corresponding to the (002) reflection of ZnO. Peaks at 31.77° and 36.25° related to the (100) and (101) reflections of ZnO were also observed for all of the samples, and thus the spectra were consistent with a typical ZnO wurtzite crystal structure (ICDD 36-1451). The predominant (002) peak indicates that the ZnO nanorod array-

nanosheet composite films exhibit c-axis orientation [26]. The intensity of the (002) plane increased with the hydrothermal exposure time because of the consolidation of the ZnO nanosheets, as seen in the surface morphological observation shown in Fig. 3 [27].

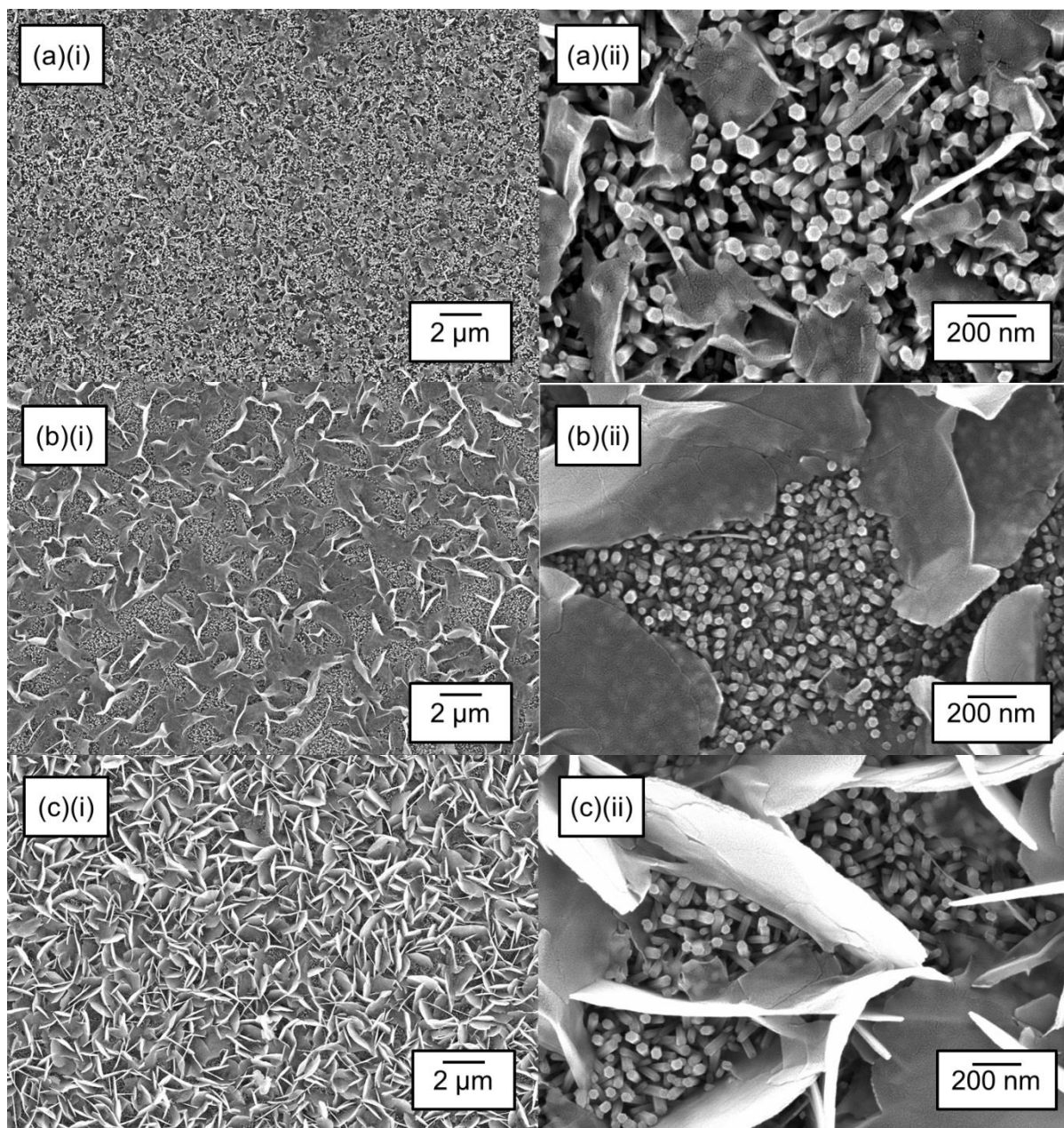


Fig. 3: Surface morphology observations of the ZnO nanorod-nanosheet composite films formed on the sol-gel seed layers after hydrothermal exposure at 80°C for (a) 4 h, (b) 12 h, and (c) 24 h.

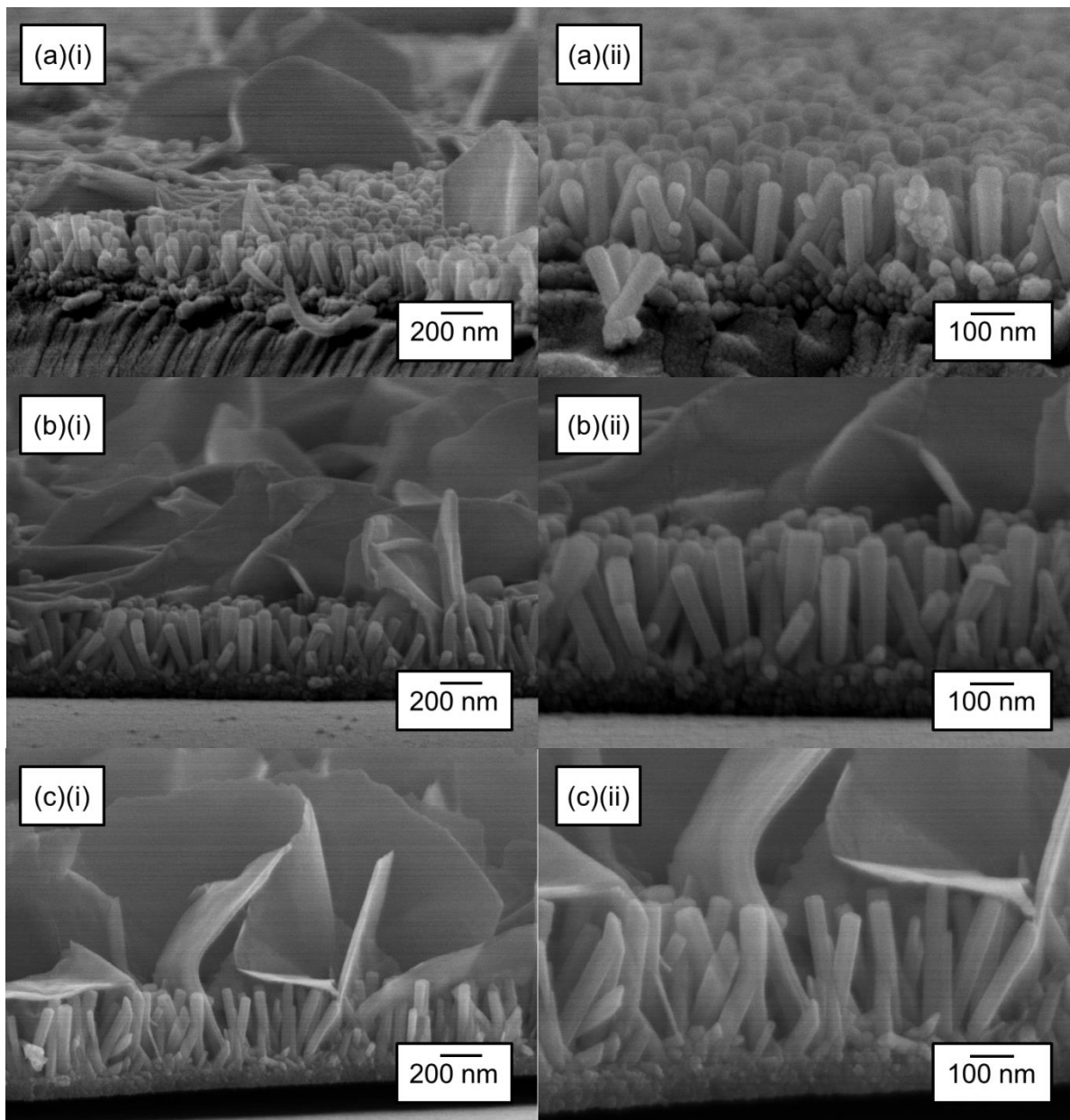


Fig. 4: Cross-sectional SEM images of ZnO nanorod-nanosheet composite films formed on seeded layers after hydrothermal growth at 80°C for (a) 4 h, (b) 12 h, and (c) 24 h.

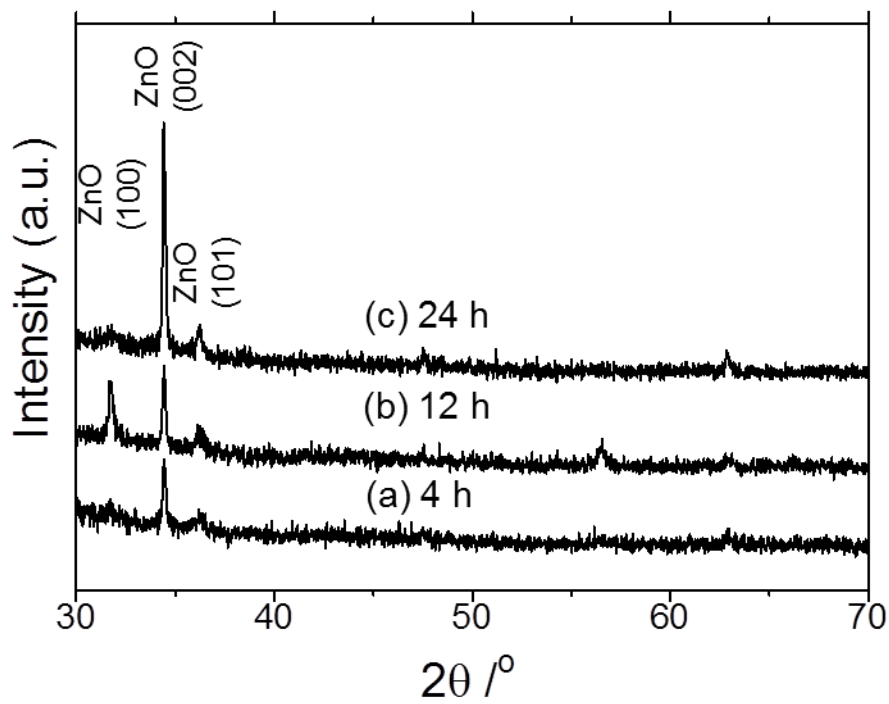


Fig. 5: XRD patterns for the ZnO nanorod-nanosheet composite films formed by growth on sol-gel seeded samples *via* hydrothermal reaction for (a) 4 h, (b) 12 h, and (c) 24 h.

The growth of the ZnO nanorod array is thought to occur *via* a self-assembly mechanism during the hydrothermal process. A schematic illustration of the possible formation mechanism of the ZnO composite nanostructures is shown in Fig. 6. In this mechanism, the presence of HMTA, a non-ionic ligand, encourages the oriented growth of the ZnO nanorod arrays. HMTA hinders the growth of the six prismatic side planes of wurtzite ZnO crystals while allowing growth along the c-axis, and thus the rod-like structure is formed [21, 28]. The chelation of HMTA on the non-polar surfaces of the nanorods prevents radial growth because HMTA inhibits the absorption of Zn²⁺ ions. The temperature used for the hydrothermal reaction must be high enough to cause decomposition of HMTA to supply hydroxyl ions for the formation of ZnO, as described in equations (1) and (2) below. When a sufficient quantity of OH⁻ is present, the hydrothermal solution reaches supersaturation, and the Zn ions will react with OH⁻ to form ZnO, as shown in equations (3) and (4).



The presence of the ZnO nanocrystal seed layer during the initial stage of the process is crucial because it provides heterogeneous nucleation sites for ZnO formation. Because ZnO is a polar crystal, each Zn atom is tetrahedrally coordinated to four O atoms, and vice versa. The alternating arrangement of Zn²⁺ and O²⁻ ions along the c-axis gives either positive or negative charges, depending on the terminating ions. These electrostatic charges attract ions

of the opposite charge and lead to the accumulation of Zn(OH)_2 or $\text{Zn(OH)}_2(\text{NH}_3)_4$ on the existing grains.

As for the nanosheet formation, the use of aqueous solution could promote the formation of the ZnO nanosheets due to the homogenization of the reactants in the medium which could affect the numbers of individual nuclei formed (Fig. 6(b)) as well as the nucleus preferential growth direction [29, 30]. Dissolution of the sol-gel seed layers during hydrothermal reaction could also contribute to the generation of ZnO clusters [30]. Agglomerations of these smaller clusters would then form larger clusters (Fig. 6(c)), and the self-assembly of the active sites could eventually promote the formation of the sheet-like structure that form the nanosheets. After that, the as-formed ZnO nanosheets were re-deposited back onto the substrate surface and were further consolidated with the hydrothermal reaction time (Fig. 6(d)) [31]. Another set of experiments was performed with the seed layer facing the bottom of the vessel during hydrothermal reaction which resulted in the formation of only well-aligned ZnO nanorods and no nanosheets were observed on the substrate surface as shown in Fig. 7. Qin *et al.* also reported the formation of bush-like ZnO nanosheets using a hydrothermal method, but the formation mechanism was not discussed [26]. It is believed that the autogenous pressure generated during the hydrothermal process prompted a higher ZnO nanosheet formation rate. The negative nature of $[\text{Zn(OH)}_4]^{2-}$ could lead to different growth rates for different planes during hydrothermal processing, and HMTA is expected to act as an organic template during the heating process up to 80°C and dynamically modify the nucleation process. With increasing Zn^{2+} and OH^- concentrations, the Zn(OH)_2 or ZnO nuclei developed under low precursor concentrations and the action of HMTA. According to Guo *et al.*, the self-assembly of a number of active sites that trigger nucleation could promote the formation of petal crystals that extend from the interface and result in the sheet-like structure [32]. However, further investigation is necessary to

understand and detail the growth mechanism responsible for the formation of the sheet-like structure. The ZnO nanorods and nanosheets are believed to form simultaneously during the hydrothermal growth process.

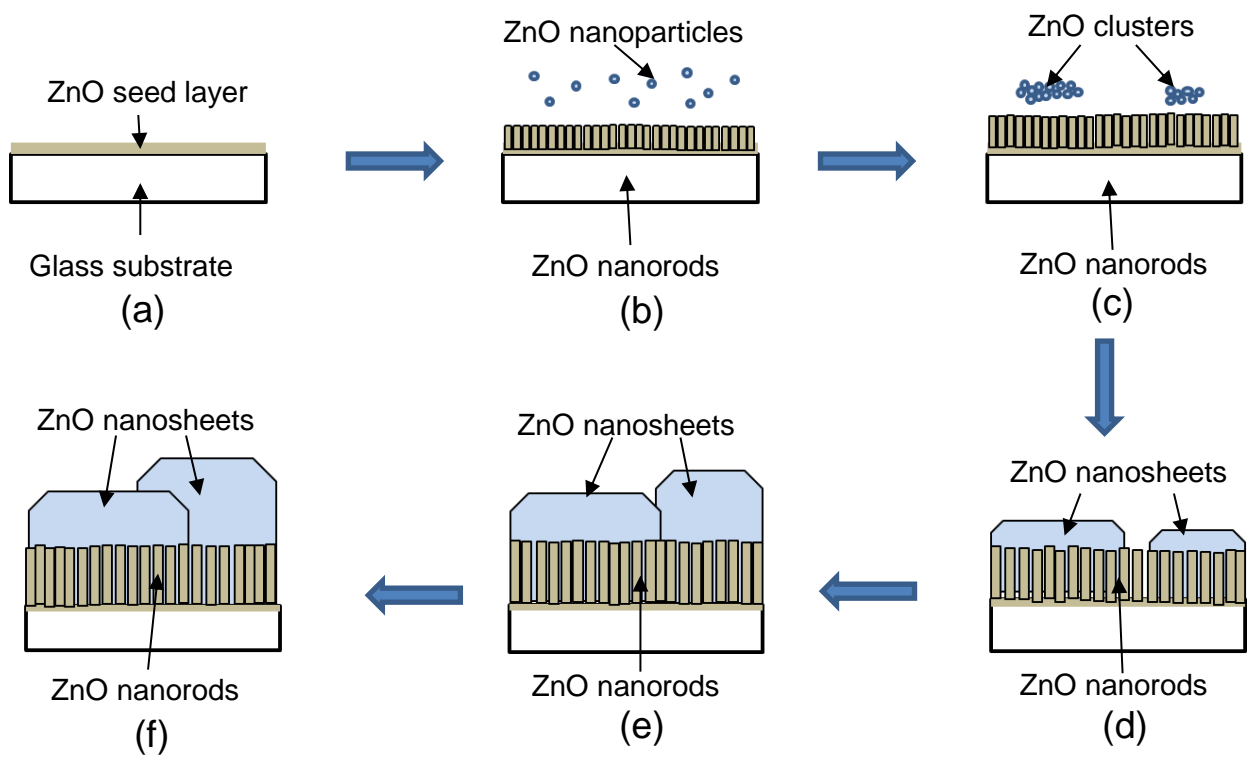


Fig. 6: Schematic illustration of the ZnO nanorod-nanosheet composite formation mechanism.

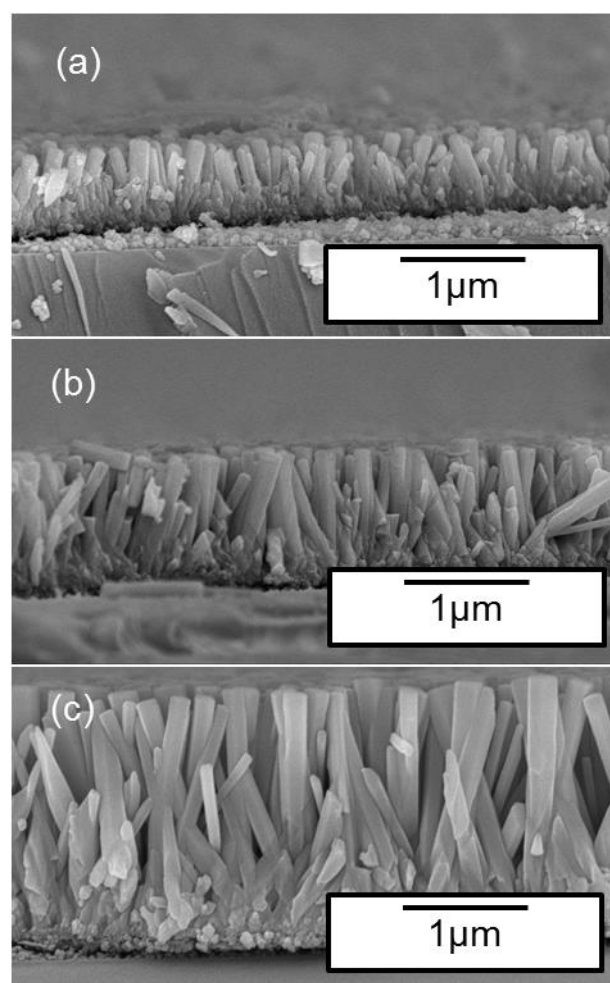


Fig. 7: Cross-sectional SEM images of well-aligned ZnO nanorod arrays formed after hydrothermal growth with the seeded surface facing towards the bottom of the vessel at 80°C for (a) 4 h, (b) 12 h, and (c) 24 h.

4.2.3.3 Luminescence properties

The room temperature PL spectra of the ZnO nanorods are shown in Fig. 8. Bands were observed around 380 nm (UV), 445 nm (blue) and 575 nm (green). The UV emission corresponds to the near band edge emission of the wide band gap of ZnO, which is caused by annihilation of the excitons by recombination [33-35]. The blue and green emissions result from the radiative recombination of photo-generated holes with singularly ionized oxygen vacancies [34] and oxygen-related vacancies [35], respectively. The observed blue emission was attributed to the nanosheets by other researchers, and was considered as having been caused by electron transitions from the shallow donor levels of oxygen vacancies and zinc interstitials to the valence band [36-38]. Wang *et al.* also reported on multiple emissions in the blue-green region for ZnO nanosheets formed by a mediated hydrothermal method [39]. The increasing visible emission with increasing hydrothermal process time could be caused by an increase in the surface defects in the nanosheets [30]. The sharp, intense UV emission indicates that the ZnO composite films formed are highly crystalline with excellent optical properties. HR-TEM images of the samples grown for 24 h were obtained. Fig. 9(a) shows an HR-TEM image of the nanorods and nanosheets. The ZnO nanosheets were polycrystalline, as indicated by the selected area electron diffraction (SAED) pattern shown as an inset in the high-resolution view shown in Fig. 9(b). Lattice fringes of 0.26 nm were observed at different orientations. It can be clearly seen that the nanosheet consisted of an agglomeration of multiple ZnO grains. The HR-TEM image of a single ZnO nanorod with a tip diameter of approximately 45 nm is shown in Fig. 9(c), and is consistent with the SEM results. A high-resolution view of the nanorod is shown in Fig. 9(d) which clearly indicates the 0.52 nm lattice fringes of the ZnO single crystal wurtzite structure at (0001) interplanar spacing. This is supported by the SAED pattern shown in the inset of Fig. 9(c). No defects such as dislocations or stacking faults were observed in the nanorods. The HR-TEM results are

consistent with the XRD results, which confirmed that the ZnO has the same crystal structure and that it grows in the [001] direction [5].

Fig. 10 shows the Raman spectra of ZnO composite films formed after 4, 12 and 24 h of the hydrothermal reaction. The symmetry of the Raman active zone-center optical phonons is represented at the point of the Brillouin zone as follows:

$$\Gamma_{\text{opt}} = A_1 + 2B_1 + E_1 + 2E_2.$$

Both of the A_1 and E_1 modes are polar phonons and can be divided into transverse (TO) and longitudinal optical (LO) phonons. The non-polar phonon modes with symmetry E_2 have two frequencies: E_2 (H), associated with the oxygen atoms, and E_2 (L), associated with the Zn sub-lattice. Among the optical modes, only the A_1 , E_1 and E_2 modes are Raman active for the ZnO single crystalline materials [40-43]. The intensities of the Raman shifts increased with hydrothermal exposure time. Four major peaks were detected at 331, 383, 438 and 580 cm^{-1} in the Raman spectra for the ZnO composite film formed after 24 h exposure. The sharp peak at 438 cm^{-1} belongs to the high- E_2 mode of the non-polar optical phonons, which corresponds to the characteristic band of the hexagonal wurtzite phase. This also confirms that the composite films formed are of good crystal quality [41-44]. The peaks at 331 cm^{-1} and 383 cm^{-1} can be assigned to the $3E_{2H} - E_{2L}$ and A_1 (TO) modes of ZnO, respectively [41,43], while the peak at 580 cm^{-1} corresponds to the E_1 mode caused by an oxygen deficiency [45], which is consistent with the photoluminescence results obtained.

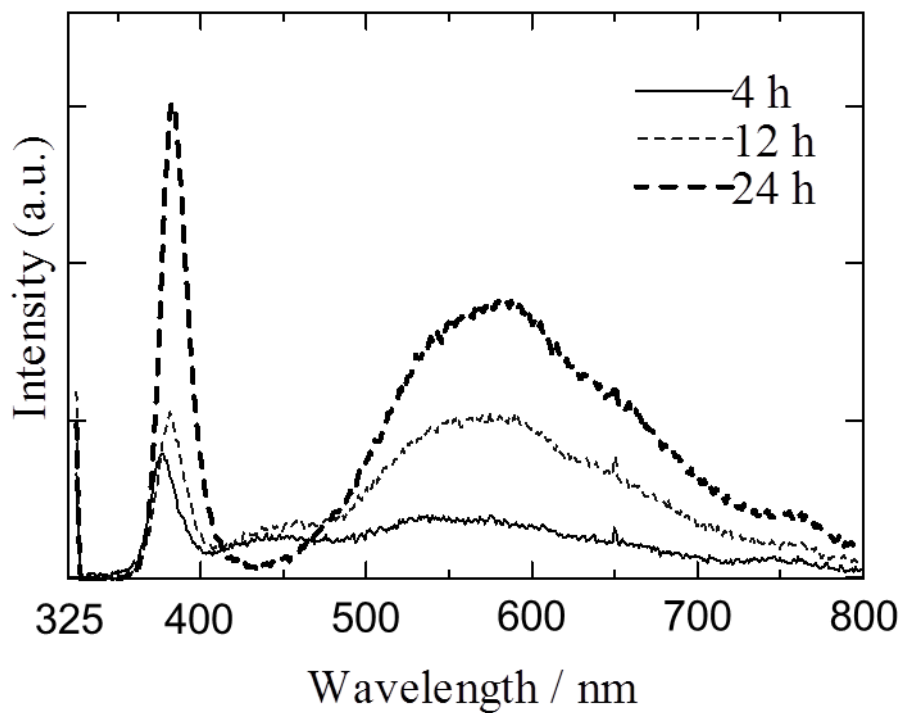


Fig. 8: Photoluminescence spectra of ZnO nanorod-nanosheet composite films formed after hydrothermal reaction at 80°C for 4 h, 12 h, and 24 h.

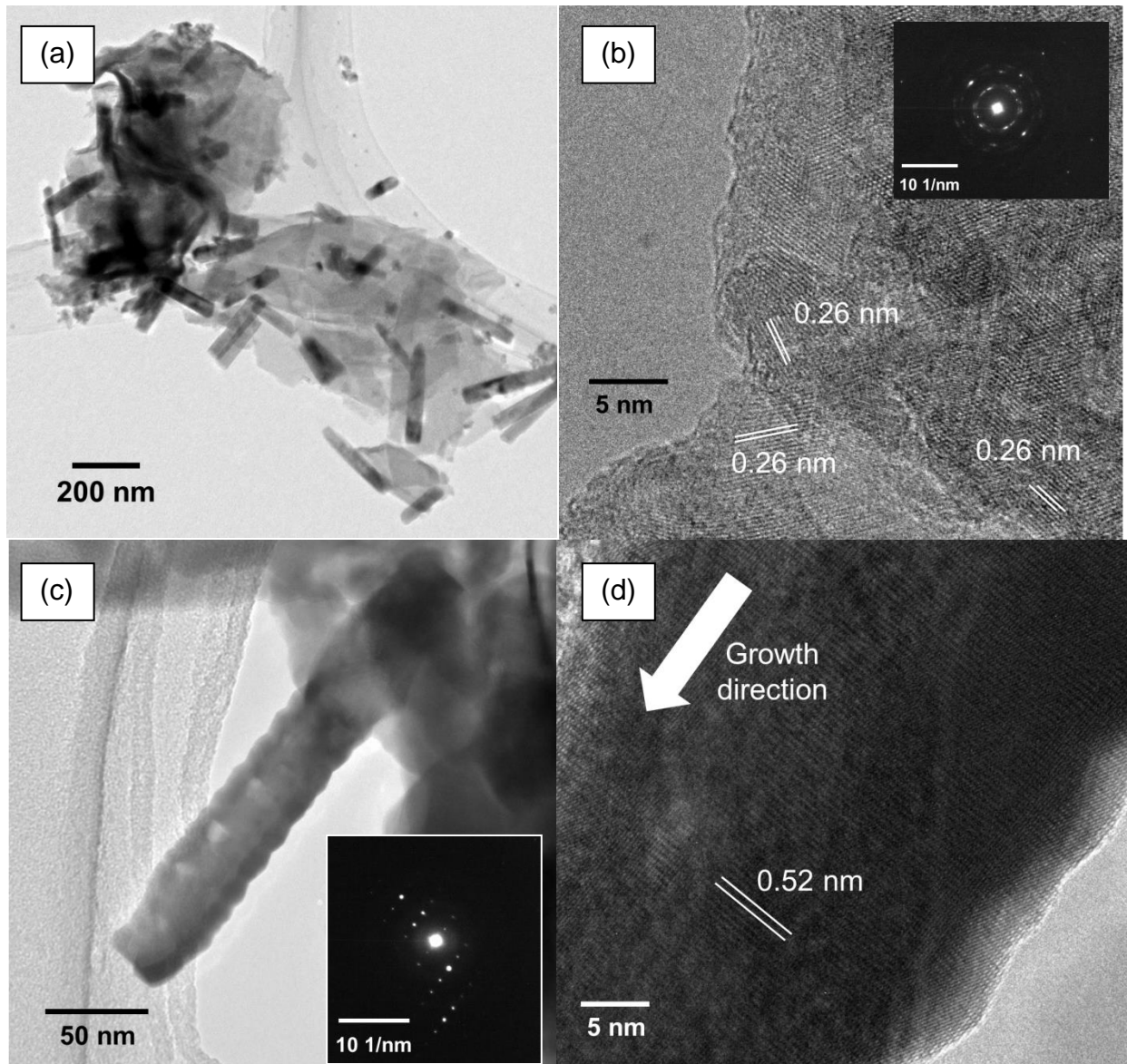


Fig. 9: HR-TEM images of ZnO nanostructures obtained after hydrothermal growth at 80°C for 24 h: (a) TEM image of the ZnO nanostructures, (b) high-resolution image and SAED image (inset) of the ZnO nanosheet, (c) TEM image and SAED image (inset) of a single nanorod, and (d) a high-resolution image of the nanorod.

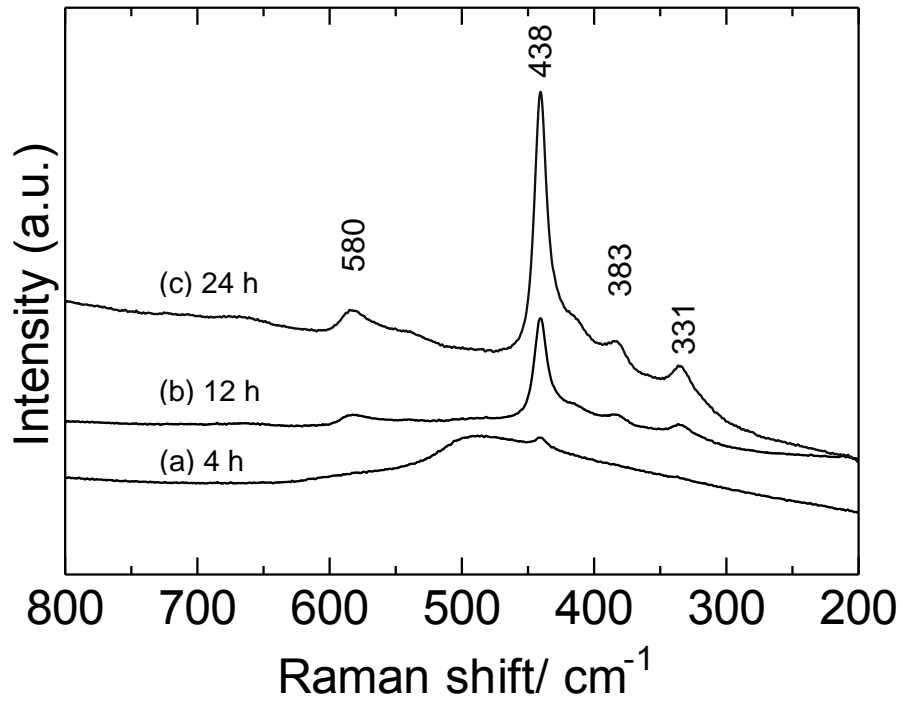


Fig. 10: Raman spectra of the ZnO composite films formed after hydrothermal reaction at 80°C for (a) 4 h, (b) 12 h and (c) 24 h.

4.2.3.4 Photocatalytic activity

The significance of the ZnO nanorod-nanosheet composite structure was evaluated by the de-colorization of MB under visible light irradiation. The photocatalytic activity of only ZnO nanorod arrays grown on the seeded substrate by hydrothermal growth of the seeded surface facing the bottom of the vessel was compared. The photocatalytic activity of the ZnO nanostructures is shown in Fig. 11 which clearly shows the gradual reduction of MB concentration with increasing exposure time as determined from the absorption band intensity of MB positioned at approximately 663 nm. Negligible photo-degradation of MB is observed after exposed to visible light irradiation for 5 h. After 5 h of visible light exposure, the photodegradation exhibits approximately 8 to 11% for the ZnO nanorods grown from 4 to 24 h, respectively. As for the nanorods and nanosheet composite structure generated after 4, 12 and 24 h of hydrothermal reaction, the photodegradation was approximately 20, 24 and 32 %, respectively. The photocatalytic results demonstrate the higher photodegradation activity of nanorods and nanosheet composite structure under visible-light irradiation. Generally, when semiconductor nanocrystals are irradiated by light with energy higher or equal to the band gap, an electron (e_{cb}^-) in the valence band can be excited to the conduction band with the simultaneous generation of a hole (h_{vb}^+) in the valence band [14]. These excited e_{cb}^- and h_{vb}^+ can recombine and get trapped in metastable surface states, or react with electron donors and acceptors adsorbed on the semiconductor surface. The photoelectron is easily trapped by electron acceptors like adsorbed O_2 , whereas the photoinduced holes can be easily trapped by electronic donors such as OH^- or organic pollutants which lead to the oxidation of the organic dyes. Besides that, the photocatalytic activity is not only dependent on the surface adsorption ability, but also relates to the type and concentration of oxygen defects on the surface of the nanostructures. Therefore, the oxygen vacancies generated on the surface of the composite structure can serve as electron capturing centers to restrain the recombination of e_{cb}^- and h_{vb}^+

and could generate active species on the surface of the semiconductor which is beneficial for the photodegradation of organic dye. Tong *et al.* reported that nanosheets structure with more surface defects generated could increase the photo-reactivity. The sheets with unique surface orientation while the particles with random orientation exhibit high density of atomic steps and ledges which serve as active sites for breaking chemical bonds [1,16]. The photocatalytic activity is clearly dependent on the morphology, specific surface area and textures of ZnO nanostructures formed [1, 15, 46].

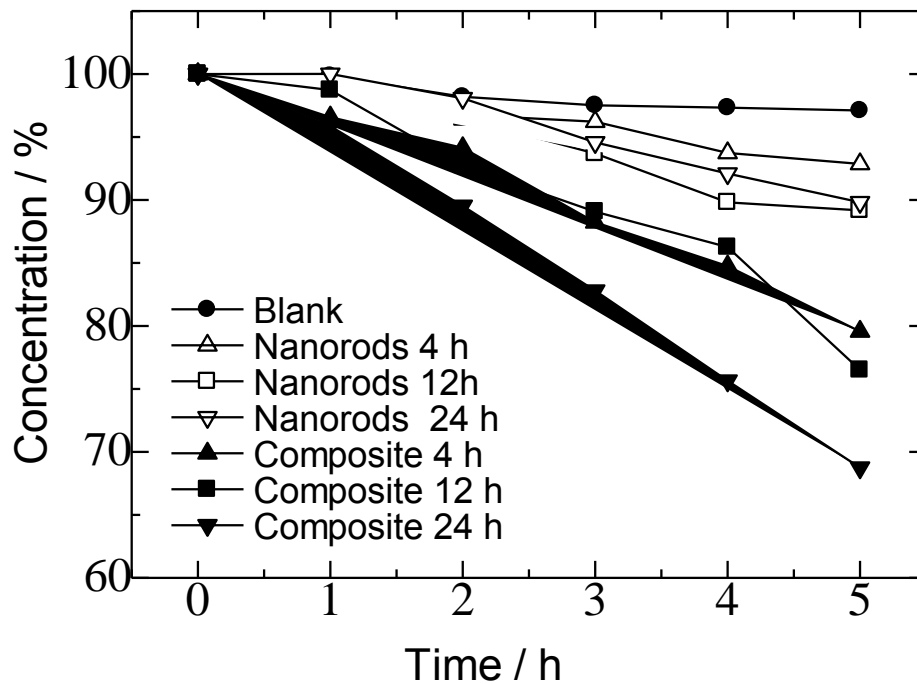


Fig. 11: Visible-light degradation of MB aqueous solution of the ZnO nanorod arrays and ZnO composite structures that consisted of nanorods/nanosheets for 1 to 5 h.

4.2.4 CONCLUSION

Well-aligned and oriented single crystal 1D ZnO nanorod array and 2D nanosheet composite films were successfully prepared using ZnO seed layers in a single step hydrothermal reaction process at a low temperature of 80°C. The photoluminescence of the ZnO composite nanostructures showed major bands in the UV, blue and green regions. XRD, HR-TEM and SAED analyses indicated that the ZnO nanostructures formed consist of single crystal ZnO nanorods and polycrystalline ZnO nanosheets. Low temperature formation using sol-gel-derived ZnO coatings and hydrothermal processing is not only cost effective but also enables the formation of ZnO composite films over a large surface area and the use of substrates with low thermal stability. The ZnO composite structure exhibits higher photocatalytic activity under visible light-irradiation and can be used for photocatalytic degradation of organic dyes. The formation of 2D nanorod and nanosheet composite in a single hydrothermal step is promising for future nanoscale scientific research and applications in photocatalytic and optoelectronic devices.

REFERENCES

- [1] A. Umar, M. S. Chauhan, S. Chauhan, R. Kumar, G. Kumar, S.A. Al-Sayari, S. W. Hwang, A. Al-Hajry, Large-scale synthesis of ZnO balls made of fluffy thin nanosheets by simple solution process: Structural, optical and photocatalytic properties, *J. Colloid Interface Sci.* 363 (2011) 521-528.
- [2] C.-Y. Kuo, R.-M. Ko, Y.-C. Yu, Y.-R. Lin, T.-H. Lin, S.-J. Wang, Tip shaping for ZnO nanorods via hydrothermal growth of ZnO nanostructures in a stirred aqueous solution, *Cryst. Growth Des.* 12 (2012) 3849-3855.

- [3] F. Xu, M. Dai, Y. Lu, and L. Sun, Hierarchical ZnO nanowire-nanosheet architectures for high power conversion efficiency in dye-sensitized solar cells, *J. Phys. Chem. C* 114 (2010) 2776-2782.
- [4] R. Wahab, S.G. Ansari, Y.S. Kim, H.K. Seo, G.S. Kim, G. Khang, H.S. Shin, Low temperature solution synthesis and characterization of ZnO nano-flowers, *Mater. Res. Bull.* 42 (2007) 1640-1648.
- [5] R. Teki, T.C. Parker, H. Li, N. Koratkar, T.M. Lu, S. Lee, Low temperature synthesis of single crystalline ZnO nanorods by oblique angle deposition, *Thin Solid Films* 516 (2008) 4993-4996.
- [6] J. Song, S. Baek, S. Lim, Effect of hydrothermal reaction conditions on the optical properties of ZnO nanorods, *Physica B* 403 (2008) 1960-1963.
- [7] T. Chen, S.Y. Liu, Q. Xie, Y.L. Jiang, G.P. Ru, R. Liu, X.-P. Qu, Patterned ZnO nanorods network transistor fabricated by low-temperature hydrothermal process, *Microelectron. Eng.* 87 (2010) 1483-1486.
- [8] P.G. Li, S.L. Wang, W.H. Tang, Low-temperature synthesis and photoluminescence of ZnO nanostructures by a facile hydrothermal process, *J Alloy Compd.* 480 (2010) 566-569.
- [9] L.H. Quang, S.J. Chu, K.P. Loh, E. Fitzgerald, The effect of post-annealing treatment on photoluminescence of ZnO nanorods prepared by hydrothermal synthesis, *J. Cryst. Growth* 287 (2006) 157-161.
- [10] Z. Zhou, Y. Zhao, Z. Cai, Low-temperature growth of ZnO nanorods on PET fabrics with two-step hydrothermal method, *Appl. Surf. Sci.* 256 (2010) 4724-4728.

- [11] H.-C. Cheng, C.-F. Chen, C.-Y. Tsay, J.-P. Leu, High oriented ZnO films by sol–gel and chemical bath deposition combination method, *J. Alloy. Compd.* 475 (2009) L46-L49.
- [12] Y. Liu, C. Pan, Y. Dai, W. Chen, Synthesis of one-dimensional ZnO nanoneedles using thermal oxidation process in the air and its application as field emitters, *Mater. Lett.* 62 (2008) 2783-2786.
- [13] J. Qiu, M. Guo, X. Wang, Electrodeposition of hierarchical ZnO nanorod-nanosheet structures and their applications in dye-sensitized solar cells, *Appl. Mater. Interfaces* 3 (2011) 2358-2367.
- [14] Z. Han, L. Liao, Y. Wu, H. Pan, S. Shen, J. Chen, Synthesis and photocatalytic application of oriented hierarchical ZnO flower-rod architectures, *J. Hazard. Mater.* 217-218 (2012) 100-106.
- [15] Y. Lu, L. Wang, D. Wang, T. Xie, L. Chen, Y. Lin, A comparative study on plate-like and flower-like ZnO nanocrystals surface photovoltage property and photocatalytic activity, *Mater. Chem. Phys.* 129 (2011) 281-287.
- [16] Y. Tong, J. Cheng, Y. Liu, G. G. Siu, Enhanced photocatalytic performance of ZnO hierarchical nanostructures synthesized via a two-temperature aqueous solution route, *Scr. Mater.* 60 (2009) 1093-1096.
- [17] Y. Yang, G. Du, X. Xin, B. Xu, Hierarchical ZnO microrods: synthesis, structure, optical and photocatalytic properties, *Applied Physics A* 104 (2011) 1229-1235.
- [18] X. Hu, Y. Masuda, T. Ohji, K. Kato, Fabrication of Zn(OH)₂/ZnO nanosheet-ZnO nanoarray hybrid structured films by a dissolution-recrystallization route, *J. Am. Ceram. Soc.* 93 (2010) 881-886.

- [19] L. Liu, M. Ge, H. Liu, C. Guo, Y. Wang, Z. Zhou, Controlled synthesis of ZnO with adjustable morphologies from nanosheets to microspheres, *Colloids Surf., A* 348 (2009) 124-129.
- [20] W.K. Tan, K. Abdul Razak, K. Ibrahim, Z. Lockman, Formation of ZnO nanorod arrays on polytetrafluoroethylene (PTFE) via seeded growth low temperature hydrothermal reaction, *J. Alloy. Compd.* 509 (2011) 820-826.
- [21] Z. Lockman, P.F. Yeo, W.K. Tan, K. Ibrahim, K. Abdul Razak, Formation of self-aligned ZnO nanorods in aqueous solution, *J. Alloy. Compd.* 493 (2010) 699-706.
- [22] D. Raoufi, T. Raoufi, The effect of heat treatment on the physical properties of sol-gel derived ZnO thin films, *Appl. Surf. Sci.* 255 (2009) 5812-5817.
- [23] Z. Liu, J. Ya, E. Lei, Effects of substrates and seed layers on solution growing ZnO nanorods, *J. Solid State Electr.* 14 (2010) 957-963.
- [24] S. Song, S. Lim, Effect of Seed Layer on the Growth of ZnO Nanorods, *J. Phys. Chem. C*. 111 (2007) 596-600.
- [25] J. Zhao, J.G. Jin, T. Li, X.X. Liu, Nucleation and growth of ZnO nanorods on the ZnO-Coated seed surface by solution chemical method, *Eur. Ceram. Soc.* 26 (2006) 2769-2775.
- [26] Z. Qin, Y. Huang, J. Qi, H. Li, J. Su, Y. Zhang, Facile synthesis and photoelectrochemical performance of the bush-like ZnO nanosheets film, *Solid State Sciences* 14 (2012) 155-158.
- [27] L.-M. Yu, X.H. Fan, J.Y. Shui, C. Lei, W. Yan, Research on the growth of ZnO nanowall by soft-solution route, *Mater. Lett.* 68 (2012) 423-425.

- [28] A. Sugunan, C. Hemant, M. Boman, J. Dutta, Zinc oxide nanowires in chemical bath on seeded substrates: Role of hexamine, *J. Sol-gel Sci. Techn.* 39 (2006) 49-56.
- [29] S. Chakraborty, A.K. Kole, P. Kumbhakar, Room temperature chemical synthesis of flower-like ZnO nanostructures, *Mater. Lett.* 67 (2012) 362-364.
- [30] J. Jiang, Z. Huang, S. Tan, Y. Ki, G. Wang, X. Tan, Preparation of ZnO nanosheets by a novel microemulsion-based hydrothermal method, *Mater. Chem. Phys.* 132 (2012) 735-739.
- [31] S. Xu, Z.L. Wang, One-Dimensional ZnO Nanostructures: Solution Growth and Functional Properties, *Nano Res.* 4 (2011) 1013-1098.
- [32] X.D. Guo, H.Y. Pi, Q.Z. Zhao, R.X. Li, Controllable growth of flowerlike ZnO nanostructures by combining laser direct writing and hydrothermal synthesis, *Mater. Lett.* 66 (2012) 377-381.
- [33] J.P. Kar, M.H. Ham, S.W. Lee, J. M. Myoung, Fabrication of ZnO nanostructures of various dimensions using patterned substrates, *Appl. Surf. Sci.* 255 (2009) 4087-4092.
- [34] L.Z. Pei, H.S. Zhao, W. Tan, H.Y. Yu, Y.W. Chen, W.F. Zhang, Single crystalline ZnO nanorods grown by a simple hydrothermal process, *Mater. Charact.* 60 (2009) 1063-1067.
- [35] M. Qiu, Z. Ye, J. Lu, H. He, J. Huang, L. Zhu, B. Zhao, Growth and properties of ZnO nanorod and nanonails by thermal evaporation, *Appl. Surf. Sci.* 255 (2009) 3972-3976.
- [36] X. Cai, X. Li, L. Liu, J. Zhu, Y. Wang, Preparation, characterization and room temperature photoluminescence properties of a zinc oxide nanosheet network grown on glass substrate by a facile chemical route, *Superlattices and microstructures* 50 (2011) 311-318.

- [37] Q. Li, H. Sun, M. Luo, W. Weng, K. Cheng, C. Song, P. Du, G. Shen, G. Han, Room temperature synthesis of ZnO nanoflowers on Si substrate via seed-layer assisted solution route, *J. Alloy. Compd.* 503 (2010) 514-518.
- [38] J. Shen, H. Zhuang, D. Wang, C. Zue, H. Liu, Growth and Characterization of ZnO Nanoporous Belts, *Cryst. Growth Des.* 9 (2009) 2187-2190.
- [39] D. Wang, Y. Zhao, C. Song, Synthesis and properties of cuboid-shaped ZnO hierarchical structures, *Solid State Sci.* 12 (2010) 776-782.
- [40] V. Gupta, P. Bhattacharya, Y.I. Yuzuk, K. Sreenivas, R.S. Katiyar, Optical phonon modes in ZnO nanorods on Si prepared by pulsed laser deposition, *J. Cryst. Growth* 287 (2006) 39-43.
- [41] W.I. Park, Y.H. Jun, S.W. Jung, G.-C. Yi, Excitonic emissions observed in ZnO single crystal nanorods, *Appl. Phys. Lett.* 82 (2003) 964-971.
- [42] R. Zhang, P.G. Yin, N. Wang, L. Guo, Photoluminescence and Raman scattering of ZnO nanorods, *Solid State Sci.* 11 (2009) 865-869.
- [43] O. Lupan, T. Pauporte, Hydrothermal treatment for the marked structural and optical quality improvement of ZnO nanowire arrays deposited on lightweight flexible substrates, *J. Cryst. Growth* 312 (2010) 2454-2458.
- [44] C. Zhang, High-quality oriented ZnO films grown by sol-gel process assisted with ZnO seed layer, *J. Phys. Chem. Solids* 71 (2010) 364-369.
- [45] W. Wang, Q. Li, Z. Liu, J. Zhang, Z. Liu, Low-temperature growth and properties of ZnO nanowires, *Appl. Phys. Lett.* 84 (2004) 4941-4943.

[46] L. Sun, R. Shao, Z. Chen, L. Tang, Y. Dai, J. Ding, Alkali-dependent synthesis of a flower-like ZnO structures with enhanced photocatalytic activity via a facile hydrothermal method, *Appl. Surf. Sci.* 258 (2012) 5455-5461.

Chapter 5

General Conclusion

The main motivation in this research work is to form functional ZnO nanostructured films by low-temperature processing methods which could enable the utilization of substrates with low-thermal stability such as organic polymers for flexible device applications. Thermal oxidation, sol-gel, hydrothermal and HWT have been demonstrated to be feasible for generation of various multi-dimensional ZnO morphologies for its optical and photo-catalytic properties, as well as DSSCs performance.

From experimental works performed in this study, it can be generally concluded as follows:

1. Thermal oxidation of metallic Zn foils can be used to generate random oriented 1-D ZnO nanorods and 2-D ZnO nanosheets. The morphologies of the nanostructures can be altered as a function of oxidation time, temperature and atmosphere. Thermal oxidations of metallic Zn foils were performed to study the formation of ZnO nanorods. It was demonstrated that oxidation of Zn foils is highly influence by the oxidation time and temperature. Randomly oriented and dendritic ZnO nanorods were formed at temperature near and above the melting point of Zn. Besides, oxidation in oxygen atmosphere was demonstrated to yield the formation of 2-D ZnO nanosheets. The optical properties of the ZnO nanostructures obtained by thermal oxidation were investigated using PL which indicated that the ZnO crystals formed possessed good crystallinity with the presence of oxygen related defects. The photocatalytic properties of the ZnO nanosheets obtained were investigated by degradation methylene orang. Formation mechanisms of these ZnO nanostructures were also proposed.

2. Novel and facile growth of ZnO nanostructures by HWT of Zn foils and sol-gel derived coatings were performed and documented. Surface oxidations of Zn foils by HWT were also investigated as a function of time. ZnO nanorods and nanosheets were obtained by HWT of chemically etched and unetched Zn foils, respectively. For etched Zn foils, ZnO nanowires were obtained after 4 h of HWT and at prolonged HWT time, ZnO nanorods were obtained and the coalescence of neighbouring nanorods due to Ostwald ripening is observed after 24 h. Interestingly, ZnO nanosheets were formed for the hot-water treated Zn foils without any chemical etching. No significant morphological change was observed for the ZnO nanosheets hot-water treated for prolonged period and coalescence of the ZnO nanosheets were also observed after 24 h. Different diffusion route of Zn ion from the substrate to the surface led to the morphological differences. However, ZnO nanostructures obtained exhibit good crystallinity as indicated by PL, Raman, HR-TEM and SAED results.

In a different study, HWT of sol-gel derived coatings as a function of time, temperature and effect of applied electric field were conducted. Dissolution and re-precipitation of dissolved species led to the formation of the ZnO nanostructures. The EF-HWT was investigated as a function of time, voltage and substrates at low-temperature of 50°C for 3 h. Granular crystallites were precipitated on the surface of the sol-gel derived ZnO film on FTO during HWT, and the shape of the precipitates was changed to hexagonal columns when an electric field was applied during HWT. The EF-HWT of ZnO gel films on Si wafer substrates influenced the morphology and orientation of the ZnO crystals formed; flower-like hexagonal ZnO crystals were obtained with increased degree of branching when higher applied voltage was used during HWT. Besides that, the optical properties of Ce-doped ZnO nanostructures obtained by HWT of sol-gel derived coating at 60°C for 30 min were also investigated.

The resultant rod-like ZnO nanostructures obtained exhibited blue shift in the UV emissions and reduced blue emissions compared to undoped ZnO nanostructured films obtained.

3. Well-aligned ZnO nanorod arrays were successfully formed on seeded ITO glass using low-temperature hydrothermal process using the optimum conditions obtained from previous reported works. Hydrothermal growth time from 4 to 24 h was investigated at 80°C. The DSSCs performances of the well-aligned ZnO nanorods were tested and efficiency up to a maximum of 0.22 % was obtained after a prolonged hydrothermal reaction time of 24 h. It was also demonstrated that the ZnO nanorod arrays formed were single crystal wurtzite structure with the preferential growth at [0001] direction. PL measurement, HR-TEM and Raman conducted further confirmed the excellent crystallinity of the ZnO crystals. The mechanism of hydrothermal growth of the well-aligned ZnO nanorod arrays was proposed as well. Besides that, ZnO composite structures that consist of both 1-D ZnO nanorods and 2-D ZnO nanosheets were obtained by hydrothermal growth of the sol-gel derived coatings on glass substrates. The simultaneous re-deposition of ZnO nanosheets generated in the aqueous hydrothermal bath and the growth of the nanorods from the coated seed layers led to this unique bi-structures formation. The photocatalytic properties of ZnO nanorod-nanosheet composite structures portrayed higher photo-degradation of MB under visible light irradiation compared only ZnO nanorod arrays.

It can be concluded that controlled formation of ZnO nano-architecture via low-temperature processes is viable using sol-gel, hydrothermal and HWT. Parameters such as temperature, time, and electric field could affect the dimensions of ZnO nanostructures formed. The ZnO nanostructures formed were demonstrated to possess good crystallinity and optical properties applicable for photocatalyst, DSSCs

and optoelectronic applications. These findings would be beneficial for applications utilizing substrates with low thermal stability for flexible devices in the future.

ACKNOWLEDGEMENTS

I would like to express my utmost gratitude to my supervisor, Prof. Atsunori Matsuda for his guidance, encouragements, invaluable supports and opportunities to learn from his undivided spirit and dedication in many aspects of life throughout my study in Toyohashi University of Technology (TUT), Japan. He has been an inspirational and motivational figure during my study and I have learnt to look for the silver lining in every obstacle that appears not only in academic but also in daily life.

I would like to acknowledge my co-supervisors, Assoc. Prof. Hiroyuki Muto and Dr. Go Kawamura for their constant vigilances and supports in every possible means. Besides that, I would like to extend my thanks to our international research collaborators Assoc. Prof. Zainovia Lockman and Assoc. Prof. Khairunisak Abdul Razak of School of Materials and Mineral Resources, Universiti Sains Malaysia for their constant guidance, encouragement and contributions over the years.

There is no word that I could use to express gratitude to my family for their unconditional love, blessings and supports. I would like to thank my lovely girlfriend, Vivien Cheng for her believe, patience, unwavering supports during my study here in Japan.

Last but not least, I would like to thank all the students, postgraduates, researchers, Mrs. Yuka Yogo of Matsuda-Muto-Kawamura laboratory for their invaluable assistance. Special thanks to Assoc. Prof. Lim Pang Boey and other Malaysian friends for their companionships and priceless help throughout my life in TUT, the memories shall be etched in my mind vividly. I am also thankful to Japan International Co-operation Agency (JICA)

for funding my PhD study in Japan and Ms. Mikayo Kurono for her kindness and assistance with JICA related matters.

Wai Kian Tan

ワイ キアン タン

Department of Functional Materials Engineering

Graduate School of Engineering

Toyohashi University of Technology

December 2013

LIST OF PUBLICATIONS

Original international publications from this thesis:

1. Zainovia Lockman, Yeo Pet Fong, **Wai Kian Tan**, Kamarulazizi Ibrahim, and Khairunisak Abdul Razak, "Formation of Self-Aligned ZnO Nanorods in Aqueous Solution", *Journal of Alloy and Compounds* 493, No.1-2, pp.699-706, March 2010.
(Chapter 1)
2. **Wai Kian Tan**, Khairunisak Abdul Razak, Kamarulazizi Ibrahim, Go Kawamura, Junichi Hamagami, Atsunori Matsuda, and Zainovia Lockman, "Formation of ZnO Nano and Sub-Micron-Rods by Chemical Process on Hot-water-treated and Non-treated Sol-gel Coating", *Malaysian Journal of Microscopy* 6, pp.58-63, October 2010.
(Chapter 1)
3. **Wai Kian Tan**, Khairunisak Abdul Razak, Kamarulazizi Ibrahim, and Zainovia Lockman, "Formation of ZnO nanorod arrays on polytetrafluoroethylene (PTFE) via seeded growth low temperature hydrothermal reaction", *Journal of Alloys and Compounds* 509, No.3, pp.820-826, January 2011.
(Chapter 1)
4. **Wai Kian Tan**, Khairunisak Abdul Razak, Kamarulazizi Ibrahim, and Zainovia Lockman, "Oxidation of etched Zn foil for the formation of ZnO nanostructure", *Journal of Alloys and Compounds* 509, No.24, pp.6806-6811, June 2011.
(Chapter 1)

5. Zainovia Lockman, Khairunisak Abdul Razak, Tan Kah Huat, **Wai Kian Tan**, Leow Cheah Li, Go Kawamura, and Atsunori Matsuda, “Formation of 1-dimensional (1-D) and 3-dimensional (3-D) ZnO nanostructures by oxidation and chemical methods”, *Materialwissenschaft und Werkstofftechnik* 43 (*Materials Science and Engineering Technology*) No.5, pp.457-460, May 2012.

(Chapter 1)

6. **Wai Kian Tan**, Leow Cheah Li, Khairunisak Abdul Razak, Go Kawamura, Hiroyuki Muto, Atsunori Matsuda and Zainovia Lockman, “Formation of Two-Dimensional ZnO Nanosheets by Rapid Thermal Oxidation in Oxygenated Environment”, *Journal of Nanoscience and Nanotechnology* Volume 13, pp.1-8, 2013.

(Chapter 2)

7. **Wai Kian Tan**, Khairunisak Abdul Razak, Zainovia Lockman, Go Kawamura, Hiroyuki Muto and Atsunori Matsuda, “Formation of highly crystallized ZnO nanostructures by hot-water treatment of etched Zn foils”, *Materials Letters* 91, pp.111-114, January 2013.

(Chapter 3)

8. **Wai Kian Tan**, Khairunisak Abdul Razak, Zainovia Lockman, Go Kawamura, Hiroyuki Muto and Atsunori Matsuda, “Optical properties of two-dimensional ZnO nanosheets formed by hot-water treatment of Zn foils”, *Solid State Communications* 162, pp.43-47, May 2013.

(Chapter 3)

9. Atsunori Matsuda, **Wai Kian Tan**, Shuhei Furukawa and Hiroyuki Muto, “Morphology-control of crystallites precipitated from ZnO gel films by applying electric field during hot-water treatment”, *Materials Science in Semiconductor Processing* 16, No. 5, pp. 1232-1239, October 2013.

(Chapter 3)

10. **Wai Kian Tan**, Khairunisak Abdul Razak, Zainovia Lockman, Go Kawamura, Hiroyuki Muto and Atsunori Matsuda, “Photoluminescence properties of rod-like Ce-doped ZnO nanostructures formed by hot-water treatment of sol-gel derived coating”, *Optical Materials*, Volume 35, Issue 11, pp. 1902-1907, September 2013.

(Chapter 3)

11. **Wai Kian Tan**, Khairunisak Abdul Razak, Zainovia Lockman, Go Kawamura, Hiroyuki Muto and Atsunori Matsuda, “Enhanced Dye-Sensitized Solar Cells Performance of ZnO Nanorod Arrays Grown by Low-Temperature Hydrothermal Reaction”, *International Journal of Energy Research* Volume 37, Issue 15, pp. 1992-2000, December 2013.

(Chapter 4)

12. **Wai Kian Tan**, Khairunisak Abdul Razak, Zainovia Lockman, Go Kawamura, Hiroyuki Muto and Atsunori Matsuda, “Synthesis of ZnO nanorod-nanosheet composite via facile hydrothermal method and their photocatalytic activities under visible-light irradiation”, *Journal of Solid State Chemistry*, 211, pp.146-153, January 2014.

(Chapter 4)